NOTE TO USERS

Page(s) not included in the original manuscript and are unavailable from the author or university. The manuscript was microfilmed as received.

134

This reproduction is the best copy available.

UMI®

Deep Etching of Silicon with XeF_2

Behraad Bahreyni

Department of Electrical and Computer Engineering
University of Manitoba
Winnipeg, Manitoba, Canada

A thesis submitted to
the Faculty of Graduate Studies
in partial fulfillment of
the requirements for the degree of

Master of Science

Copyright © 2001 by Behraad Bahreyni

National Library of Canada

Bibliothèque nationale du Canada

Acquisitions and Bibliographic Services

Acquisitions et services bibliographiques

395 Wellington Street
Ottawa ON K1A 0N4
Canada

395, rue Wellington
Ottawa ON K1A 0N4
Canada

Your file Votre référence

Our file Notre référence

The author has granted a non-exclusive licence allowing the National Library of Canada to reproduce, loan, distribute or sell copies of this thesis in microform, paper or electronic formats.

L'auteur a accordé une licence non exclusive permettant à la Bibliothèque nationale du Canada de reproduire, prêter, distribuer ou vendre des copies de cette thèse sous la forme de microfiche/film, de reproduction sur papier ou sur format électronique.

The author retains ownership of the copyright in this thesis. Neither the thesis nor substantial extracts from it may be printed or otherwise reproduced without the author's permission.

L'auteur conserve la propriété du droit d'auteur qui protège cette thèse. Ni la thèse ni des extraits substantiels de celle-ci ne doivent être imprimés ou autrement reproduits sans son autorisation.

0-612-62689-X

Canada

THE UNIVERSITY OF MANITOBA

FACULTY OF GRADUATE STUDIES

*****

COPYRIGHT PERMISSION

DEEP ETCHING OF SILICON WITH XeF_2

BY

BEHRAAD BAHREYNI

A Thesis/Practicum submitted to the Faculty of Graduate Studies of The University of Manitoba in partial fulfillment of the requirement of the degree

Of

MASTER OF SCIENCE

BEHRAAD BAHREYNI © 2001

Permission has been granted to the Library of the University of Manitoba to lend or sell copies of this thesis/practicum, to the National Library of Canada to microfilm this thesis and to lend or sell copies of the film, and to University Microfilms Inc. to publish an abstract of this thesis/practicum.

This reproduction or copy of this thesis has been made available by authority of the copyright owner solely for the purpose of private study and research, and may only be reproduced and copied as permitted by copyright laws or with express written authorization from the copyright owner.

To the people of my country, Iran

Abstract

Fabrication of microelectromechanical systems (MEMS) requires systems for depositing and selectively removing of parts of a substrate material. The most commonly used material in micromachining of different MEMS devices is silicon. Therefore, depositing and etching of silicon is of great importance in micromachining.

One of the candidates for selective etching of silicon is xenon difluoride. XeF_2 etches silicon isotropically in its gaseous form without a need for plasma generation. XeF_2 is extremely selective to silicon compared to other common materials in micromachining; such as SiO_2, Si_3N_4, aluminum, and copper.

In this thesis, design and fabrication of a XeF_2 etching system is described. The

system can both be controlled manually or by a computer. Different etching methodologies were examined and the results are presented. These experimental results are compared with the theoretical calculations.

The second part of the thesis deals with simulation of the etching process. The simulation which is described in this report could predict the odd shape of the etching profiles after deep etching of samples with XeF_2. The simulation algorithms are based on a theory which was developed for explaining the shape of etched profiles.

Acknowledgments

I want to thank my advisor, Dr. Cyrus Shafai, for all his support and encouragement. His patience and generosity in sharing his time and knowledge benefited me greatly. For this, I shall be eternally grateful.

I would also like to thank professor H. C. Card, professor G. E. Bridges, professor D. J. Thomson, and Dr. D. R. Oliver for their guidance and valuable discussions that we had.

I also thank many of my friends and colleagues; especially Paul Bugyik, Dr. Kin Yip Sze, Jeremy Johnson, and all students in room 470.

I am grateful to our talented technicians: Mr. Bill Bourbonnais, Mr. Allan McKay, Mr. Al Symmons, and Mr. Ken Biegun. Their help made completion of this project possible.

My parents have supported me for all my life. If I have done anything that can be considered a success, it is a direct result of their encouragement and guidance. My heartfelt thanks go in a special way to them.

Last but not least, I want to thank my fiancée, Solmaz, for her love and patience. While I was working on this project, she tolerated my occasional irrational behavior with fortitude.

Table of Contents

Abstract......ii

Acknowledgments......iv

List of Figures......xi

List of Tables......xvi

List of Symbols......xvii

Chapter 1: Introduction......1

I. Motivation......1

II. Organization of Thesis......2

Chapter 2: Microelectromechanical Systems and Micromachining......4

I. What Are Microelectromechanical Systems?......4

II. Integrated Circuit Processes......9

III. Bulk Micromachining......11

A. Wet Etching of Silicon......12

B. Dry Etching of Silicon.......14
IV. Surface Micromachining.......16
V. The Selectivity Issue.......16
VI. Bonding.......18
VII. High Aspect Ratio Processes.......19
VIII. Mechanical Transducers.......20
A. Piezoresistive Sensors.......22
B. Piezoelectric Sensors.......22
C. Capacitive Sensors.......23
D. Optical Sensors.......23
E. Resonant Sensors.......24
IX. Other MEMS Applications.......25

Chapter 3: Xenon Difluoride Etching of Silicon.......26
I. Xenon Difluoride Properties.......26
II. The Etching Mechanism.......28
III. Silicon Etch Rate in a XeF_2 Ambient.......31
IV. Xenon Difluoride Etching Systems.......33
A. Continuous Flow/Amount Etching Method.......33
B. Pulse Mode Etching.......34
V. The Designed XeF_2 Etching System.......37
VI. Control Software.......41

VII. Alternative Etching Methods....47

A. Triple Pulse Method....47

B. Quick Pulse Method....48

VIII. Calculation of Etch Rate and Etch Depth....48

Chapter 4: Experimental Results....52

I. Sample Preparation....52

II. Comparison of Different Etching Techniques....53

III. Microstructure Fabrication Results....55

IV. Trenching Effect....61

V. Loading Effect....63

VI. Corrosion of Materials after Long Exposure to XeF_2....64

Chapter 5: Simulation of the Etching Process....66

I. Definition of Problem....66

II. The Simulation Program: Details and Algorithms....67

A. Main Program....67

B. Simulation....72

III. Simulation Results....76

Chapter 6: Conclusions....81

I. Summary....81

II. Future Work....82

Appendix A: Hardware and Electronic Details....84

I. Hardware and Electronics....84

A. Hardware....84

B. Electronics....85

Appendix B: Flowchart of Etching Control Software....89

Appendix C: Simulation Program Code....95

Appendix D: Etching Data for Different Etching Methods....115

I. Sample with an Initial Surface Area of ~60mm^2....115

A. Basic Pulse Method....115

B. Triple Pulse Method....116

C. Quick Pulse Method....116

II. Sample with an Initial Surface Area of ~110mm^2....117

A. Basic Pulse Method....117

B. Triple Pulse Method....117

C. Quick Pulse Method....118

III. Sample with a Surface Area of ~85mm^2....118

A. Basic Pulse Method....118

B. Triple Pulse Method....119

C. Quick Pulse Method....120

Appendix E: Experimental Data for Trenching Effect....121

I. Dependance of Trenching Effect on Hole Diameter....121

II. Dependance of Trenching Effect on Number of Etching Pulses....125

A. Results after 4 Etching Pulses....126

B. Results after 7 Etching Pulses....127

C. Results after 10 Etching Pulses....128

III. Comparison of Simulation and Experimental Results....129

Appendix F: Fabricated System....132

References....135

List of Figures

Figure 2−1.(a) Optical bench for optical CD readout signal processing, (b) A magnetic micromotor....5

Figure 2−2. A micromachined accelerometer....7

Figure 2−3. Basic process flow of IC fabrication....10

Figure 2−4. Different profiles resulted from different etching methods....13

Figure 2−5. A MEMS filter....24

Figure 3−1. A simplified schematic of a plasma etching system....27

Figure 3−2. Simplified schematic of a reactive ion etching system....27

Figure 3−3. Schematic of a simple XeF_2 etching system....34

Figure 3−4. Schematic of a pulse etching system....35

Figure 3−5. Pressure changes inside the expansion and etching chambers during an etching cycle....36

Figure 3−6. Simplified schematic of the initial design of the XeF_2 etching system....37

Figure 3−7. Original design with the expansion chamber added to it....39

Figure 3−8. Software interface before starting the etch....43

Figure 3−9. Software interface in manual mode........44

Figure 3−10. Software interface in automatic mode........46

Figure 3−11. Change in number of XeF_2 molecules during an etching pulse........50

Figure 3−12. Etch rate as a function of time........50

Figure 3−13. Etch depth as a function of time........51

Figure 4−1. Comparison of different etching methods........54

Figure 4−2. A released cross. The smaller photo in right corner is taken at the same position but 75µm below the sample surface........55

Figure 4−3. A released bridge. Note cracking of the oxide layer due to etch−induced stress at sharp points........56

Figure 4−4. A fabricated circular membrane........57

Figure 4−5. SEM image of the etched silicon surface........58

Figure 4−6. AFM image of the etched silicon surface........58

Figure 4−7. Etching profiles for holes with different diameters: (a) expected and (b) observed profiles........59

Figure 4−8. Variation of etch depth with hole diameter........60

Figure 4−9. The etch profile for small size mask opennings........60

Figure 4−10. The etch profile at the bottom of a large hole. The etch depth around the center of the hole is about 23µm versus 27µm at the edge........61

Figure 4−11. Profilometer plot of a relatively large hole. The etch depth at the center of this whole is 6µm less than that of the edges........62

Figure 4−12. Profilometer plot Illustrating the loading effect between two adjacent holes. 63

Figure 4−13. Cross sections of the etch profiles resulting from etching through two close openings in mask. Note that the etch depth at each point depends on its distance from the other hole..64

Figure 4−14. A piece of an aluminum film which was attacked by XeF_2 during a long etch..65

Figure 5−1. Simplified flowchart of the simulation program..69

Figure 5−2. Comparison of Gaussian random variables. one generated in simulation program and the other one with Matlab..71

Figure 5−3. Flowchart of the simulation subroutine..74

Figure 5−4. Different etch profiles which are resulted by changing λ............................76

Figure 5−5. Simulation results showing the trenching phenomenon for and its changes with λ. The hole with is 400μm and the reaction probability was set to 0.01..................77

Figure 5−6. Simulation results showing the loading effect for two neighbor holes. The hole diameters are 200μm each, the distance between them is 100μm, and the reaction probability was set to 0.01..78

Figure 5−7. The effect of changing the reaction probability on the simulated profile. The hole width is 200μm and the mean free path is 20μm..79

Figure A−1. Initial design for control board (only one of the four similar circuits is shown)..86

Figure A−2. Final electronic circuitry for control board...87

Figure B−1. The main subroutine in automatic mode....90

Figure B−2. The etch subroutine....91

Figure B−3. The purge subroutine....92

Figure B−4. Timer subroutine....93

Figure B−5. Subroutine for reading the pressure....94

Figure E−1. Profile of a 60μm hole....122

Figure E−2. Profile of a 158μm hole....122

Figure E−3. Profile of a 249μm hole....123

Figure E−4. Profile of a 411μm hole....123

Figure E−5. Profile of a 576μm hole....124

Figure E−6. Profile of a 924μm hole....124

Figure E−7. Profile of a 595μm hole....126

Figure E−8. Profile of a 895μm hole....126

Figure E−9. Profile of a 570μm hole....127

Figure E−10. Profile of a 995μm hole....127

Figure E−11. Profile of a 617μm hole....128

Figure E−12. Profile of a 930μm hole....128

Figure E−13. Experimental and simulation results for a 60μm hole....130

Figure E−14. Experimental and simulation results for a 160μm hole....130

Figure E−15. Experimental and simulation results for a 250μm hole....130

Figure E−16. Experimental and simulation results for a 580μm hole. The actual trench

depth is 2.9μm versus 5μm for simulated result. 130

Figure E−17. Experimental and simulation results for a 1000μm hole. The actual trench

depth is 4.9μm versus 7μm for simulated result. 131

Figure F−1. Final setup of the system..132

Figure F−2. Another view of the etching system...133

Figure F−3. Computer interface...133

List of Tables

Table 2−1. Comparison of the etch rates of common wet etchants for different silicon crystal orientations....13

Table 2−2. Some of the commonly used materials in microelectronics and their plasma etchants....15

Table 2−3. The etch rate of Si, SiO_2, and Si_3N_4 for different wet and dry etchants....17

List of Symbols

ε Dielectric permitivity

ε_0 Permitivity of vacuum

A Surface area of each of capacitor plates;

Surface area of those parts of silicon substrate which are exposed to XeF_2

d Distance between a capacitor plates;

Gas molecule diameter

C Capacitance

R Silicon etch rate;

Universal gas constant

ν_0 Pre–exponential factor in rate equation

N_A Avogadro number

k Boltzmann constant

V Volume

T Temperature

E_a Effective activation energy

n_{Si} Density of silicon atoms in bulk silicon

N Number of XeF_2 molecules in etching chamber during the etch

N_0 Initial number of XeF_2 molecules in etching chamber

λ Mean free path of a molecule

P Pressure

Chapter 1: Introduction

I. Motivation

Different kinds of microelectromechanical systems (MEMS) and their fabrication techniques have been investigated by many research groups with different backgrounds. This is mainly due to the potential for great improvements in reliability and reducing the cost of making and maintaining a system. In fact, the effect of introduction of MEMS to system design, especially in sensor design area, is usually compared to the integrated circuit revolution and its impact on electronics engineering and later on all aspects of modern life. The fabrication methods for MEMS devices have their roots in microelectronic fabrication.

Micromachining, a term which is used for MEMS fabrication processes, requires numerous systems for different purposes. Similar to microelectronic fabrication, the three main techniques which are used in micromachining are deposition/growth, etching, and doping. The systems which are used for these processes are sometimes modified versions of those used in microelectronic industry, like furnaces and mask aligners, or they may be mainly designed and used for micromachining, like systems for making high aspect ratio

microstructures.

In micromachining, sometimes it is necessary to use one layer as a mold to form another structure. This layer will be removed after that structure is made out of some other material. In this case the first layer is called *"sacrificial layer"*. Obviously the etchant which is used for etching the sacrificial layer has to be as selective as possible to minimize etching of the main structure. One of the most commonly used materials as a sacrificial layer is polysilicon. Thus an etchant which can etch polysilicon or silicon selectively compared to other materials can be very useful. One of the candidates for this purpose is XeF_2.

In this thesis, design and fabrication of a system for etching silicon with XeF_2 are explained. Different etching methods and their experimental results are compared. The observed oddities in the shape of etching profiles resulting from deep etching of substrate through a hole on mask are explained. A simulation program was written to verify the explanation for observed profiles. The simulated results closely matched the experimental observations.

II. Organization of Thesis

Chapter 2 introduces microelectromechanical systems and their basic fabrication methods. Common types of MEMS devices are also briefly introduced.

Chapter 3 discusses the XeF_2 properties and its silicon etching mechanism. Different

etching systems and methods are described and compared with each other. The design for the etching system is also explained in this chapter.

In Chapter 4 the experimental results are presented. Results for making various microstructures and usually from different points of view are shown.

Chapter 5 describes the simulation software and its algorithms. After explaining the problem, the algorithms are fully explained. Finally the simulation results for different etching conditions are presented.

Finally in Chapter 6 conclusions are given. This chapter also contains some suggestions for the future work based on this thesis.

There are six appendices for this thesis. In Appendix A the hardware details of the etching system are described.

Appendix B shows the flowcharts for the control software. This is included in this thesis as a reference for readers who wish to make updates to the software.

Appendix C contains the C code for the simulation software, and similar to Appendix B, its main purpose is making future work easier.

Appendix D includes the etching data, such as pressure and pulse duration, for some of the samples whose results were used in thesis.

Appendix E contains figures that illustrate the trenching effect and its dependance on different parameters. These experimental results are also compared to simulations.

Finally, Appendix F includes photos of the actual system setup in laboratory.

Chapter 2: Microelectromechanical Systems and Micromachining

I. WHAT ARE MICROELECTROMECHANICAL SYSTEMS?

Microelectromechanical Systems (MEMS) contain extremely small mechanical elements (a few microns to 100's of microns), often integrated together with electronic signal processing circuitry. MEMS devices are manufactured in a similar fashion to electronic microchips. The most significant advantage here is not necessarily that the system can be miniaturized, but rather that the lithographic techniques that now mass-produce thousands of complex microchips can simultaneously be used to manufacture mechanical sensors and actuators. As a result, the price of these components may eventually be reduced to just pennies, as has happened with integrated circuits.

Microengineering refers to the technologies and practice of designing and fabricating three dimensional structures and devices with dimensions on the order of micrometers to perhaps a few millimeters (Figure 2–1(a) [1] and Figure 2–1(b) [2]). The two construction technologies of microengineering are microelectronics and micromachining. Microelectronics, producing electronic circuitry on silicon chips, is a

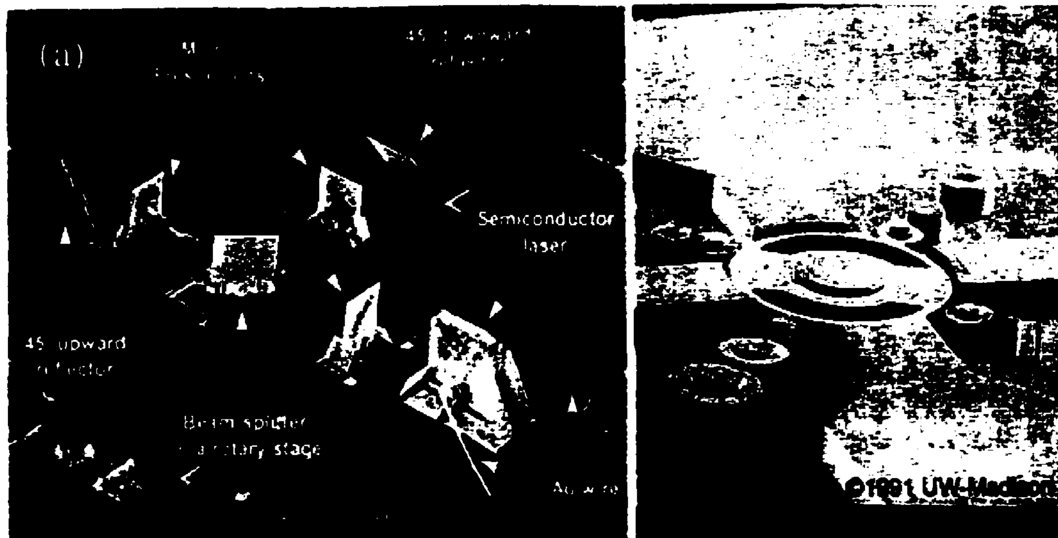

Figure 2-1.(a) Optical bench for optical CD pickup head from [1], (b) A magnetic micromotor from[2].

well developed and mature technology. Micromachining is the general name for various techniques used in order to produce the structures and moving parts of microengineered devices or making sensors with very small dimensions. One of the main goals of microengineering is to be able to integrate microelectronic circuitry into micromachined structures, in order to produce completely integrated systems (microsystems). Such systems could have the same advantages of low cost, reliability and small size as silicon chips produced in the microelectronics industry. An example model of a microsystem is that of a control system; many proposed microsystems take this form. Microsensors detect changes in the parameter to be controlled. Electronic control logic then operates microactuators based on information from the sensors to bring the parameter to be controlled within the desired limits. But not all devices need to follow this control-system scheme. For instance, an accelerometer designed to inflate an air-bag in the event of a car

crash may not only incorporate a micromachined acceleration sensor, but also electronics to condition the signal and detect a rapid deceleration as well as microactuators to apply a force on the sensor allowing the device to be tested when the driver starts the car.

Microsystems may be constructed from parts produced using different technologies on different substrates connected together; i.e. a hybrid system. For example, a silicon chip would be used to implement control circuitry, whereas the actuators it controls could be micromolded in plastic or electroplated metal. Alternatively, all components of a system could be constructed on a single substrate using one technology (a monolithic system). Hybrid systems have the advantages that the most appropriate technology for each component can be selected to optimize system performance. This will often lead to a shorter development time, since microfabrication techniques for each component may already exist. Thus compromises will not have to be made to ensure that each component can be fabricated without damaging components already existing on the substrate. Monolithic devices will typically be more compact than hybrid devices and also more reliable (fewer interconnections that can go wrong, for example). Moreover, once the fabrication process has been developed, they can be manufactured more cheaply since less assembly is required.

A significant problem facing microengineers is that of assembling many microscopic components. Potential solutions include self–assembling systems and desktop factories staffed by microrobots! At some point many microsystems will have to interact with macroscopic systems. Often it may be that only a critical component of a

system has to be microengineered and supported by a complex system produced using more conventional engineering techniques. It is easy to underestimate the problems involved in mounting and packaging microdevices, and then integrating them with macroscopic supporting systems.

Figure 2-2. A micromachined accelerometer, from [3].

When considering such small devices, a number of physical effects have different significance on the micrometer scale compared to macroscopic scales. Interest in microengineering has initiated, or renewed, interest in a number of areas dealing with the study of these effects on microscopic scales. This includes such topics as micromechanics, which deals with the moving parts of microengineered devices, or microfluidics, which discusses the behavior of fluids in microchannels or capillaries.

Silicon micromachined devices have seen the greatest application, since silicon micromachining techniques are well developed micromachining techniques. This is due to

silicon wide use by the microelectronics industry. Silicon is also the primary substrate material used in the production of microelectronic circuitry, and so it is the most suitable candidate for the eventual production of microsystems.

Most of the larger companies in MEMS area are focussing on the larger markets, such as automotive sensors (pressure, directional acceleration, and gas sensors) for engine management and safety systems (Figure 2-2) [3]. However, there are a number of other applications which will be important in upcoming years. These include:

- Gas and chemical sensors for environmental monitoring:
    - Pd gate FET's
    - SnO sensors
- Biomedical sensors for monitoring and analysis:
    - Blood pressure monitors
    - Blood gas analysis
    - DNA analysis
    - Electrophoresis columns
- RF and optical components for communications:
    - Filters and oscillators
    - Low loss transmission lines
    - Switching devices
    - Other optical components (lenses, splitters, diffractive elements)
- Sensor arrays for improved reliability and performance

- Mass data storage

In addition to the above mentioned areas, there are other windows being opened to the microengineering world as this field is further explored and its capabilities are found to match the demand of other technologies demands. For more information about MEMS, the reader is referred to [4], [5], [6], [7], and [8].

II. INTEGRATED CIRCUIT PROCESSES

Integrated circuit (IC) processing is a mature technology for the fabrication of electronic devices and systems. Micromachining has inherited a great deal from the basic IC fabrication processes and being familiar with these processes is essential in order to understand the micromachining processes.

The steady advances in IC fabrication technology have been the basis for the microelectronics revolution, from the discrete germanium transistors of the 1950's to the 4G bit DRAM's of today. This section provides an overview of basic processes used to fabricate silicon ICs with the goal of introducing the technology and the terminology. Only an outline of the information related to the major process steps is given below. For a more detailed overview of all these processes the reader can refer to many available textbooks on this subject such as [9] and [10].

The main process steps employed in IC fabrication are (Figure 2-3): thin film deposition/growth, lithography, selective doping, and selective etching. Thin film

formation processes are used for a variety of materials. In a standard IC fabrication foundry the most commonly used thin film layers are: (1) epitaxial layers, (2) dielectric films, such as silicon dioxide and silicon nitride, (3) polysilicon films, and (4) metallization films. These films are used not only to build the active components, but also

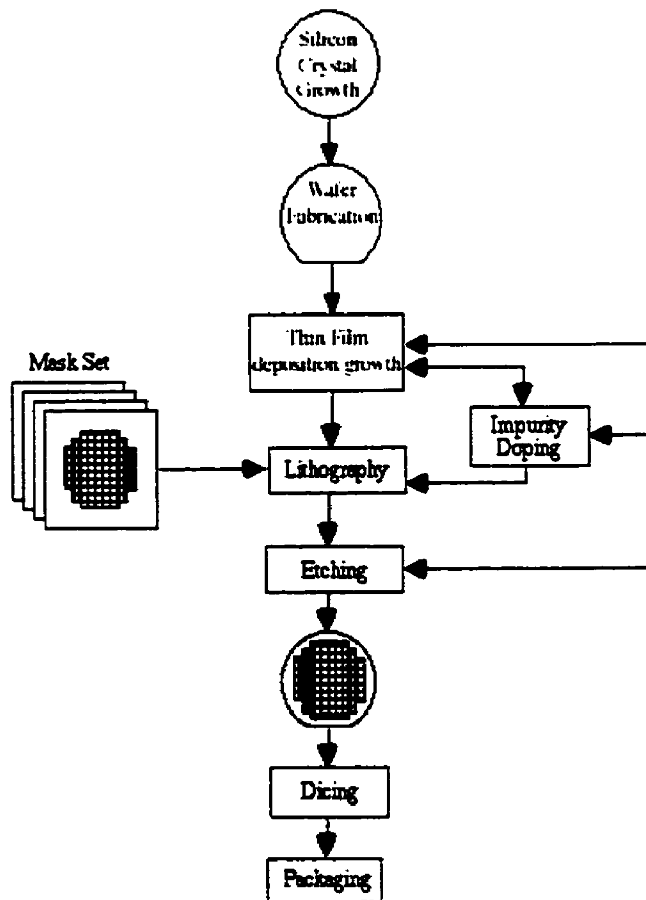

Figure 2-3. Basic process flow of IC fabrication

the interconnections and passive components in the circuit. Along with film processes, impurity doping is employed to modify the electrical properties of the wafer or thin film.

Doping may be done by thermal diffusion or ion implantation of dopant atoms. Lithography processes are used to transfer the pattern from a mask to the thin film or substrate surface. The unwanted segments of the film or substrate are then etched away to complete the pattern transfer. This cycle is repeated for each mask layer in the device design. Once the processing is completed, the wafers are probed for yield and diced into chips. These chips are encapsulated or packaged in various ways as final devices. Since most MEMS devices use silicon IC processes, the following discussion will be limited to silicon ICs. There are two classifications of micromachining: bulk and surface; both are based on silicon IC technology.

III. Bulk Micromachining

Bulk micromachining was developed during the 1970's as an extension of integrated circuit technology. It was used for fabrication of three dimensional structures [11]. Bulk micromachining of silicon uses wet and dry etching techniques in conjunction with etch masks and etch stops to sculpt micromechanical devices from the silicon substrate. Extensive reviews of bulk micromachining by anisotropic etching of silicon have been published [11] , [13].

There are two key capabilities that make bulk micromachining of silicon a viable technology. First, anisotropic etchants of silicon such as ethylene diamine pyrocatechol (EDP), potassium hydroxide (KOH), tetramethyl ammonium hydroxide (TMAH) and

hydrazine are available which preferentially etch single crystal silicon along given crystal planes. Second, etch masks and etch–stop techniques are available which can be used in conjunction with silicon anisotropic etchants to selectively prevent regions of silicon from being etched. As a result, it is possible to fabricate microstructures on a silicon substrate by appropriately combining etch masks and etch–stop patterns with anisotropic etchants.

A. Wet Etching of Silicon

In general, wet etching of silicon is used for shaping and polishing, as well as for characterizing structural and compositional features. The fundamental etch reactions are electrochemical, involving oxidation–reduction, followed by dissolution of the oxidation products.

One of the most important characteristics of the etching process is the directionality (or profile) of the etching process. If the etch rate in all directions (i.e. x, y, and z) is the same, the etch process is said to be *isotropic* or *non–directional*. The etching of single crystal silicon, or polycrystalline and amorphous silicon in HNA (HF, HNO_3, and CH_3COOH) etchant systems will result in such profiles. Etch processes which are *anisotropic* or *directional* have different etch rates for different directions. An example of this etch profile is the etching of <100> single crystal silicon in KOH–water or ethylene diamine pyrocatechol–water (EDP) etchants. Examples of isotropic and anisotropic etching of silicon are shown in Figure 2–4. The extreme case of directional etching in which the lateral etch rate is zero (referred to here as a *vertical profile*) is also shown.

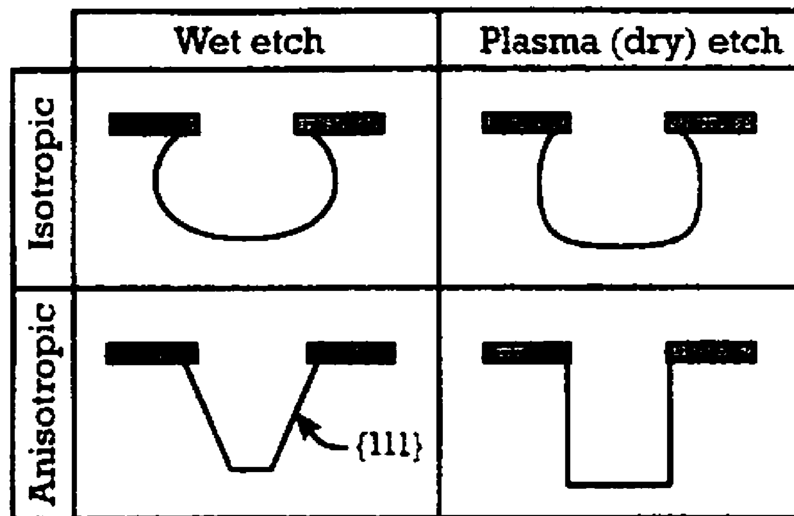

Figure 2-4. Different profiles resulted from different etching methods.

This profile can be achieved by etching <110> single crystal silicon with KOH-water. The etch rates of common anisotropic wet etchants for (100) and (111) planes are given in Table 2-1.

In some cases it is necessary to agitate the sample during the etch. This helps

Etchant	***(100) Etch Rate (μm/min)***	***(111) Etch Rate (μm/min)***	***(100)/(111) Etch ratio***
KOH	1.4	3.5×10^{-3}	400/1
EDP	0.75	0.02	35/1
TMAH	1	0.03-0.05	10-35/1

Table 2-1. Comparison of the etch rates of common wet etchants for different silicon crystal orientations.

remove the byproducts from the surface. Thus, the etchant molecules can react with substrate more easily. Agitation usually results in higher etch rates and more uniform

profiles.

In order to control the etching process, there are a variety of etch–stop methods to terminate etching at specified regions, such as high boron doping of those regions, electrochemical etch–stop, and P–N junction etch–stop. It should be mentioned that these methods can not be applied to all etchants and may not be suitable for some applications.

B. Dry Etching of Silicon

Dry etching is usually preferred to wet etching for many reasons. Dry etching is usually done in a plasma environment, which is much easier to start and stop than immersing samples into wet etchants and, generally, there are many more variables for controlling the etch process. Also, plasma etchants are usually less sensitive to the small changes of temperature across the wafer. These reasons generally make plasma etching more reliable and repeatable than wet etching. Plasma etching can have extremely high anisotropy. There are usually fewer particles in a plasma environment compared to a chemical solution which means plasma is a cleaner etching method. Finally, plasma etching produces less chemical waste than wet etch [12].

The etching is performed by reactive ions that are generated in a plasma environment. In fact, the only reason for plasma generation is breaking the bonds in chemically stable molecules and producing ions from those molecules. Different gases are used for plasma generation to etch the different materials that are commonly used in microelectronics. Some of these materials and their corresponding etchants are listed in

Table 2–2.

The most common form of dry etching for micromachining applications is reactive ion etching (RIE). Ions are accelerated towards the material to be etched, and the etching reaction is enhanced in the direction of travel of the ion. Thus, RIE is an anisotropic etching technique. Deep trenches and pits (up to ten or a few tens of microns) of arbitrary shape and with vertical walls can be etched in a variety of materials including silicon, oxide and nitride. Unlike anisotropic wet etching, RIE is not limited by the crystal planes in the silicon.

The reader can refer to [12] and [13] for more information about these techniques.

IV. SURFACE MICROMACHINING

Material	***Etchant***
Si	CF_4/O_2, CF_2Cl_2, CF_3Cl, $SF_6/O_2/Cl_2$
SiO_2	CF_4/H_2, C_2F_6, C_2F_6, C_3F_8, CHF_3/O_2
Si_3N_4	$CF_4/O_2/H_2$, $CF_4/O_2/H_2$, C_2F_6, C_3F_8, CHF_3
Al	BCl_3, BCl_3/Cl_2, $SiCl_4/Cl_2$
Organics	O_2, CF_4/O_2, SF_6/O_2
GaAs	BCl_3/Ar, $Cl_2/O_2/H_2$, H_2, CH_4/H_2
InP	CH_4/H_2, C_2H_6, Cl_2/Ar
Au	$C_2Cl_2F_4$, Cl_2, $CClF_3$

Table 2–2. Some of the commonly used materials in microelectronics and their plasma etchants.

Surface micromachining evolved directly from IC fabrication methods of

deposition, patterning, and etching, though there are major differences. Often, thicker films are required for mechanical behavior and as some of the layers are sacrificially removed to allow for free–moving parts, other layers must be resistant to sacrificial etchants such as hydrofluoric acid which may be used for etching silicon dioxide. Photolithography is relied upon for accurate placement and definition as MEMS dies have much more topography than IC die. These thicker layers also challenge etch technology, though Deep Reactive Ion Etching (DRIE) is predominately the etching method of choice. Surface micromachining is typically limited to a layer thickness of ~5 μm.

Examples of commercial surface micromachined MEMS include micro–accelerometer chips (e.g. ADXL family by Analog Devices Inc.). These devices are used as sensing element in vibration sensors, in automobile air–bag deployment mechanism, and in controlling mirror arrays in portable projectors.

V. The Selectivity Issue

In both bulk and surface micromachining, removing the unwanted sections of a thin film or substrate plays a very important role in microstructure fabrication. The etch depth can be as high as a few hundred microns. In such cases, choosing proper materials as the masking layer or the etchant is critically important. The most commonly used materials for masking are silicon dioxide and silicon nitride. Polysilicon or crystalline silicon are usually the materials that are needed to be, either completely or partially, removed. Thus

Etchant	*Si (μm/min)*	*SiO_2 (nm/min)*	*Si_3N_4 (nm/min)*	*Reference*
KOH	1.4	7.7	0	11
TMAH	1	0.05–0.25	0.05–0.25	11
HNA	1.5	8.7	2	14
DRIE	2	5		13
Cl_2/He	0.5	38	56	14
BrF_3	5	0.3	2.5	26
XeF_2	10	0	0	27

Table 2–3. The etch rate of Si, SiO_2, and Si_3N_4 for different wet and dry etchants.

it is very important to use an etchant which is as selective as possible to silicon. In Table2–3 the selectivities of some of the common etchants to silicon. SiO_2, and Si_3N_4 are listed.

Noting that BeF_3 is extremely dangerous and the high cost of plasma etching systems, XeF_2 seems to be the best candidate for selective etching of silicon. Under normal conditions, neither XeF_2 nor BrF_3 attacks photoresist, aluminum, copper, or stainless steel [14], [26]. This allows a person to employ the photoresist layer that he has already used for his lithography, as a masking layer. This can greatly reduce the fabrication complexity. However, XeF_2 can attack SiO_2 and Si_3N_4 in a plasma ambient or under UV light exposure [25].

VI. BONDING

The construction of any complicated mechanical device requires not only the

machining of individual components but also the assembly of components to form a complete system. In micromachining, bonding techniques are used to assemble individual micromachined parts to form a complete structure. Usually entire wafers or individual dies are bonded together. A primary application of silicon wafer bonding is in the fabrication of Silicon On Insulator (SOI) devices, where a wafer bonding and thinning process is used to produce a bulk–quality layer of single–crystal silicon over a thin film of thermally grown silicon dioxide. SOI wafers are then used to fabricate devices with reduced parasitic capacitance and leakage (i.e. higher device performance) in comparison with conventional silicon devices fabricated on bulk silicon.

When used in conjunction with micromachining techniques, wafer bonding allows the fabrication of three dimensional structures which are thicker than a single wafer. This is important for micropumps and microvalves where more than one cavity is needed in series in the thickness direction. Several processes have been developed for bonding silicon wafers. Silicon direct bonding is used to bond a pair of silicon wafers together directly, face to face. Anodic bonding is used to bond silicon to glass.

Wafer bonding processes add substantial flexibility to the device design and also solve some of device packaging problems. Examples of wafer bonding applications are packaging for pressure transducers, accelerometers, sealed cavities, and thermally isolated structures, and fluid control devices. A review of bonding techniques is given in [15] and [16].

VII. High Aspect Ratio Processes

High aspect ratio processes provide a means for fabricating micromechanical components with small lateral dimensions in comparison with their heights. Relatively thick and narrow structures offer high rigidity in the direction perpendicular to the substrate and compliance in the lateral directions. For microactuator applications, thick, high aspect ratio devices offer the possibility of compact production of high torque/force ratios, because of the larger interaction areas [17].

LIGA is probably the best known method of fabricating high aspect ratio structures [18]. LIGA is an acronym derived from the German words Lithografie, Galvanik, Abformung, which means lithography, electroforming, and injection molding. In this process, high intensity, low divergence, hard X-rays are used as the exposure source for the lithography. These X-rays are usually produced by a synchrotron radiation source. PMMA (polymethylmethacrylate) is used as the X-ray resist. The capabilities of this fabrication process for high-aspect-ratio fabrication are substantial. Thicknesses of several hundreds of microns and aspect ratios of greater than 100 to 1 (height to width) have been achieved. The sidewalls of the plated structures are almost vertical and smooth and they can be even used for optical components [19]. Also, by means of subsequent replication processes, such resist reliefs may be transformed into complementary relief structures and a wide variety of materials may be utilized. This replicating method has the potential to make the process reasonably cost effective. However, a synchrotron is

necessary for LIGA, and since only a few exist in the world, the number of research groups that can currently use this process is limited. There has been a great deal of research on LIGA–like methods using high aspect ratio lithography and films [20], [21].

VIII. MECHANICAL TRANSDUCERS

A transducer is a device that converts one physical quantity to another. The change in the resistance of some materials upon the application of stress to them is one example (piezoresistive effect). Deformation of a piezoelectric crystal under an applied electric field is another. Sensors and actuators are special types of transducers. In the present context, a sensor is a device that converts one physical or chemical quantity to an electrical signal, to be processed by the microsystem. Similarly, an actuator is a device which converts an electrical quantity into a physical or chemical one. Many of the sensors described below have been developed within the microelectronics industry and do not involve special micromachining techniques. However, some of these sensors can be enhanced by the use of micromachining techniques (e.g. for thermal isolation). Microactuators are required to drive the resonant sensors and make them oscillate at their resonant frequency. They are also required to produce the mechanical output required of particular microsystems; this may be moving micromirrors to scan laser beams or switching them from one fiber to another [22], to drive cutting tools for microsurgical applications, to drive micropumps and valves for microanalysis or microfluidic systems,

or these may even be microelectrode devices to stimulate nervous tissue in neural prosthesis applications [23]. A variety of methods exist for achieving microactuation like: electrostatic, magnetic, piezoelectric, hydraulic, and thermal. Of these, electrostatic and piezoelectric methods currently look most promising, although the others have their place. Electrostatic actuation is possibly the most common and well developed method, but it does suffer a little from wear and sticking problems. Magnetic actuators usually require relatively high currents (hence high power). However, unlike electrostatic actuators, magnetic actuators can be used for both pushing and pulling objects. Thermal actuators also require relatively large amounts of electrical energy and the generated heat also has to be dissipated. A detailed description of these methods is beyond the scope of this thesis.

The mechanical sensors that will be discussed here can be categorized into two groups. The first uses physical mechanisms to directly sense the parameter of interest (e.g. distance, strain). The second type uses microstructures to enable the mechanical sensors to detect parameters of interest that cannot be measured directly with the first type of sensor (e.g. acceleration). In almost all of these cases, releasing of a mechanical microstructure is necessary.

A. Piezoresistive Sensors

The change in resistance of a material with an applied strain is termed the piezoresistive effect. Piezoresistors are relatively easy to fabricate in silicon, being just a

small volume of silicon doped with impurities to render it n–type or p–type. Also the signal detection circuitry is simple. They have been used in a variety of applications where the measurement of the strain is desired or in applications that some other mechanical quantity (e.g. pressure or force) is first transformed to stress, which is then measured by piezoresistors .

B. Piezoelectric Sensors

When a force is applied to a piezoelectric material, a charge is induced on its surface which is proportional to the applied force. The applied force can thus be computed by measuring the electrical potential that appears across the crystal. Common piezoelectric crystals used for microengineered devices include zinc oxide and PZT (PbZrTiO3 – lead zirconate titanate), which can be deposited on microstructures and then patterned. The piezoelectricity property can also be used for microactuation and moving objects within very small distances. Piezoelectric actuation has been widely used in scanning probe microscopy where it is desirable to be able to move the probe on the surface of the sample over very small distances and with high accuracy.

C. Capacitive Sensors

For two parallel conducting plates, separated by an insulating material, the capacitance between the plates is given by:

$$C = \epsilon \frac{A}{d} \qquad (2-1)$$

where A is the area of the plates, d is the distance between them, and ε is the dielectric

permitivity which depends on the material between the plates. For air, ε is 8.854×10^{-12} F/m and is usually denoted by ε_0. It is assumed that the circumferences of the plates are much larger than the distance between them, so that fringing effects can be neglected. It can be seen that the measured capacitance is inversely proportional to the distance between the two plates. It is possible to use this technique to measure small displacements (microns to tens of microns) with high accuracy (sub–nanometer); however the instrumentation required to measure capacitance changes can be complex. In Figure 2–2 a micromachined accelerometer which employs capacitive sensing for measuring the amount of acceleration of the central proof mass is shown.

D. Optical Sensors

Silicon is a reflective material, as are many other materials used in semiconductor device fabrication (e.g. aluminum). Thus optical means may be used to sense displacement or deformation of microengineered cantilevers, membranes, etc. A laser is directed at the surface to be monitored in such a way that interference fringes are set up. By analyzing these fringes, displacement or deformation may be detected and quantified. One area where this technique is often employed is atomic force microscopy (AFM) for monitoring the deflection of a cantilever on which the sensing tip is mounted.

E. Resonant Sensors

These are based on micromachined cantilevers, or bridges, or similar structures which are driven to oscillate at their resonant frequency. Changes in the resonant

frequency of the device are typically sensed using different techniques, including piezoresistivity, optical techniques, or capacitive sensing. The resonant frequency of a bridge is related to the force applied to it (between anchor points), its length, thickness, width, mass, and the modulus of elasticity of the material from which it has been

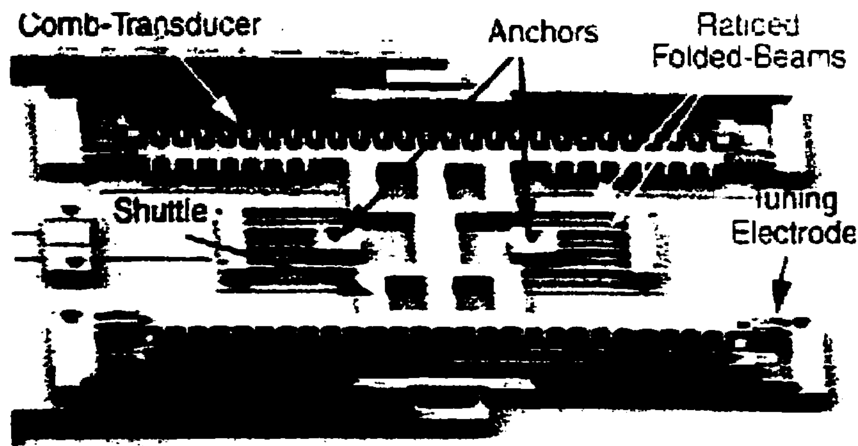

Figure 2–5. A MEMS filter from [24].

fabricated. If the membrane that the bridge is mounted on is deformed, for instance, if there is greater pressure on one side than the other, then the force applied to the bridge results in change to the resonant frequency.

Alternatively, a resonant device may be used as a biosensor, by coating it with a material that binds to the substance of interest. As more of the substance binds to the device, its mass will be increased, again altering the resonant frequency. In Figure 2–5 a MEMS filter is shown, which first converts an electrical signal to mechanical vibrations which are then converted back to an electrical signal [24].

IX. OTHER MEMS APPLICATIONS

In addition to sensors area, the MEMS devices have numerous other applications in other fields. A few examples are: RF devices, biomedical applications (BioMEMS), microfluidics, microtribology, microactuation, etc.

Coverage of all these topics is beyond the scope of this thesis and the interested user can refer to the references.

Chapter 3: Xenon Difluoride Etching of Silicon

I. *Xenon Difluoride Properties*

Xenon difluoride (XeF_2) is a white crystalline solid at room temperature, with rocksalt–size grains. It has a sublimation pressure of about 4Torr at room temperature. The gas will form HF in presence of water vapor, which is a potential safety hazard. However, with caution and proper ventilation, it can be handled safely. If necessary, an acid scrubber should be connected to the exhaust of the etching system.

XeF_2 is member of a family of fluorine based silicon etchants which includes ClF_3, BrF_3, BrF_5, and IF_5 [25], [26], [37]. All of these compounds can be used for etching of silicon. XeF_2 is more than 10^4 times more reactive than F_2 molecules itself and hence, in many experiments it has been used as a source for fluorine atoms. XeF_2 etches silicon isotropically, with etch rates as high as 15μm/min [27] in its gaseous form (non–plasma). At low pressures, the etch rate is linearly proportional to pressure. XeF_2 is extremely selective to silicon with respect to other common materials in semiconductor industry (Table 2–3), such as aluminum, silicon dioxide, silicon nitride, and even photoresist. This

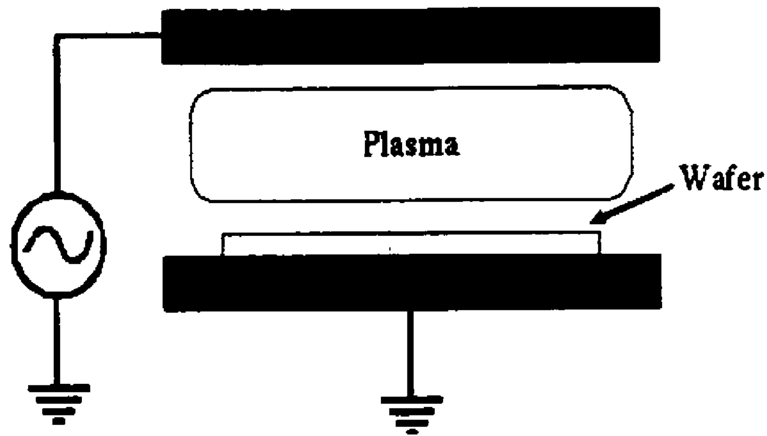

Figure 3−1. A simplified schematic of a plasma etching system.

makes XeF_2 a very attractive material, especially for post−CMOS processing of integrated circuits and systems [35]. This property makes XeF_2 an inexpensive alternative for plasma etching in many applications, since a XeF_2 etching system set up is much simpler than a plasma or reactive ion etching one. As can be seen in Figure 3−1 and Figure 3−2 , both

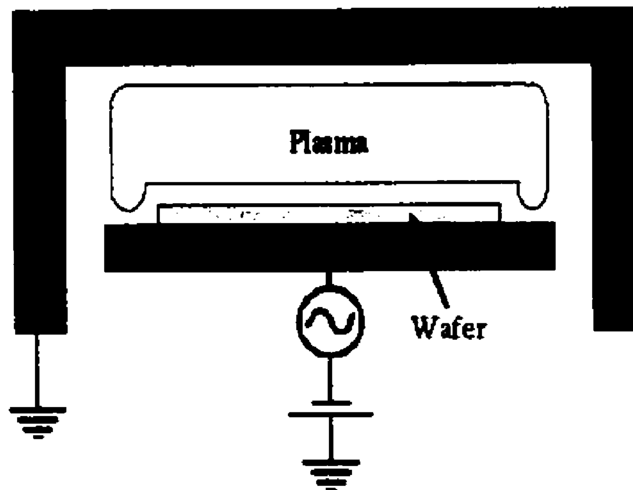

Figure 3−2. Simplified schematic of a reactive ion etching system.

plasma and reactive ion etching require a high power RF voltage source. Both methods are also sensitive to the pressure inside the etching chamber and the gas ratios.

A XeF_2 etching system is considerably simpler and less sensitive to different etching parameters. The most important factors for etching silicon with XeF_2 are time and etching pressure. Both of these parameters may be easily controlled.

Currently, many different companies produce XeF_2 with high purity (>99%) at prices starting from a few dollars per gram.

II. The Etching Mechanism

It has been well known that radicals generated in a fluorocarbon plasma produce volatile species as a consequence of chemical reactions which occur at the surface of silicon and its compounds. For example, F atoms and CF_3 radicals generated in gas phase by plasma–induced dissociation of CF_4 react with silicon to form SiF_4 (volatile).

In almost all cases, the etching mechanism of a solid material by exposing to gas phase particles with or without a plasma can be described by the following sequence of steps: (1) non–dissociative adsorption of gas phase species at the surface of the material to be etched; (2) dissociation of this adsorbed gas; (3) reaction between the adsorbed atoms and the solid surface to form an adsorbed product molecule; (4) desorption of the product molecule into gas phase; (5) and finally the removal of non–reactive residue (e.g. carbon, which can be burnt) from the surface [25]. These steps can be best explained by

illustrating them in an example like reaction of silicon with CF_3 radicals:

Step 1: Non–dissociative adsorption:

$CF_3\ (gas) + Si \rightarrow CF_3\ (ads.) + Si,$

Step 2: Dissociative adsorption:

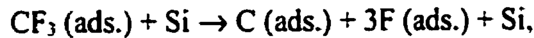

$CF_3\ (ads.) + Si \rightarrow C\ (ads.) + 3F\ (ads.) + Si,$

Step 3: Formation of product molecule:

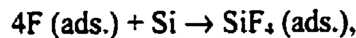

$4F\ (ads.) + Si \rightarrow SiF_4\ (ads.),$

Step 4: Desorption of product molecule:

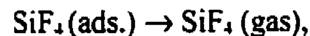

$SiF_4\ (ads.) \rightarrow SiF_4\ (gas),$

Step 5: Residue removal:

$C(ads.) + 4F\ (ads.) \rightarrow CF_4\ (gas).$

The first step almost always occurs since attractive forces between the non–dissociated molecule and the surface usually exist. This step may involve a *"precursor state"* where the molecule is mobile and diffuses through a thin boundary layer on the surface until it dissociates, possibly at a step, vacancy, or other defect. The resulting atoms may continue to diffuse or may become attached to a given surface site. On the other hand, sometimes the first four steps occur almost simultaneously, with very low or no diffusion. Finally, for atomic fluorine, the first two steps would be combined and labeled *"adsorption"*, but the conceptual framework would be similar.

If any of the above five steps does not occur, the reaction will not proceed. The available data shows that the second step (dissociative chemisorption) either does not

occur or occurs slowly for most of the molecules, such as CF_4, CF_3H, $CFCl_3$, and CCl_4. Therefore, it is the role of a plasma environment to change such non–reactive particles into reactive species. On the other hand, studies have shown that carbon is easily deposited on a silicon wafer, but is removed from it with some difficulty, which causes problems during the fifth step. For silicon at room temperature, the steps 3 and 4 occur at the same time. Thus if there is a gas which does not leave residue on surface and which dissociatively chemisorb, it can be used for etching of silicon simply by exposing silicon to an ambient atmosphere of that gas. An obvious candidate is F_2, but due to the strong chemical bond between the fluorine atoms, the reaction probability between F_2 and silicon is very small. The next candidates can be the noble gas compounds of fluorine such as XeF_2. At room temperature, the XeF_2–Si reaction is more than 10^4 times faster than F_2–Si reaction.

The approximate reaction equation for XeF_2 and silicon is given by:

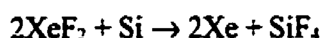

$$2XeF_2 + Si \rightarrow 2Xe + SiF_4$$

Significant quantities of fluorine are always observed on the surface of the samples etched by XeF_2. However, no data has been available that shows any indication of adsorbed xenon [25]. This implies that XeF_2 is dissociatively adsorbed on these surfaces and after the reaction the xenon atom, being a noble gas, is immediately desorbed into the gas phase. However, etching of silicon does not start instantaneously upon exposure to XeF_2 since a fluorosilyl layer on the surface has to be formed. During the etching, two stable products, SiF_4 and Si_2F_6, and a free radical, SiF_3 are formed. The relative amount of

each of these products depends on doping and XeF_2 flux [28].

Due to the weak chemical bond between xenon and fluorine atoms, one may essentially consider XeF_2 as a source of fluorine atoms. To verify this assumption, many research groups have investigated the differences between the reaction of XeF_2 and fluorine atoms with silicon, for example [29], [30], [31], [32], [33], and [34]. These studies indicate that although XeF_2 decomposes relatively easily, there are some differences between etching silicon with XeF_2 and fluorine atoms. For example one of the byproducts in both cases is SiF_2 which forms a surface layer that can affect how fast the reaction proceeds. It has been observed that the ratio of SiF_4 to SiF_2 molecules resulting from the reaction between XeF_2 and silicon is smaller than that of the reaction between fluorine atoms and silicon. This might be one of the sources of the existing difference between reaction probabilities of XeF_2 and fluorine atoms with silicon [35]. It is also suggested that adsorption plays an important role in reaction of XeF_2 with silicon but not with F atoms [31].

III. Silicon Etch Rate in a XeF_2 Ambient

Due to the extremely high observed selectivity of XeF_2 to silicon, presentation of very thin layers of other materials like SiO_2 can prevent the etch to proceed. So sample preparation is required before etching. In most cases the native oxide should be removed by an HF dip for a few seconds. This high degree of selectivity can be explained by the

fact that fluorine atoms attack silicon spontaneously, but reaction with other materials, especially silicon compounds such as silicon dioxide and silicon nitride, requires not only fluorine atoms but also high temperatures and/or radiation [37]. In fact, it is known that XeF_2 will attack silicon compounds, such as Si_3N_4 or SiO_2, in an plasma environment or under ultra violet radiation [25].

The reaction rate (i.e. etch rate) of silicon with XeF_2 can be described by an Arrhenius equation of the form [34]:

$$R = v_0 \cdot \frac{N}{kV} \cdot T^{1/2} \cdot e^{-E_a/kT} \qquad (3-1)$$

where R is the etch rate of silicon in µm/min, v_0 is a pre–exponential factor (1.9×10^{-14} kcal.cm^4/min/K$^{3/2}$), N is the number of XeF_2 atoms in volume V (cm^3) above the silicon surface, k is the Boltzmann constant (1.987×10^{-3} kcal/mole/K), T is the absolute substrate temperature (K), and E_a is the effective activation energy (−3.2 kcal/mole).

If one assumes that the etching process is chemical reaction limited and the XeF_2 concentration is uniform in the etching chamber, the changes in the number of XeF_2 atoms, N, can be expressed as:

$$-\frac{dN}{dt} = 2\,RA\times n_{Si} \qquad (3-2)$$

where A is the silicon opening area of the etching sample and n_{Si} is the atomic density of bulk silicon.

If we combine equations 3−1 and 3−2, we can find the changes in number of XeF_2

atoms as a function of time:

$$N = N_0 . e^{-C\frac{A}{V}t} \quad (3-3)$$

where N_0 is the initial number of XeF_2 atoms and C is a constant.

This equation shows that the number XeF_2 molecules decreases exponentially as the etch proceeds. In other words, this means that the etch rate decreases with time for a known amount of XeF_2. However this equation must be used carefully since area of the exposed silicon changes considerably due to the removal of silicon atoms from the surface and more importantly, due to surface roughness.

These equations will be used to calculate the etch rate and etch depth for different etching methods which are explained later in this chapter.

IV. Xenon Difluoride Etching Systems

A. Continuous Flow/Amount Etching Method

There are two common methods of etching silicon using XeF_2. In the simpler method, silicon can be etched by either using a constant flow of XeF_2 or putting the sample in a chamber with a known pressure of XeF_2 during the whole etching period [36], [39]. A schematic of a system to etch silicon with either of these methods is shown in Figure 3–3. To start etching, first the etching chamber is filled with nitrogen through V_2, and then is vented down to a pressure of 25mTorr or less by closing V_2 and opening V_3.

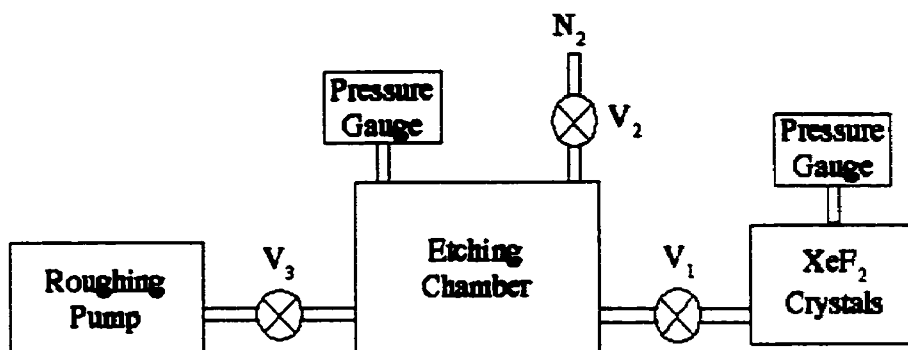

Figure 3-3. Schematic of a simple XeF_2 etching system.

Then both of the valves are closed, and if the pressure inside the XeF_2 crystal chamber is equal to the desired value, V_1 is opened for a limited time so that the pressure inside the etching chamber reaches to its predetermined value (normally around 0.1~3Torr). The ultimate pressure inside the crystal chamber can not exceed the sublimation pressure of XeF_2. The system will remain in this state for a specified time during which the etching is required to be in progress. As mentioned earlier, due to the necessity of formation of a fluorosilyl layer, the etching does not start instantaneously upon the exposure of the silicon to XeF_2 [27].

B. Pulse Mode Etching

Exposing silicon to a constant flow/amount of XeF_2 results in widely varying performance depending on the quantity, age, and history of the crystals in the source chamber. The effect of these phenomena can be reduced by employing another method which is called pulse method [27], [35]. In this method, instead of exposing silicon to a constant flow or amount of XeF_2 during the whole etching time, the required time is

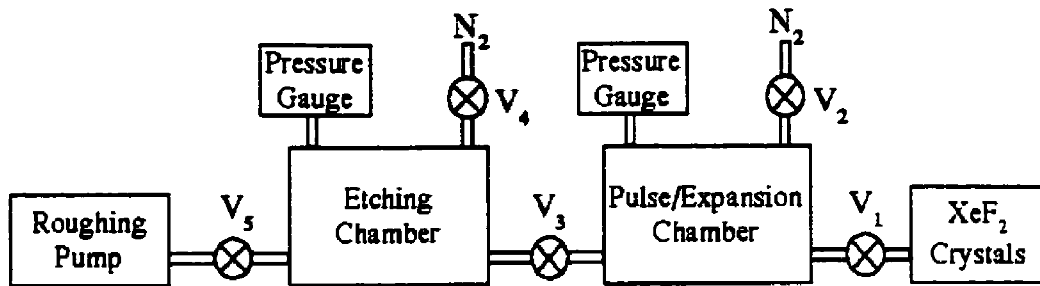

Figure 3–4. Schematic of a pulse etching system.

divided into a few smaller periods. The rest of the process is basically the same as the one that was described earlier. In some cases, there is another chamber added to the etching system (*"expansion chamber"* in Figure 3–4). This chamber improves the control on the pressure of etching chamber. To perform a single cycle of etching, first both etching and expansion chambers are filled with nitrogen through V_2 and V_4, while other valves are closed. Then these chambers are pumped down to a pressure of 50mTorr or less by opening V_3 and V_5 and keeping the other valves closed. The expansion chamber is filled with XeF_2 vapor from the sublimating crystals in the source chamber, while the etching chamber is pumped down to lower pressures. Once the target pressures are reached (typically 1–3Torr in the expansion chamber and around 20mTorr in etching chamber), the expansion chamber is isolated from the source, the etching chamber is isolated from the pump, and the two chambers are connected together. The pressures equilibrate in less than a second and etching begins afterwards. Changes in the pressures of the etching and expansion chambers are shown in Figure 3–5 [27]. The slight change of the pressure

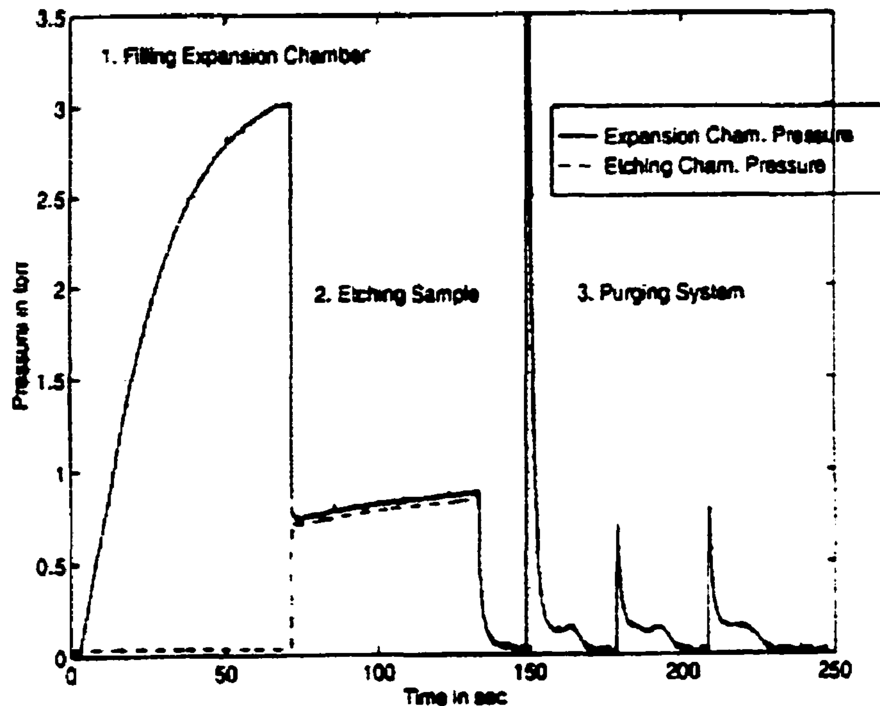

Figure 3–5. Pressure changes inside the expansion and etching chambers during an etching cycle from [27].

inside the etching chamber during the etching period is due to the formation of byproduct compounds resulting from the reaction between XeF_2 and silicon.

Since XeF_2 does not attack aluminum, chambers and pipes can be made of aluminum, rather than stainless steel which is more difficult to shape. The vacuum pump used in these systems is usually a mechanical roughing pump without any special oil. However, there is a possibility of formation of HF in oil.

V. THE DESIGNED XeF_2 ETCHING SYSTEM

A complete XeF_2 etching system was designed and successfully tested. A schematic of the initial configuration of the system is shown in Figure 3-6. [35] and [37] show that pulse etching with XeF_2 would result in more uniform profiles and is more repeatable than putting the samples exposed to a constant flow of the gas or leaving them in a chamber filled with XeF_2 for a long time. Thus, the system was designed for pulse mode etching. To perform etching pulses, vacuum valves are needed to open or close the paths through which the gases can flow. Due to the fact that the etching pulses may be as short as tens of seconds in duration, one should be able to open or close the valves in much

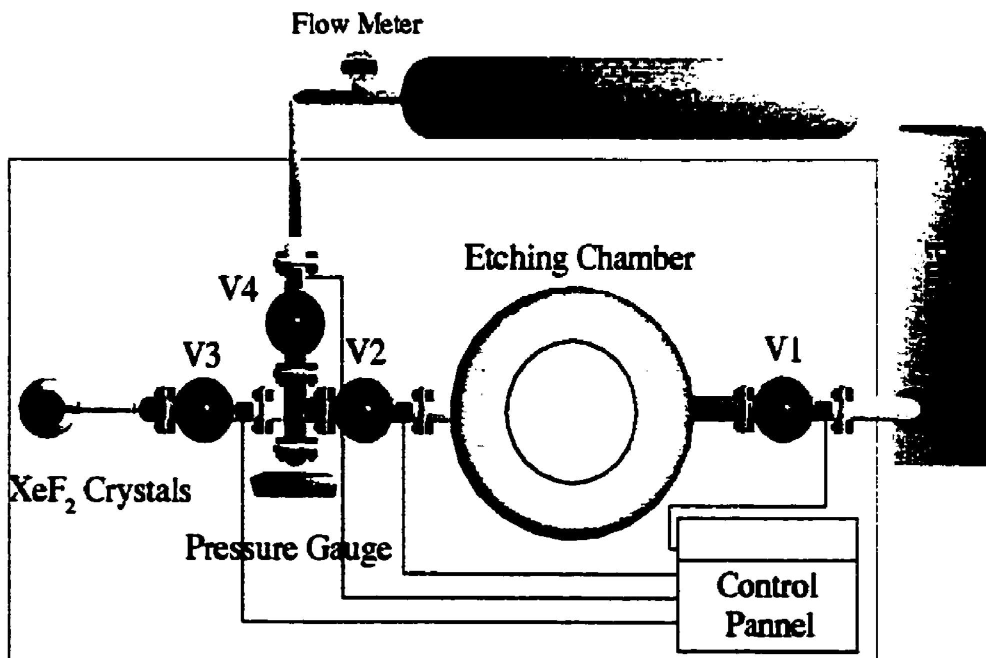

Figure 3-6. Simplified schematic of the initial design of the XeF2 etching system

shorter intervals in order to not affect the timing of the etch. Pneumatic valves are suitable for this application. As mentioned earlier, since XeF_2 does not attack either aluminum or stainless steel, the valve body, pipes, and the chambers can be made out of these two materials. In the fabricated system the main etching chamber and most of the pipes were made of aluminum due to the relative ease of shaping it with respect to stainless steel. The valves and the flanges were made of stainless steel. To connect different vacuum parts to each other, ConFlat type flanges were chosen because of their simplicity, low leakage, and ease of maintenance.

As can be seen in Figure 3-6, there are two valves between the crystal chamber and the main etching chamber. This increases the flexibility of the design, since an expansion chamber can be easily added between these valves. This design also allows the use of only one pressure gauge to measure the pressure inside either the crystal/expansion chamber or the etching chamber, by appropriate opening and closing of V_2 and V_3. The tradeoff of using a single pressure gauge is not being able to read the pressures of both chambers at the same time. However, this is not necessary in most cases.

The selected valves were pneumatic valves which could be opened or closed by a sending an electrical signal to a solenoid which was mounted on them. This allows the user to remotely control the operation of the system by a simple control board (Appendix A).

A series of etches was performed with the system described above on many samples. After these tests, the initial electronics and hardware designs were modified. In

the first design, to fill the main chamber with XeF_2 and establish a reasonable pressure level for etching, the crystal chamber needed to be connected directly to the etching chamber for a relatively long time (up to a minute). This procedure involves the risk of contaminating the XeF_2 crystals. To avoid this potential problem, an expansion chamber was added to the system (Figure 3–7).

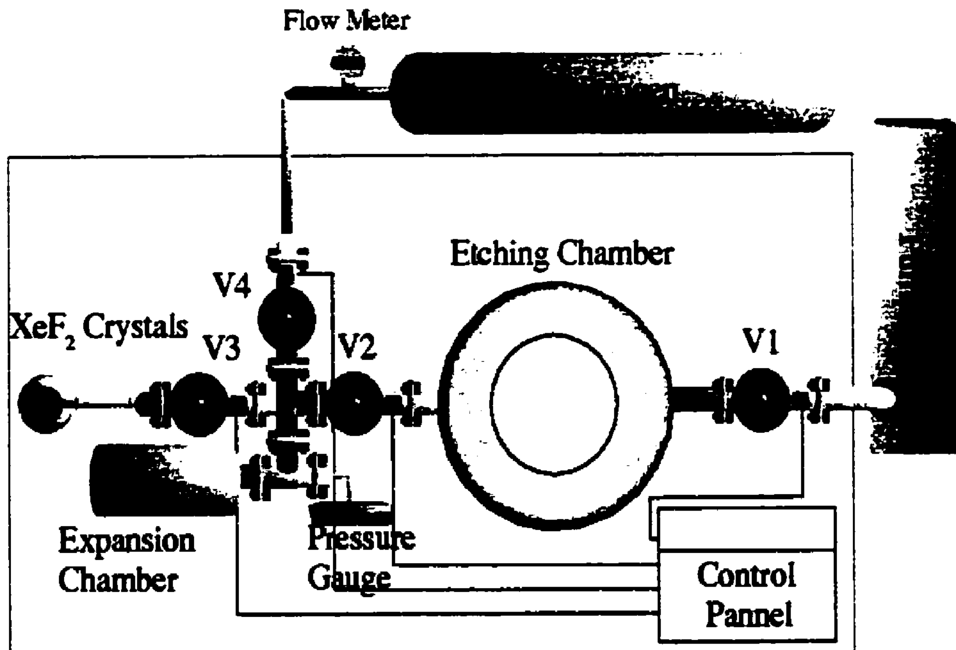

Figure 3–7. Original design with the expansion chamber added to it

The expansion chamber was easily added to the system by taking off the pressure gauge from its initial position and attaching a vacuum Tee to where the pressure gauge had been. The expansion chamber was connected to one of the connections and the pressure gauge was connected to the other one.

Although this design could reduce the risk of crystal contamination, it also introduced a new problem. The way the etch was performed with the added expansion chamber is as follows. First the expansion chamber is connected to the crystal chamber while the main chamber is pumping down to low pressures. When the pressure inside the expansion chamber is high enough, the valve between the expansion and crystal chambers (V_3 in Figure 3–7) is closed, the etching chamber is isolated from the vacuum pump (V_1 closed), and the etching and expansion chambers are connected to each other (V_2 opened). The XeF_2 gas, which has already filled the expansion chamber, will flow into the etching chamber. In less than a second the pressure inside two chambers equilibrates and XeF_2 starts to etch silicon [27]. However, after this initial suction of XeF_2 gas into the main chamber, movement of those XeF_2 molecules, which are in currently the expansion chamber, to etching chamber will be governed by diffusion (ignoring the slight and slow increment of the pressure inside the etching chamber). Since the distance between the etching and expansion chamber is very long compared to the mean free path of the gas molecules at the etching pressure (30cm vs. ~20μm), it will take a very long time for the XeF_2 molecules inside the expansion chamber to migrate to the etching chamber where they can react with silicon.

The mean free path of a gas molecule can be found from the following equation [37]:

$$\lambda = \frac{RT}{\sqrt{2}\pi d^2 N_A P} \qquad (3-4)$$

where R is universal gas constant (8.3145 J/mole K), T is temperature in Kelvin, d is the molecule diameter (m), N_A is the Avogadro number (6.022×10^{23}), and P is pressure (Pascal). It can be seen that for common etching pressures (0.3−3Torr) the mean free path lies in the range of 10−100μm.

If it is desired to perform multiple short pulses (~10's of seconds) at a certain pressure, this technique will end up in consuming a much larger quantity of XeF_2 compared to the amount of the gas which is actually needed to etch away the same amount of silicon. This is due to the trapping of a considerable amount of almost fresh XeF_2 gas in the expansion chamber which will be pumped out of the system during the purge cycles. In fact, when pumping down the etching chamber after each etching pulse, it was observed that the silicon was etched, although the pressure was dropping rapidly.

VI. CONTROL SOFTWARE

It has always been desirable to automate the controlling of a system to a computer. Thus, a computer program was written to control the whole system with accurate timings and pressure readings. This software offers the user with many different options based on the desired etching sequence. The communication with the pressure gauge is established through a serial connection (RS−232). To change the status of the valves, the computer sends appropriate commands, based on the pressure readings and timing of the etch, to a card inserted into a PCI slot inside the computer. This card converts the software

commands into electrical signals and sends them to the main control board. The control board is designed so that the user can put it in manual control mode and solely takes the control of the system. The other option is putting the system in automatic control mode and letting the computer control the operation of the system according to user settings for timings and pressure levels in different chambers during each of the etching steps.

XeF_2 can be a safety hazard. In presence of water vapor (e.g. moisture in air), it forms HF which is extremely dangerous. Thus, in all of the design steps of both software and hardware, the user safety and maintaining a robust and tolerant configuration was considered carefully.

LabView was used to write the control software, due to its readily available controls and the user friendly interface.

The control software is written so that almost all the process variables are adjustable and the user can set them when running the application program. At the beginning, default values for total number of etching pulses, duration of each pulse, minimum XeF_2 pressure before starting the etch, number of purging cycles after completion of the etch, and the purging pressure are displayed. Also, the user has the option to perform the etch in a *"time based"* mode. In this mode, the crystal and expansion chambers are connected to each other for a certain amount of time to fill the expansion chamber with XeF_2 gas. When operating the system in this mode, it is assumed that the gas pressure inside the expansion chamber will be within a proper range after that time has elapsed. This feature was added after it was observed that sometimes it takes a very long time for the pressure

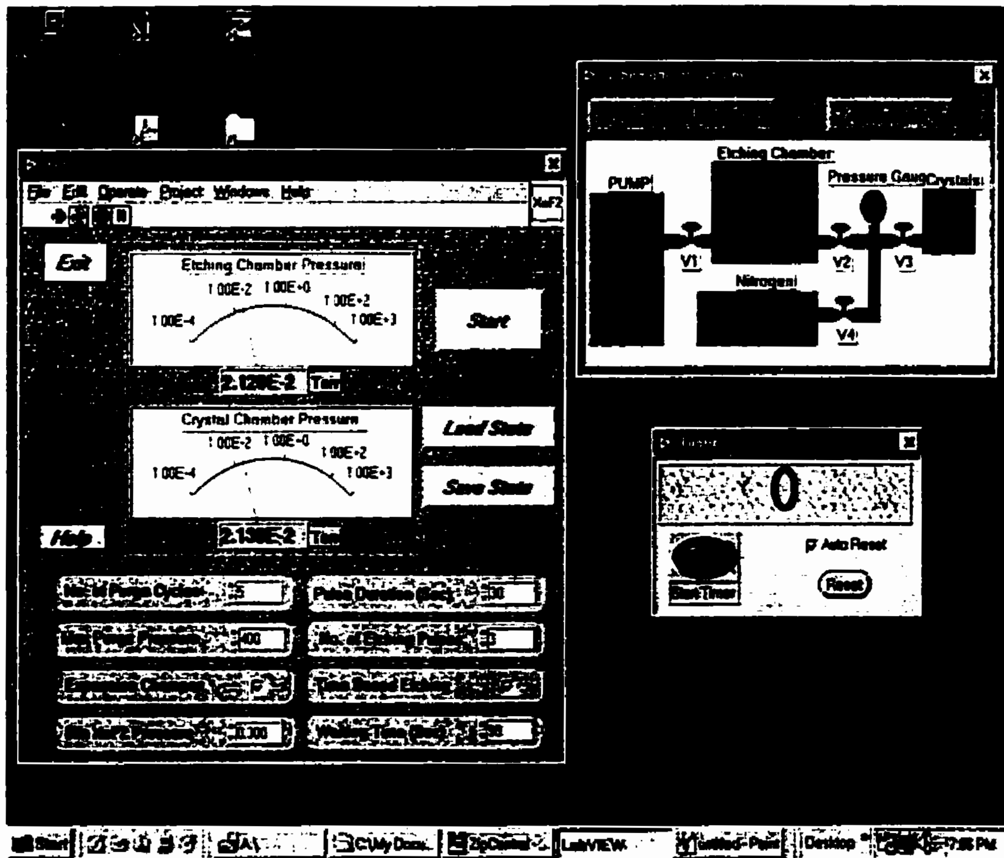

Figure 3–8. Software interface before starting the etch.

to rise a little bit. This might be due to the problems with the pressure gauge or the aging of crystals. In such cases this option can reduce the overall time that is needed to complete the whole etching. Also there is an option of connecting the crystal and etching chambers directly to each other while etching is in process. This should normally be avoided, but having this option lets the user to perform etches at higher pressures or when the expansion chamber is detached from the system. The user can modify all values and save them to a file or load them from a previously saved data (Figure 3–8).

After setting the etch parameters, the user has the option to do the etch in either fully *"automatic"* mode or in a so called *"manual"* mode, in which he can close or open different valves by clicking on appropriate locations on the screen. Figure 3–9 illustrates the interface in manual mode.

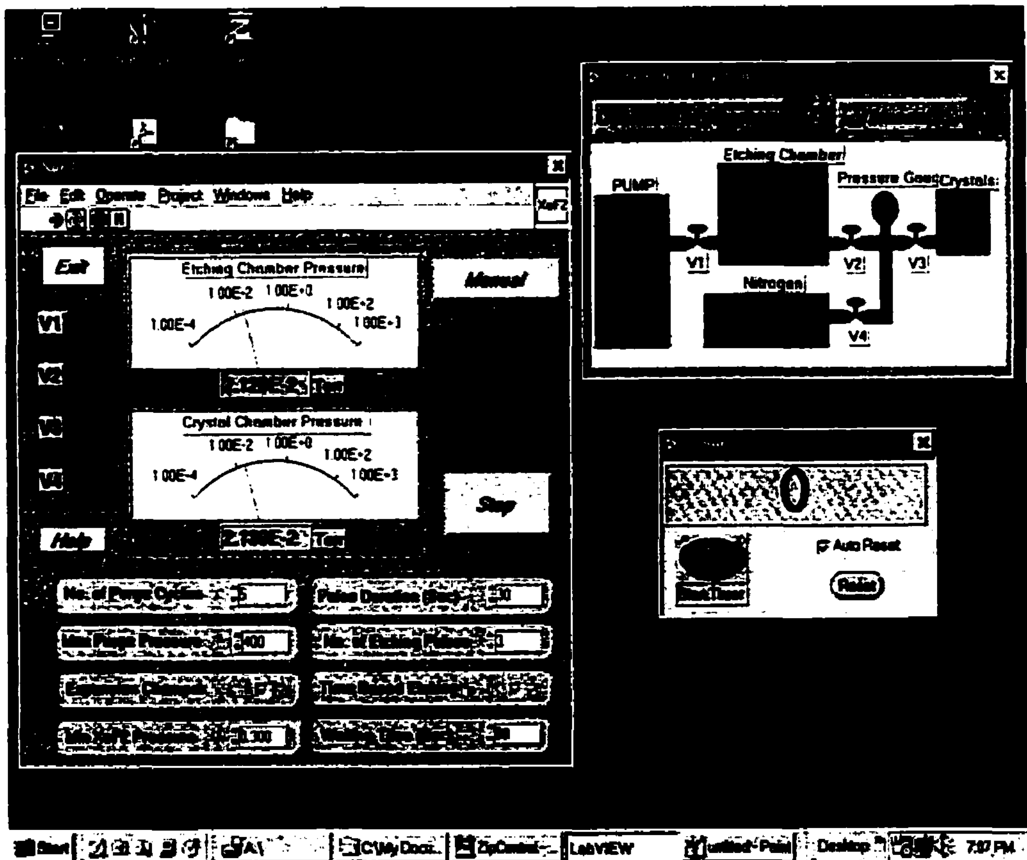

Figure 3–9. Software interface in manual mode.

This software manual mode is preferred to the one from the main control board, since the user is provided with a timer and schematic diagram of the system, on which the gas flow inside the system and the situation of any of the valves can be easily verified.

The schematic and the timer run in different windows, so the user can place them anywhere on the screen. The timer has two modes of operation. In default mode, the timer automatically resets whenever the situation of any of the valves changes. In the other mode, timer resets when the user clicks on the *"Reset"* button in timer window. Having this timer is especially useful when the user wants to perform etching in manual mode.

In automatic mode, the computer controls the system based on user settings. To control the system in this mode, the *Manual/Automatic* switch on main board must be put in *Automatic* position. The user has to select automatic control mode in software, too. During the whole process, computer checks and monitors the pressure levels inside different chambers frequently (in 200msec intervals) and performs the proper action based on its readings and timings. The etching starts when the user clicks on *"Etch"* button in automatic mode (Figure 3-10). The etching and expansion chambers are filled with nitrogen and pumped down to vacuum a few times to ensure that the contamination level is low. Then main chamber is evacuated to the lowest possible pressure (~0.1mTorr). The system remains in this state until the pressure inside the crystal/expansion chamber reaches the desired value. Main chamber, which is now disconnected from the vacuum pump, is connected to the crystal/expansion chamber and the reaction between XeF_2 gas and silicon starts instantaneously. The valve between crystal chamber and main chamber should be closed as soon as possible to prevent contamination of XeF_2 crystals in crystal chamber. The system keeps this state until the end of etching period. Then the main chamber is connected to the pump to stop the reaction. The chamber is filled with

nitrogen and pumped down again. This procedure is repeated for as many times as required. After completion of etch, the main chamber is purged with nitrogen a few times to push the remaining XeF_2 gas out of the main chamber and exhaust pipe.

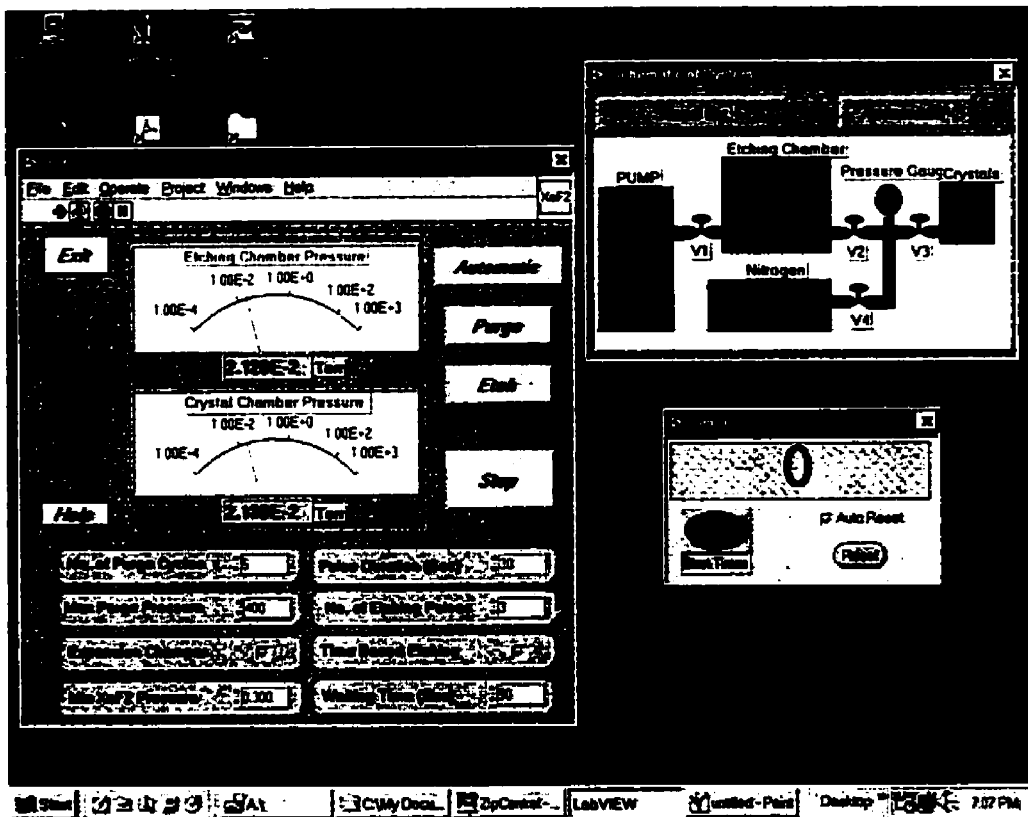

Figure 3-10. Software interface in automatic mode.

VII. Alternative Etching Methods

A. Triple Pulse Method

To use XeF_2 more efficiently two alternative pulse etching methods were examined. In the first method, the total devoted time to each etching pulse is divided into 3 shorter pulses such that the length of these shorter pulses were around 50%, 30%, and 20% of that of the original pulse. To perform the etch, the expansion chamber is filled with XeF_2 and then connected to the etching chamber. The system will remain in this state for the first fraction of the original pulse. Then the etching chamber is disconnected from expansion chamber and pumped down to low pressures to remove the consumed gas from the etching chamber. During this period, the expansion chamber remains isolated. The two chambers will be connected to each other for the second time after pumping down the etching chamber. Due to the existing pressure difference between two chambers most of the XeF_2 from the expansion chamber will be sucked into the etching chamber and react with silicon, but this time at a lower pressure. This procedure can be repeated one more time to ensure that most of the gas that originally was in the expansion chamber has been used. Then both etching and expansion chambers are purged and the expansion chamber can be filled with XeF_2 to continue with another pulse.

This method can be useful when the exact value of the etch rate is not important or when the etch is self-terminating.

B. Quick Pulse Method

The other etching method that was tried enables etches at relatively high pressures (i.e. high etch rates) but has a higher risk of crystal contamination. In this method, after the initial purges, the expansion and crystal chambers are always connected to each other (V_3 open in Figure 3-7). This will cause the XeF_2 pressure inside the expansion chamber to be around the sublimation pressure of XeF_2 crystals. To perform the etch, the etching chamber is pumped down to high vacuum and then isolated from the vacuum pump (V_1 closed). Then the expansion chamber is momentarily connected to the etching chamber (hence the name *"quick pulse"* method). Since the pressure equilibrates very fast, the connection time can be in the order of one or two seconds. The etching chamber will be filled with XeF_2 gas after this step, initiating the etching. After the etch is done, the etching chamber is pumped down to vacuum again, and if necessary, this procedure can be repeated. In this method the etch is always done at high pressures and hence the etch rate is expected to be relatively high. Also controlling the etch process is easier than the previous method. However, the risk of crystal contamination is also higher.

VIII. Calculation of Etch Rate and Etch Depth

The equations derived in section III can be used to estimate the etch depth and etch rate based on the number of XeF_2 molecules inside the etching chamber. However, it should be noted that those equations assume that all of the gas molecules will eventually

react with silicon, which is not necessarily true. A gas molecule may react with the main reaction byproducts or it may not react with anything, like what happens to some of the gas molecules at the far end of the expansion chamber which may not travel to the etching chamber.

The calculations are done for the basic and quick pulse methods. Repeating them for the triple pulse method is not necessary, since the triple pulse method is similar to the basic method. It will be shown that most of the gas inside the chamber is consumed after the first minute of etching and the etch rate drops to almost zero after that.

To use equations 3−1, 3−2, and 3−3, one should know the etching chamber volume, etching pressure, and the area of silicon surface exposed to XeF_2. For the designed system, the etching chamber volume for basic and quick pulse methods are 1650cm^3 and 1100cm^3, respectively. The etching pressure for quick pulse method is assumed to be around 1.3Torr and for basic pulse method it is considered to be around 1Torr [27]. The surface area of the samples that were etched in the system was about 0.85mm^2. However, it should be noted that this area will change considerably during the etch and an effective surface area of 0.9mm^2 was assumed for calculations.

Figure 3−11 shows the change in number of XeF_2 molecules in the etching chamber as a function of time. It can be seen that the total number of XeF_2 decreases exponentially (governed by equation 3−3). This will cause the etch rate to drop as well (Figure 3−12), since according to equation 3−1, the etch rate is directly proportional to the number of XeF_2 molecules in chamber. The average etch rate for the 2.5min pulse for basic and

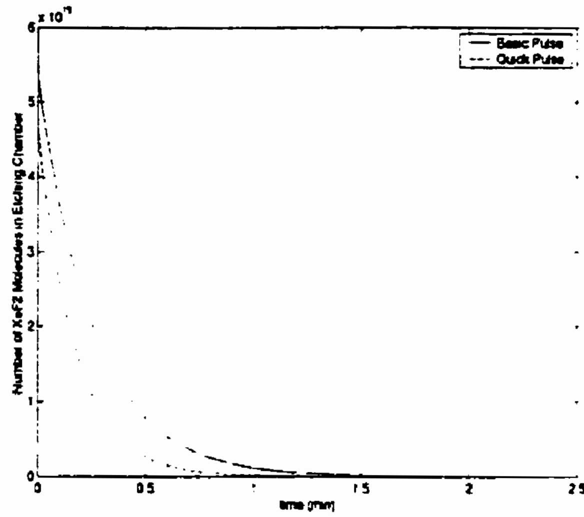

Figure 3–11. Change in number of XeF_2 molecules during an etching pulse.

quick pulse methods is 2.36μm/min and 3.54μm/min, respectively. This shows that, as

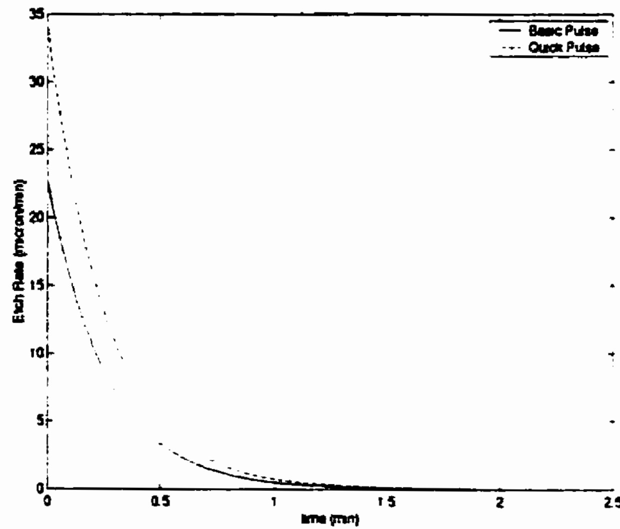

Figure 3–12. Etch rate as a function of time.

expected, the etch rate for quick pulse method is larger than basic pulse method.

Figure 3−13 illustrates the increase in etch depth as a function of time. Due to the consumption of the XeF_2 molecules, the etch depth is almost constant after the first minute of the etch.

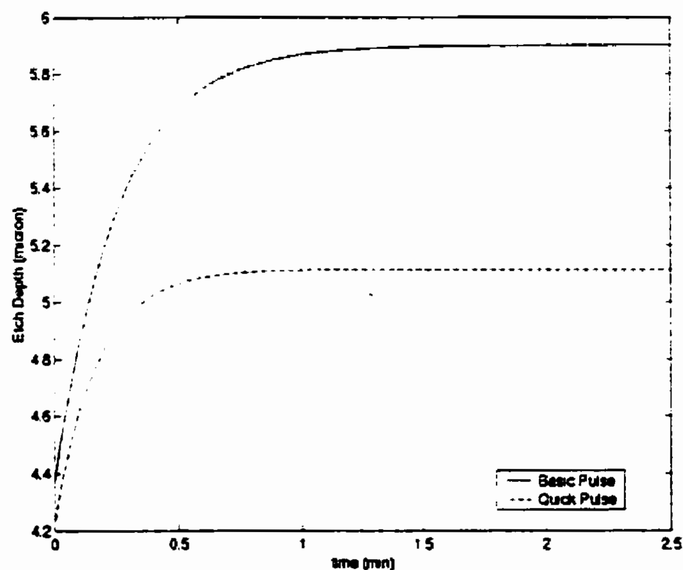

Figure 3−13. Etch depth as a function of time.

It can bee seen that the etch depth for quick pulse method is smaller than that of basic pulse method. This is due to the smaller number of gas molecules inside the etching chamber before the etching begins.

Chapter 4: Experimental Results

I. Sample Preparation

To test and calibrate the etching system several microstructures were fabricated (bridges, cantilevers, and circular membranes) from an oxide layer grown on wafer surface.

We prepared our samples by first growing a thermal oxide layer on surface of regular silicon wafers. The oxide layer was grown in a furnace at 1000°C. There was a flow of nitrogen and DI water vapor over the silicon wafers to increase the oxide growth rate. The thickness of the oxide layer for different experiments was between 1μm and 2μm. Lithography techniques were then employed to transfer the patterns from masks to a positive photoresist layer (Olin Hunt HPR 506) which was spun on top of the oxide layer.

The masks were made in Cadence and saved as a postscript file. This file was then printed on mylar sheet by a high resolution printer (2400 dpi). The mylar sheet was then cut into smaller pieces. Each piece was taped to a piece of glass and used as a mask for photolithography with UV light, to protect select regions of the wafer with photoresist during subsequent etching of SiO_2. The exposed photoresist was developed using Olin

Hunt HPRD 519 positive photoresist developer.

Using a 10:1 BHF (Buffered HF) solution, the oxide was removed from those locations where the underlying silicon was to be exposed to XeF_2. Numerous cantilevers and bridges were patterned on the oxide layer, mainly to estimate the stress in the grown oxide layer. To make circular membranes, many holes with different diameters were patterned on the oxide layer. In addition to SiO_2 masks, photoresist was also used as the masking layer. However, these group of samples were only used for investigation of the etch profile and not for making microstructures. These samples were then etched in the system. Different samples were etched by different numbers of etching pulses and pulse durations to investigate the operation of the system and etching mechanism of XeF_2. In almost all cases, the etching pressure was set to be around 0.3Torr based on the readings from the pressure gauge. The etch rate at this pressure was found to be around 1–2μm/min which is consistent with the data from different references [35], [37], [39].

II. Comparison of Different Etching Techniques

As mentioned in chapter 4, different etching methods were investigated. The results of a series of etches in different methods with roughly the same etching conditions are given in Figure 4–1. The reader can refer to Appendix D for the exact etching data. For the results shown below, the pulse duration was set to be 150 seconds for all three different modes of operation. The etching pressure, except for the quick pulse method, was around

0.3Torr during the etch. However, due to the problems with the pressure gauge, the actual etching pressure should be higher than 0.3Torr.

The basic pulse method yields the highest etching depth. As calculated in Chapter 3, this is due to existence of a larger number of XeF_2 molecules in the etching chamber compared to the quick pulse method. Quick pulse method results in a slightly higher etch depth than triple pulse method, which is due to the etching at a higher pressure of XeF_2. However, the etch rate for quick pulse method should be the highest of all of these methods at the beginning of each pulse.

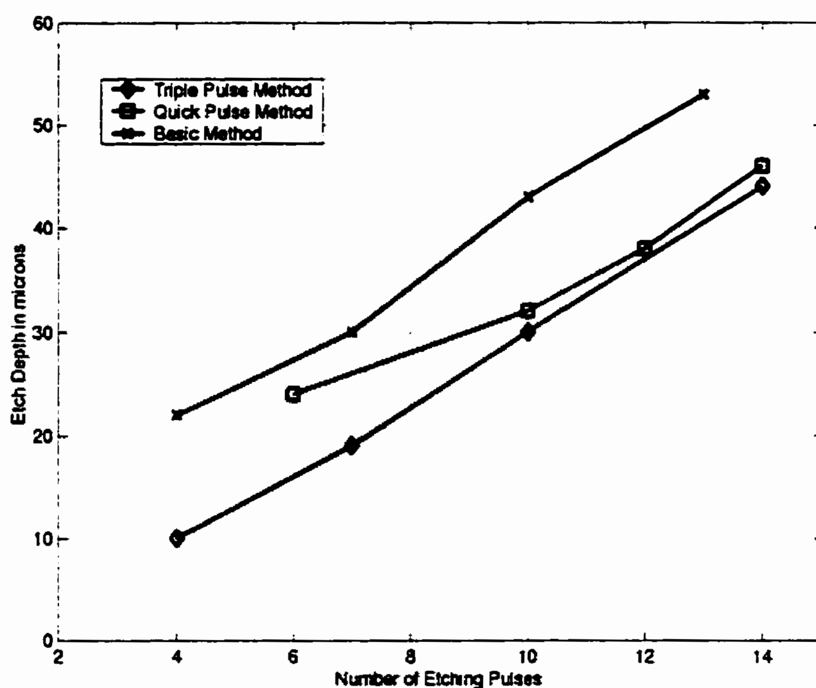

Figure 4–1. Comparison of the etch depth at the center of a 500μm hole after etching the sample with different methods.

Considering the small difference between the etch depths of these three methods, it can be concluded that the triple pulse method is probably the best method in terms of low risk of crystal contamination and efficient using of XeF_2.

III. Microstructure Fabrication Results

It was expected that the thermally grown oxide layer would be stressful and this was approved by inspection of the released structures. All of the structures, such as the

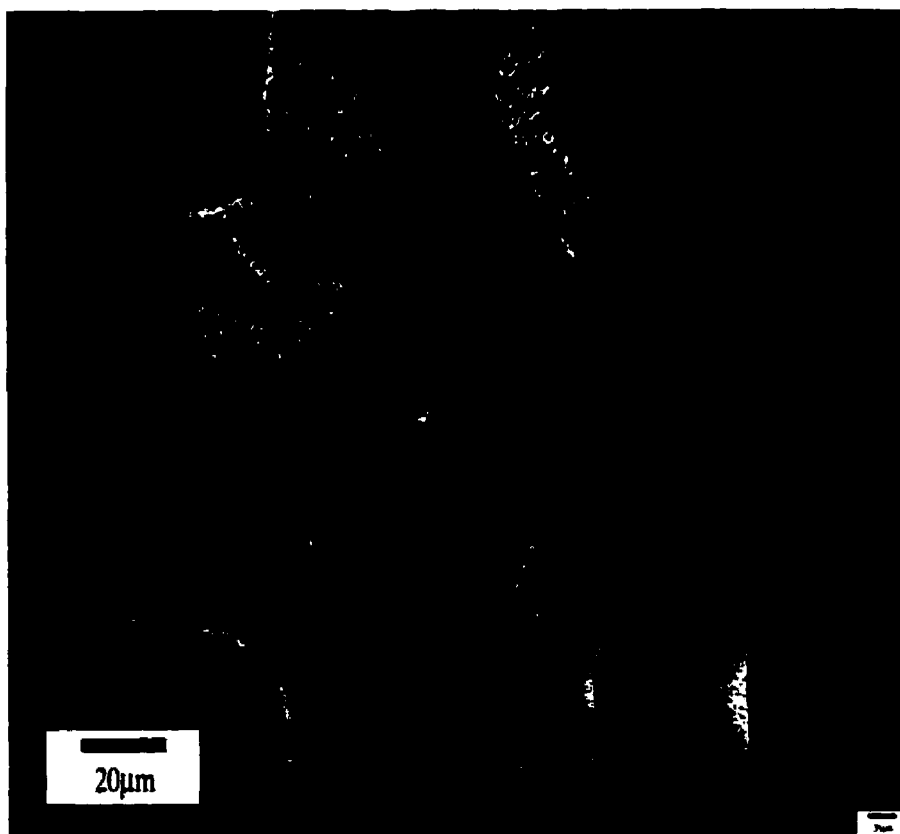

Figure 4–2. Dark field image of a released cross. The smaller photo in right corner is taken at the same position but 75μm below the sample surface.

released cross shown in Figure 4–2, were curved upwards and even some of them were broken. Moreover, the released oxide around the edges of structures was buckled. This clearly shows existence of compressive stress in the oxide layer. One can also identify some cracks at sharp points (Figure 4–3), which is an implication of etch induced stress in a thin film [38]. A number of circular membranes with different diameters were also fabricated (Figure 4–4).

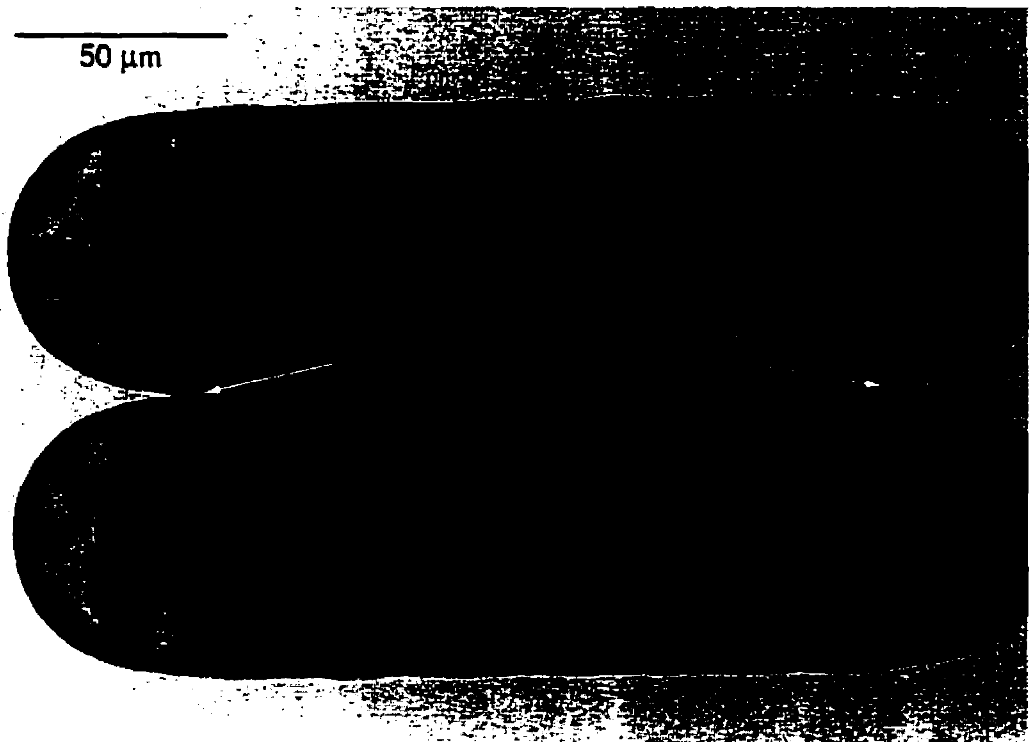

Figure 4–3. A released bridge. Note cracking of the oxide layer due to etch–induced stress at sharp points.

In figures 4–2, 4–3, and 4–4, it can be seen that there is some oxide roughening at the outer edges of the structures. These samples were etched in two steps. After the first etching step, the samples were exposed to the atmosphere. This might result in sticking of

some water molecules to the underside of the oxide layer. These water molecules could react with XeF_2 during the second etch step and form HF, which etched silicon dioxide.

The silicon surface of all the etched samples was rough. Figure 4–5 and Figure 4–6 illustrate the SEM and AFM images of this phenomenon.

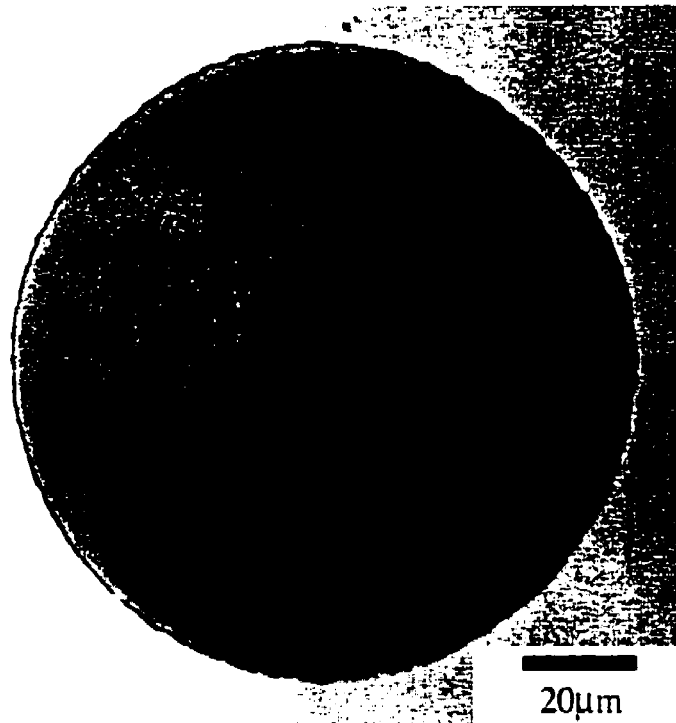

Figure 4–4. A fabricated circular membrane.

The most interesting phenomenon that was observed dealt with etching through the circular holes. As mentioned earlier, a number of holes with different diameters were etched on the oxide mask. XeF_2 could penetrate through these holes to etch the underlying silicon and since it is an isotropic etchant, it would eventually form a circular membrane.

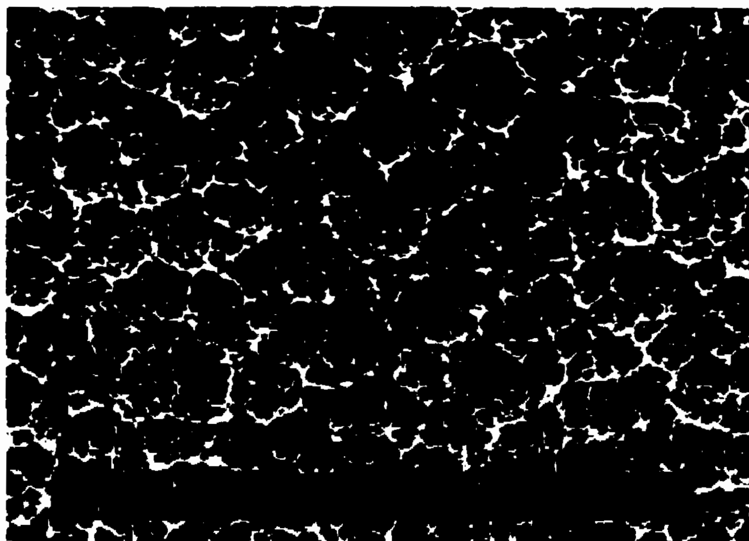

Figure 4–5. SEM image of the etched silicon surface.

membrane.

One expects the etch depth to increase with the hole diameter for relatively small holes and to be almost constant for larger holes. If one assumes that there is a constant flux of gas molecules impinging on the surface, there will be a greater number of gas

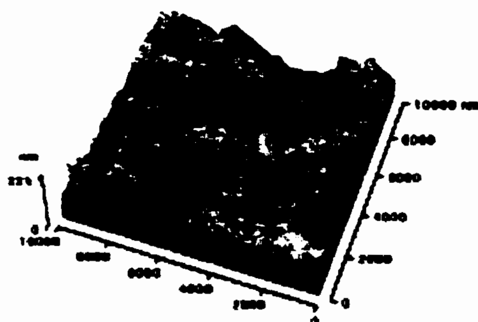

Figure 4–6. AFM image of the etched silicon surface.

molecules that can pass through the hole on the mask. Also it seems to be reasonable to assume that maximum etch depth corresponds to the biggest holes and the etch depth at the center is almost constant for large holes as can be seen in Figure 4–7 (a). But experimental results did not support this prediction.

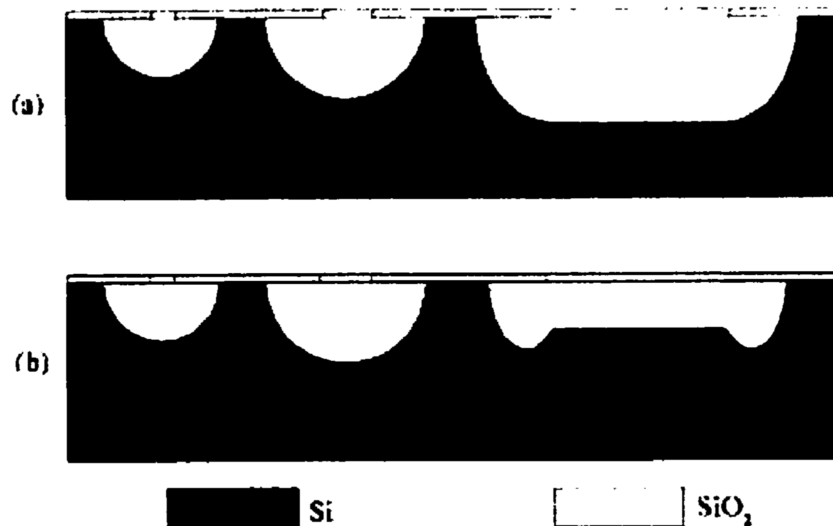

Figure 4–7. Etching profiles for holes with different diameters: (a) expected and (b) observed profiles

The etch depth for small holes (20–100μm) was smaller than medium size holes (100–200μm) and it increased with the hole diameter (Figure 4–8). For very large holes (>1mm) the etch depth near their centers was almost the same, which was in agreement with what was expected. What was found to be interesting was the etch profile at the edges of these large holes was not a simple spherical–shape sidewall connected to a flat surface as in isotropic wet etching. But it rather had a more sophisticated shape as shown

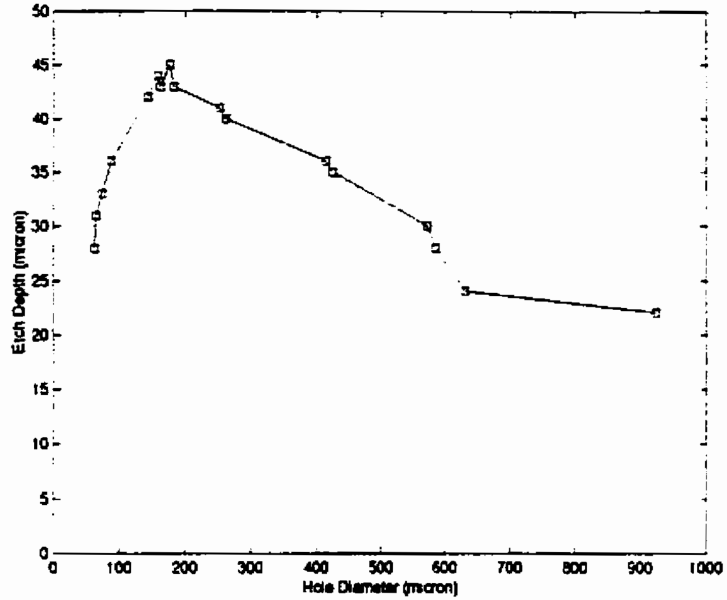

Figure 4–8. Variation of etch depth with hole diameter.

in Figure 4–7 (b). There was another interesting phenomenon dealing with the etch depth of these large holes. Etch depth at the centers of these holes was smaller (>25%) than what it was for medium size holes. Even at the edges where the profile had its maximum

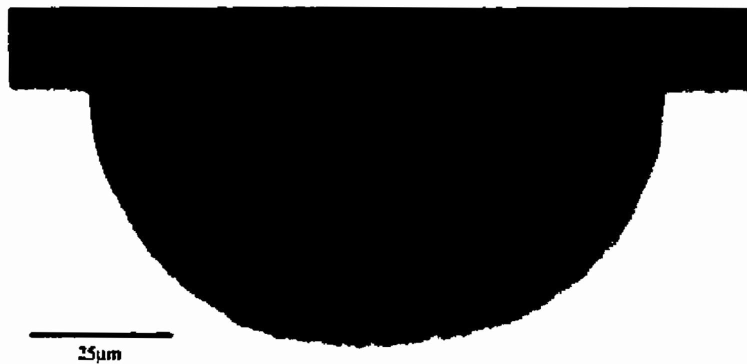

Figure 4–9. The etch profile for small size mask opennings.

Figure 4−10. The etch profile at the bottom of a large hole. The etch depth around the center of the hole is about 23μm versus 27μm at the edge.

depth, it was still something close to 10% less than the etch depth for medium size holes. The etch profiles for small and large hole are illustrated in Figure 4−9 and Figure 4−10. Some research groups, such as [26] and [27], had observed similar phenomena even with etchants other than XeF_2 (BrF_3), but no complete and satisfactory explanation was given.

IV. Trenching Effect

It is believed that the unexpected shape of the etched region (Figure 4−11) can be explained by considering the edges of structures as places with a higher reaction probability. When a gas molecule impinges on a solid surface, it may not react with the surface. A reaction probability should be assigned for each impingement to take this into account [39]. For very large holes, there is a relatively large open area around the centers of holes. Thus, if after hitting the surface, a gas molecule does not stick to the surface, there is a lot of room for it to move away from the surface. However, at the edges of the structures, there is a silicon sidewall surrounding the open area and above that there is the

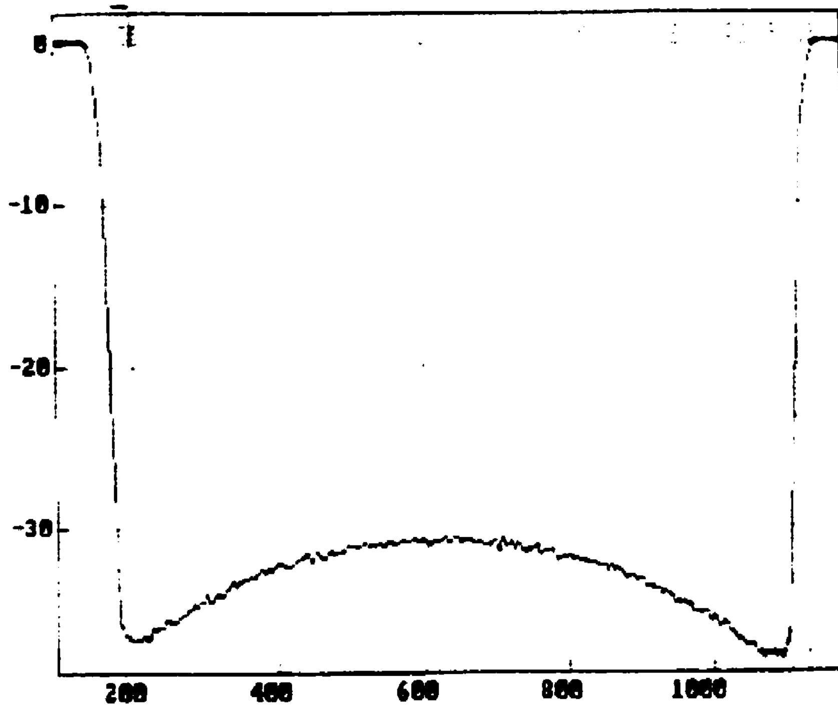

Figure 4-11. Profilometer plot of a relatively large hole. The etch depth at the center of this whole is 6mm less than that of the edges.

released dielectric film. There is a higher probability for the gas molecules to react with silicon in this areas, because if it does not react with the hole bottom upon its first impingement, after bouncing back, it may hit the silicon sidewall or the dielectric mask. Then it may either react with the sidewall or bounce back from it (or from the released section of dielectric mask which overhangs above this area). The higher reaction probability at edges can also be considered as a virtual increase in the number of gas molecules at those areas. This discussion is valid if the distances are on the order of the mean free path of the gas molecules at that given pressure. For the pressures that the

XeF_2 etch is usually performed, the mean free path for XeF_2 molecules is between 10–100μm which is close to the etch depth for our samples.

V. Loading Effect

The smaller etch depth at the centers of large holes compared to that of small holes can be described to be a consequence of local depletion of etchant molecules. Around the centers of large holes whose diameters are much bigger than the mean free path of the gas molecules, many of the gas molecules have the chance of reacting with silicon. This

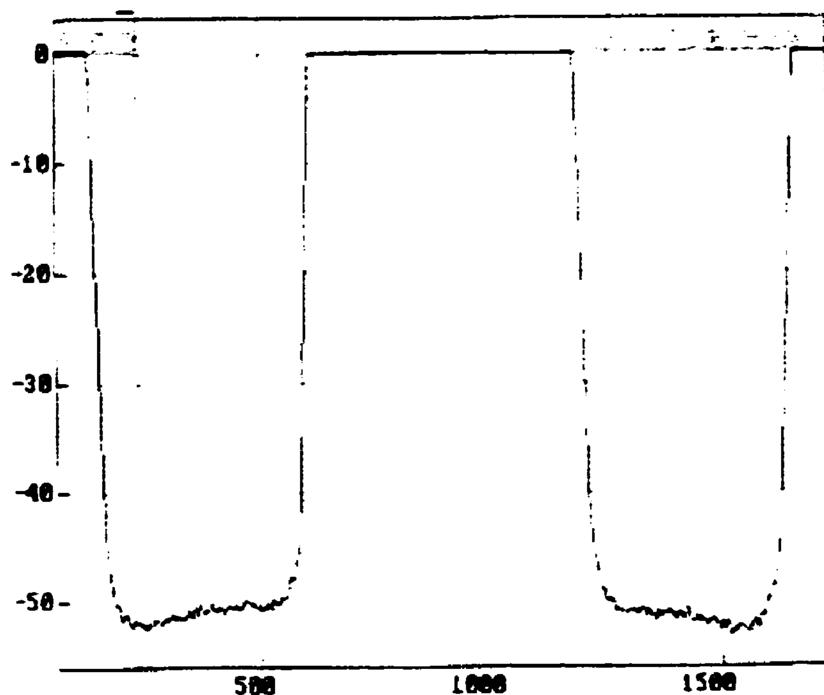

Figure 4-12. Profilometer plot Illustrating the loading effect between two adjacent holes.

causes the number of reactive XeF_2 molecules above these regions to be less than other places, which results in a slower etching of silicon and therefore, a smaller etch depth.

It can also be observed that some loading effect exists when there are two closely spaced openings in the mask (Figure 4–12 and Figure 4–13).

This phenomenon can also be explained by the local depletion of XeF_2 molecules. The only difference between this case and the previous one is in consumption of reactive XeF_2 molecules by a neighboring hole.

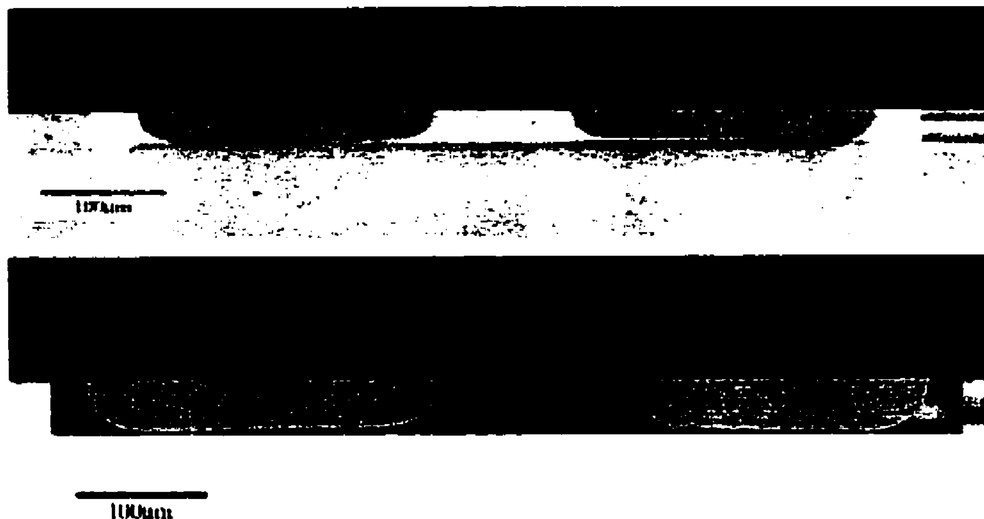

Figure 4–13. Cross sections of the etch profiles resulting from etching through two close openings in mask. Note that the etch depth at each point depends on its distance from the other hole.

VI. Corrosion of Materials after Long Exposure to XeF_2

While performing the experiments, it was noted that XeF_2 can attack materials other than silicon, provided that the exposure time is long enough. For example, an

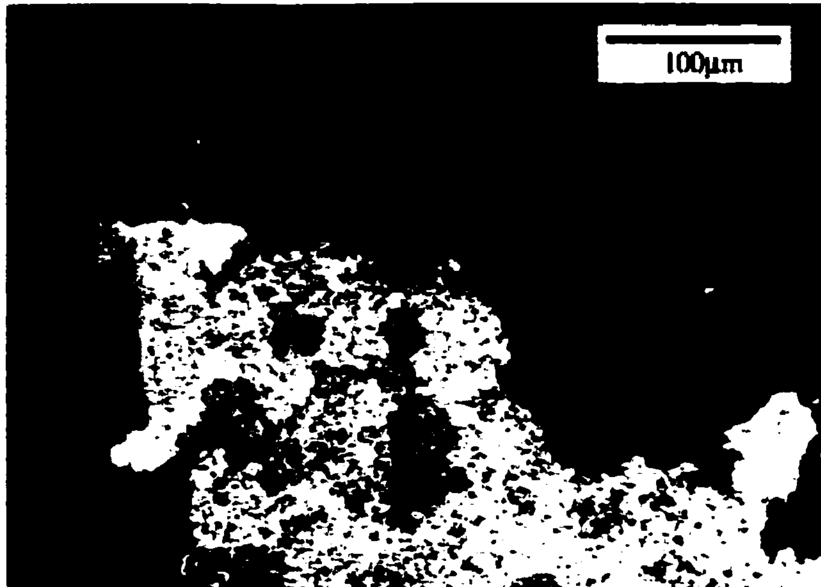

Figure 4–14. A piece of an aluminum film which was attacked by XeF_2 during a long etch.

aluminum thin film (~600nm) is shown in Figure 4–14. It was corroded after performing a long XeF_2 etch (~1hr). This contradicts what other groups have previously reported and can be due to an extended amount of exposure time.

Chapter 5: Simulation of the Etching Process

I. Definition of Problem

As mentioned in previous chapters, after observing the etched profiles and the unexpected shape of them, a theory to explain these phenomena (i.e. trenching and loading effects) was developed. To verify this theory, a simulation of the behavior of XeF_2 molecules during the etching period was written.

Initially, a program was written in Visual Basic and run on a PC. This preliminary test of the theory was promising and confirmed the theory. But the simulation was very slow and would take a very long time (more than 48hrs) before we could see any noticeable result. Thus it was decided to write the code in C and perform the simulation on more powerful UNIX workstations and save the processed data to files. The saved files were then transferred to a Macintosh computer.

The saved data was displayed using an application program (Image SXM) and the format of the data file can be changed very easily, if desired. This also enabled the implementation of the simulation on different machines, like Sun Ultra Sparc and IBM RS/6000 workstations, which have different graphic programming methods. But since

the simulation program complied to ANSI C regulations and the saving method for all those platforms was the same, saved files could be exported to the mentioned application program. The other reason for choosing UNIX was its power to deal with huge amounts of data at the same time. UNIX also provides the user with the opportunity to perform long and time consuming computations, which may take days or even weeks to complete, in background. As mentioned earlier, the chosen programming language was C due to its efficiency in compilation and, as a result, faster simulations.

To simulate the etch, a gas molecule is considered to be somewhere in chamber. Then the motion of this gas molecule is simulated by moving it in random directions and with random radii. This will continue until the gas molecule hits the silicon. Based on the reaction probability which is assigned to that gas molecule, it may either react with silicon or bounce back and continue moving around. Each of these steps will be explained in more detail in the next section. For most cases that are shown in this chapter, the simulation time was between 24 to 48hrs.

II. The Simulation Program: Details and Algorithms

A. Main Program

When the simulation program is executed, the user will be asked to enter simulation parameters. He has to enter a scaling factor and the number, width, and position of the holes on mask. Then the values for mean free path (MFP) of the gas molecules, reaction

probability, a smoothing factor, interval between two successive saving of data, and finally total number of output files have to be entered. The position of each hole is determined by entering its distance from the previous hole.

The width of the window for displaying the results was set to be 1000 pixels. Since each pixel represents 1μm, if it is desired to run the simulation for a virtually bigger piece of silicon, a larger scaling factor (>1) should be entered, but one should note that this will often result in a longer computation time. If the chosen scaling factor is greater than one, the simulation will be performed for that bigger window. After completion of simulation, the user will be provided with all the data files which will represent different segments of the simulation window (each 1000 pixels wide) and also with a single file which is a compressed form of the bigger window to fit it into the viewing window.

In the simulation, each pixel is considered to be equal to 1μm. To resemble a reaction between a silicon atom and a gas molecule, the corresponding value of that pixel is changed. But this means that each impingement removes a cluster of silicon atoms, since the dimensions of silicon atoms are much smaller than 1μm. The mentioned smoothing factor is introduced to compensate for this. The corresponding value for each pixel will change only after that pixel (i.e. silicon atom) is hit by gas molecules as many times as the smoothing factor.

After getting the necessary data from user, two arrays of random variables will be constructed which will be used as look-up tables during the simulation (Figure 5-1). This reduces computation load on CPU which translates into faster simulations. To

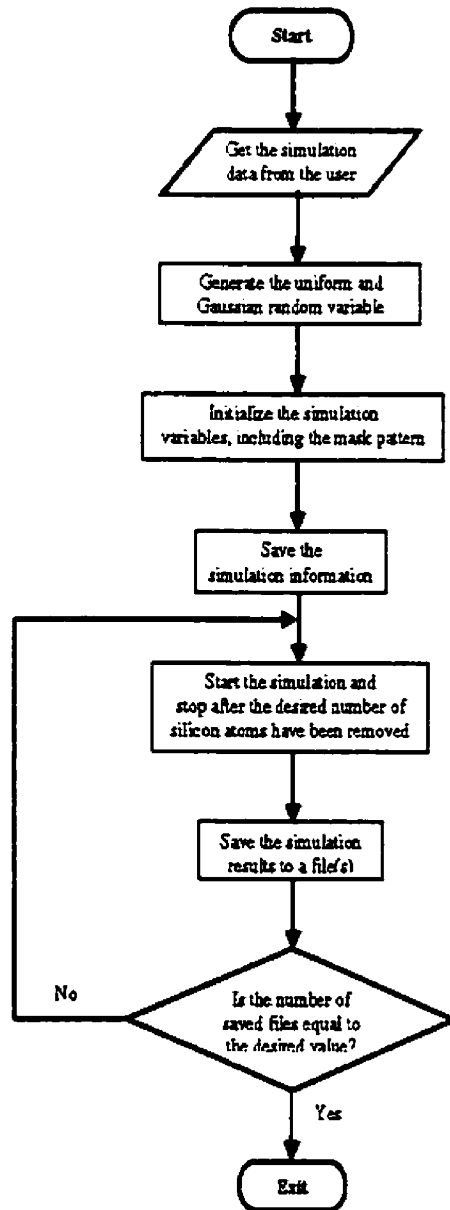

Figure 5-1. Simplified flowchart of the simulation program.

reduce the correlation between those processes that use these arrays as sources for random variables each array consists of many (32768) elements which are independently generated. One of these arrays represents a uniformly distributed random variable ranging from 0 to 1. This array is used for determining the direction of a gas molecule after it collides with another one in free space. The direction of a gas molecule after collision is totally random and can be anything between 0° and 360°. This array is also used to make the second random variable array which represents a Gaussian random variable. It is also used for the initial placement of a newly generated gas molecule. Finally, to determine whether a reaction should happen or not, a randomly chosen element of this array will be compared to the reaction probability. To generate a Gaussian random variable, the well known central limit theorem was used [40]. This theorem states that, under very general conditions, the sum of a large number of independent random variables will have a Gaussian distribution. To create an array of Gaussian random variables, the array of uniform random variables was used. 50 randomly chosen elements of that array were added together and the expected mean (25) was subtracted from the result to form a random variable with zero mean. The result was divided by a scaling factor afterwards. To verify generation of a Gaussian random variable, the generated array was saved to a file and later compared with a Gaussian random variable created by Matlab (Figure 5–2). If necessary, the variance of this generated Gaussian random variable can be adjusted by changing the number of those elements of the uniform random variable which were used to generated the second array.

However, if one makes the variance too small the distribution approaches to a single value random variable (i.e. delta function). This was observed to add to the computation time. On the other hand, if one tries to make the variance big, the distribution will not remain Gaussian.

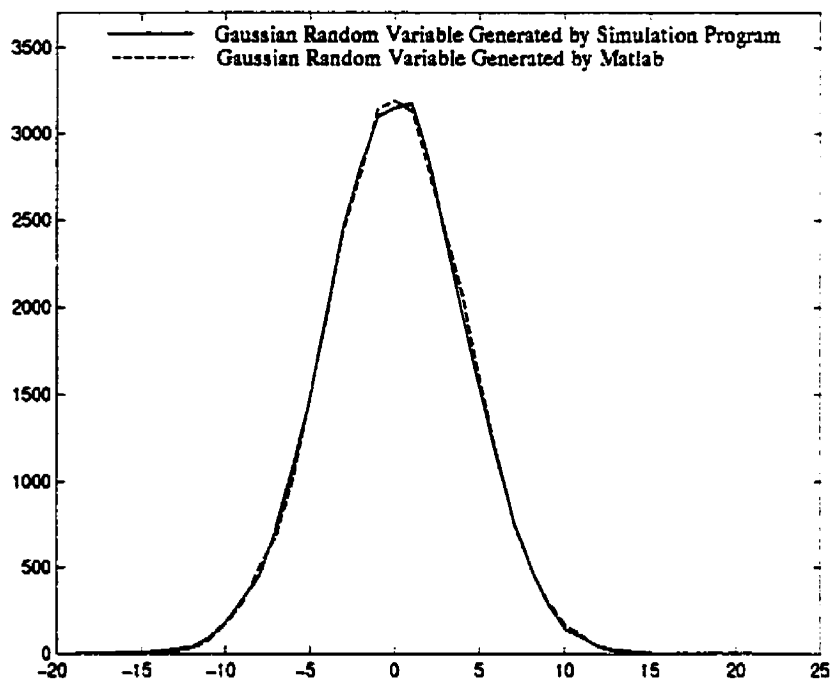

Figure 5−2. Comparison of Gaussian random variables, one generated in simulation program and the other one with Matlab.

The Gaussian array is used for two purposes; one is to determine the distance that a gas molecule travels before its next collision with another gas molecule. This distance is assumed to have a Gaussian distribution with a mean equal to the MFP of gas molecule.

An array consisting of different possible values for travel distance of the gas molecule is generated using the original Gaussian array. The Gaussian array is also used to calculate the reflection angle when a gas molecule hits mask.

Different variables and especially an array which holds the data for silicon, mask and the empty space above the mask, are initialized using the user data. The mentioned array contains all the information about mask pattern at the beginning, then will be used during the simulation and contains the simulated etch profile, and finally will be saved to a file as the simulation results.

B. Simulation

The simulation starts afterwards (Figure 5–3). First a gas molecule is assumed to be at a random position above the mask. The initial distance of the gas molecule from the mask does not affect the etch profile, since the horizontal location of the molecule is random. However, it was noted that the number of gas molecule impingements on the mask before its reaction with silicon, does depend on this distance. This could be easily verified by checking the value of a counter in the main program which kept track of the number of collisions and impingements on mask. The gas molecule impingements on top of the mask are of no importance to our simulation. This number of unnecessary impingements, and hence calculations, seemed to have a minimum when the gas molecule was initially generated at a distance of about 3 MFP's above the mask. The gas molecule then travels randomly in space. For each movement, the direction is totally

random between 0° and 360° and the radius is a Gaussian random variable with a mean equal to the MFP of the as molecule. This kind of motion resembles the gas molecule collisions with other gas molecules. This tracking of the gas molecule position will continue until the distance between the current position of the gas molecule and the etching window is bigger than a few MFP's or the molecule hits silicon or mask. If the molecule moves far away from the edges of etching window (>10 MFP's), it will be *"forgotten"* and a new one will be *"generated"* randomly inside the window to reduce the computation time.

If the gas molecule hits the mask, it should bounce back almost elastically. Three cases were examined. In the first case, it was assumed the collision was completely elastic and the reflection angle was equal to the impingement angle. In the second case the reflection angle was assumed to be independent of the impingement angle and a random value was assigned to it. Also the effect of assigning a Gaussian distribution to the reflection angle with a mean value equal to the impingement angle was examined. The first and third methods resulted in roughly similar profiles. However, the second method of calculating the reflection angle resulted in distorted profiles. Between the first and third method, the first one is preferred because of its shorter calculation time.

While the gas molecule continues its travel above the silicon surface and mask, it is always checked to see if the current and next positions of the gas molecule are on the same side of mask. This prevents the gas molecule to penetrate through the mask. In case that those two points are on two different sides of the mask, it is assumed that the gas

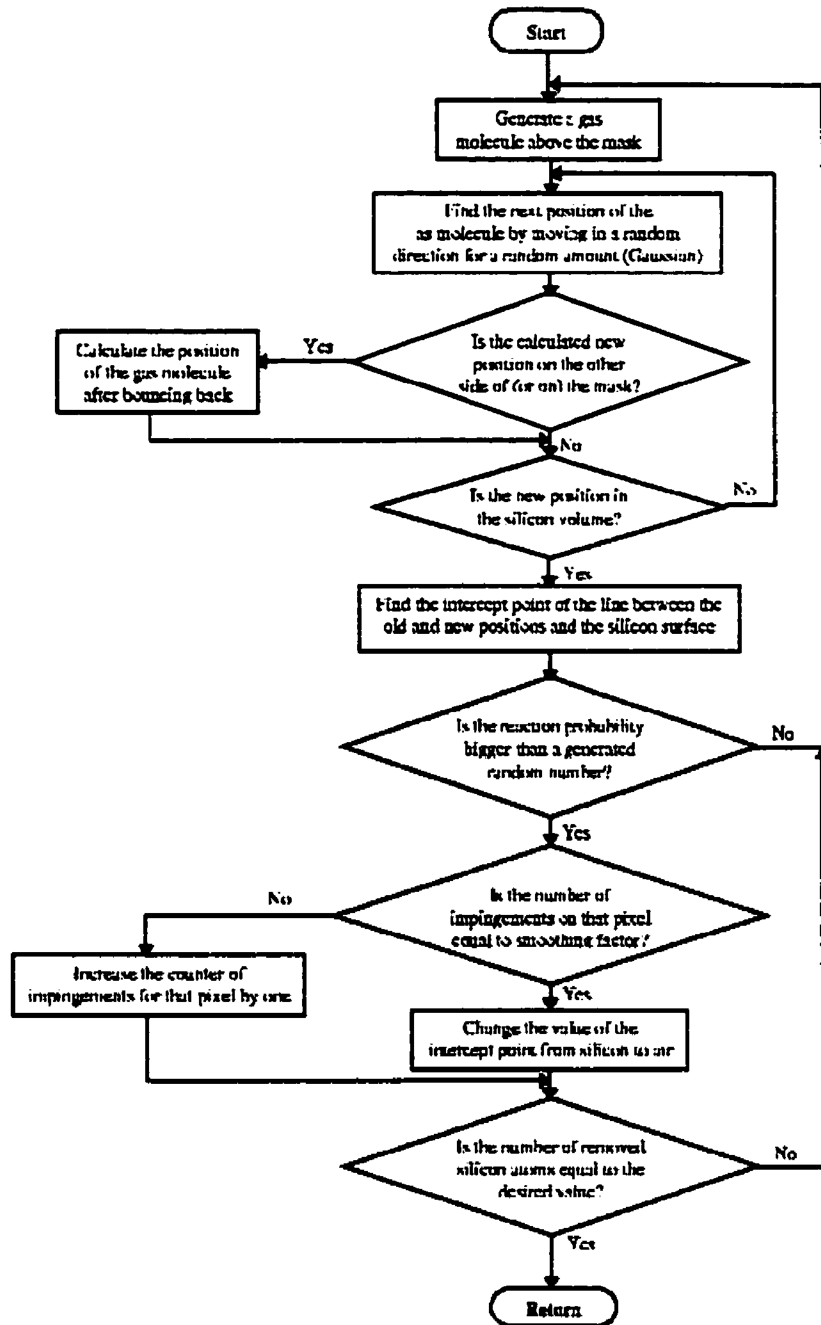

Figure 5−3. Simplified flowchart of the simulation subroutine.

molecule has hit the surface and a new position based on its impingement angle will be assigned to it.

Tracking of the gas molecule continues until the next location of it is found to be inside the silicon volume. In this case, the point on the silicon surface that the gas molecule would hit, is found. This point lies on a line which connects the current and next locations of the gas molecule to each other. To find the intercept point of this line and silicon surface, a successive series of movements will be done. First, location of the middle point between the current and next locations is calculated. Then if this point is inside the silicon volume, the next location is moved to this point. But if it happens to be in the empty space, the current location will be moved to that position. This procedure will be repeated until the distance between the current and next locations is less than 2 pixels (i.e. one atom).

Since the gas molecule reacts with silicon with a certain reaction probability, a random number will be generated and compared to the value of the reaction probability that the user had entered. If this random number is bigger than the specified reaction probability, the reaction will take place, which means that the silicon atom located on the intercept point will be removed. If the reaction does not happen, the molecule bounces back and continues its traveling in the empty space.

The data is saved after a certain number of silicon atoms have been removed. This interval and number of output files are set by user.

III. Simulation Results

A series of simulations were performed for different values of simulation parameters. Based on the developed theory, the most important factor which determines the final shape of the etch profile, is the ratio of the mean free path of the gas molecule to the mask opening diameter. This explanation was approved by the simulations.

As can be seen in Figure 5–4 the etch profile changes with λ which stands for mean free path. For the three cases shown in Figure 5–4 the reaction probability was set to be 0.01 and the hole diameters are 10μm, 50μm, and 100μm, respectively. In this figure, the changes in profile of the 50μm hole are particularly interesting. As can be seen, for small

Figure 5–4. Different etch profiles resulted from changing λ.

λ the trenches at the edges of the hole can be identified and the hole is considered as a large one. When the λ is made bigger, the profile approaches to that of a medium size hole and, finally, if λ still becomes bigger, the profile will look like the profile of a small hole (i.e. spherical).

The trenching effect can be viewed better in Figure 5-5. In this figure, the simulation

Figure 5-5. Simulation results showing the trenching phenomenon for and its changes with λ. The hole with is 400μm and the reaction probability was set to 0.01.

was performed for a single hole with different values for λ. These results support the discussion in Chapter 4 about the relation between trenching effect and the mean free path of the gas molecule. Interestingly, the simulation results also exhibit the surface roughness that was seen on the etched samples.

The simulation is able to predict the loading effect where there were two closely spaced openings on mask (Figure 5–6). It can be seen that this phenomenon is also related to the mean free path of gas molecules. As discussed in Chapter 4, we can observe one profile is loaded by its neighbor when the distance between two holes is in the order of ten's of the mean free path of the gas molecule. If the mean free path is much smaller than the distance between two neighboring holes, then the effect of those two holes on each other's profiles can be ignored. Also, if the mean free path is almost as big as the distance between holes, gas molecules can travel through the space between holes. This means that we should not see that much of loading effect when the mean free

Figure 5–6. Simulation results showing the loading effect for two neighbor holes. The hole diameters are 200μm each, the distance between them is 100μm, and the reaction probability was set to 0.01.

path is comparable to the distance between the neighbor holes.

Initially different values for the reaction probability were used. However, while its effect is not as important as the mean free path, it affects the profile. It was noticed that the simulation results with the reaction probability set to 0.01 would match the

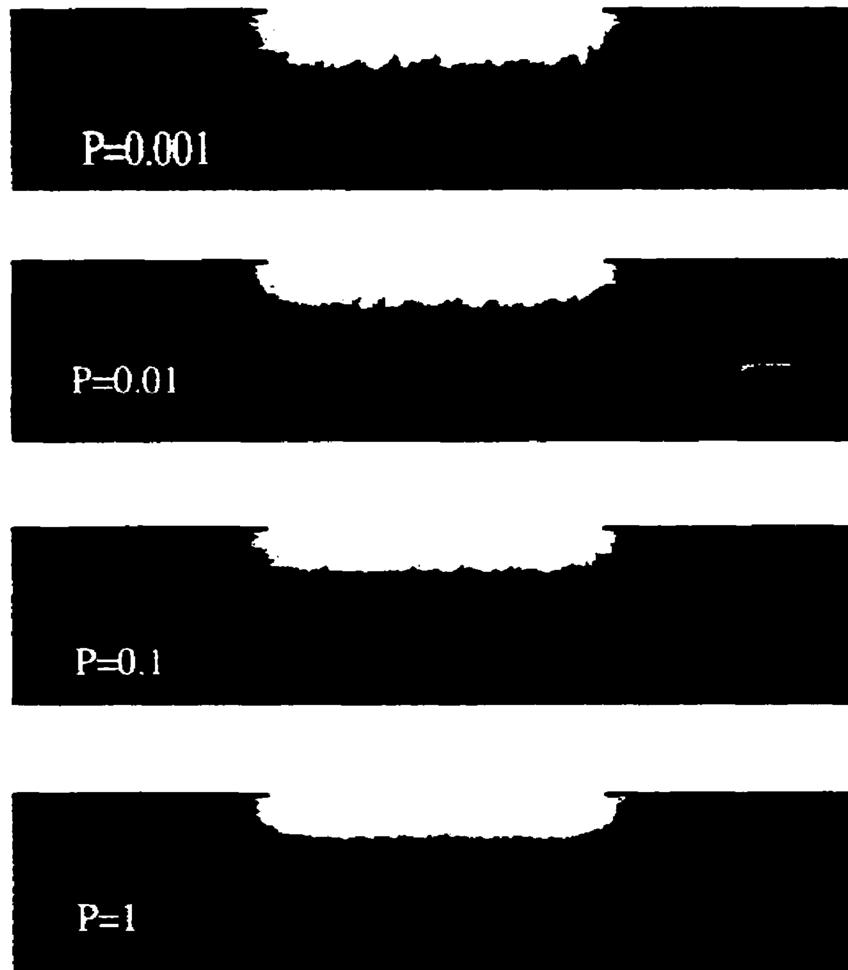

Figure 5–7. The effect of changing the reaction probability on the simulated profile. The hole width is 200µm and the mean free path is 20µm.

experimental results best (Figure 5–7). This is on close agreement with the reaction probability of silicon with XeF_2 measured to be 0.013 in [34]. In Figure 5–7 the effect of changing the reaction probability within a range of four orders of magnitude is illustrated. Based on the simulation, it seems that the reaction probability plays an important role for the observed surface roughness.

The reaction probability was changed by factors of 2 to 3 around the values shown in Figure 5–7 and no significant change was observed in profile. Thus, the overall shape of the etch profile is not sensitive to small changes in reaction probability.

Chapter 6: Conclusions

I. Summary

In this thesis design and testing of a XeF2 etching system was described. The etching system was successfully made and used for etching numerous samples with different methods. The system can be solely controlled either manually or by a computer. The manual control is useful for investigation of novel etching methods or for system maintenance. It is also possible to leave the system control to a computer and a control software for this purpose was written on a PC. All the etching parameters can be set by user. The system design is flexible and this allows the user to investigate many different etching techniques. Benefits and drawbacks of each of them were explained and the experimental results were presented.

A simulation program was written which supported the explanation for the odd etching profile. Many of the etching parameters can be set and the effect of varying these parameters on the simulation results were tested and discussed. The simulation results closely agree with the experimental ones and proved to be useful for prediction of the etching profile.

II. Future Work

The future work related to this project can be divided into two major areas. The first area deals with physical experiments that can be done with the designed system. This may include, but is not limited to, investigation of novel etching methods, finding ways to increase or control the etch rate, or improving the efficiency of system in terms of XeF_2 usage (e.g. finding a way to circulate the gas inside the chambers). For example, effects of applying an electric or magnetic field to the sample during the etch may lead to interesting results.

The other area for future work is related to the simulation of the etching process. The first possibility is extending the current two dimensional simulation to a three dimensional one. This will require a huge amount of computation and ways for optimizing the code for this particular purpose have to be found. It will be very useful if a model for the etch can be proposed. This will reduce the computation time by orders of magnitude and will also provide a better insight about the etch process. The current simulation will predict the final etch profile based on the etching parameters. Prediction of important etching factors, such as etch rate, can be a very useful feature that may be added to this code and contribute to a complete simulation application. With some modifications, most of the algorithms used in this simulation software can be applied to simulation of other types of dry etching, such as plasma etching or reactive ion etching.

Chapter 6: Conclusions

Appendix A: Hardware and Electronic Details

I. Hardware and Electronics

In this section details of the hardware of the etching system will be described. In first section the hardware (e.g. valves, pressure gauge, and connections) will be explained. After that, the electronic circuitry of the system will be analyzed.

A. Hardware

XeF_2 does not attack aluminum. Thus, it was decided to make the main chamber and all those parts of the system which required welding or machining out of aluminum, which is easier to work with than stainless steel. The viewing window is a piece of acrylic which is bolted to the lid of the main chamber. Viton O–rings were used for both the main lid and the viewing window. Valves and almost all the other parts purchased from vacuum component vendors were all made of stainless steel (except aluminum to stainless steel adaptors).

Pneumatic valves with solenoids mounted on them were chosen. This enabled opening or closing of the valves from a remote control panel. The chosen valves require

compressed air with a pressure of 80 to 100psi for operation. The solenoid on each valve needs a 110V–60Hz electrical command signal for actuation.

All the flanges and connections are ConFlat (except for the pump connector), with copper O–rings. Using ConFlat flanges makes the system maintenance easier while providing very low leak rate for the connections.

XeF_2 crystals are in an aluminum cylinder which has its own manual valve. This valve is open only when the system is in use and it is closed at all other times for safety reasons.

Pressure inside the system is monitored by a pressure gauge which employs convection for its measurements. The pressure gauge can measure pressure from 0.1mTorr to 1000Torr which spans over the entire pressure rage that we may have inside the system. It shows the pressure on its LED display, which is necessary in manual mode of operation. Upon receiving a proper command, it will send the pressure data via an RS–232 serial connection to the requesting device (e.g. a personal computer). However, the pressure transducer seemed to be attacked by XeF_2 (or possibly, formed HF) and failed. Thus, the values that we had for pressure might not be the correct values.

B. Electronics

All the signals for opening or closing valves are sent from the main control panel. On control panel, user can select from two modes of operation: (1) manual, where user opens or closes the valves based on his own readings of pressure or timings and (2) automatic, where the user, after setting the values for timings, number of pulses, pressure

levels, etc. leaves the control of the system to a personal computer (PC). In manual mode, each valve is controlled by a corresponding switch on control panel while in automatic mode, this is done by PC commands.

To send signals to the control board, a data acquisition (DAQ) board was inserted into one of the PCI slots of the mother–board of a personal computer. This card contains an 8255 chip which has three 8 bit output/input ports. The data on each of these ports is set/read by sending proper commands to this IC. This card sends data to the main control board through a ribbon cable.

The circuit configuration that we initially used for the main control board is shown in Figure A–1 . In this design, next to each switch is a circuit for filtering out the fluctuations that are caused when switch is opened or closed. This is done by adding a

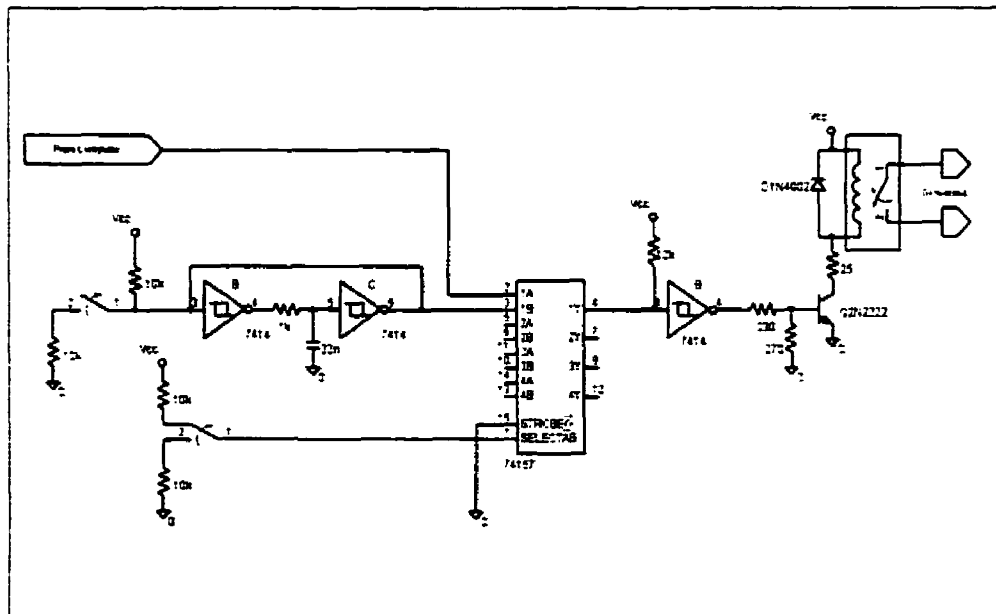

Figure A–1. Initial design for control board (only one of the four similar circuits is shown).

20–50msec delay in signal path. A multiplexer is placed after the filters which selects the command signal to the valves to be from either the switches or the computer. The electronic circuitry after the multiplexer is essentially for deriving the relays, including transistors, fly–back diodes, etc. The relays convert the low voltage digital signals to 110V, 60Hz pulses and at the same time, isolate the high voltage circuit form the low

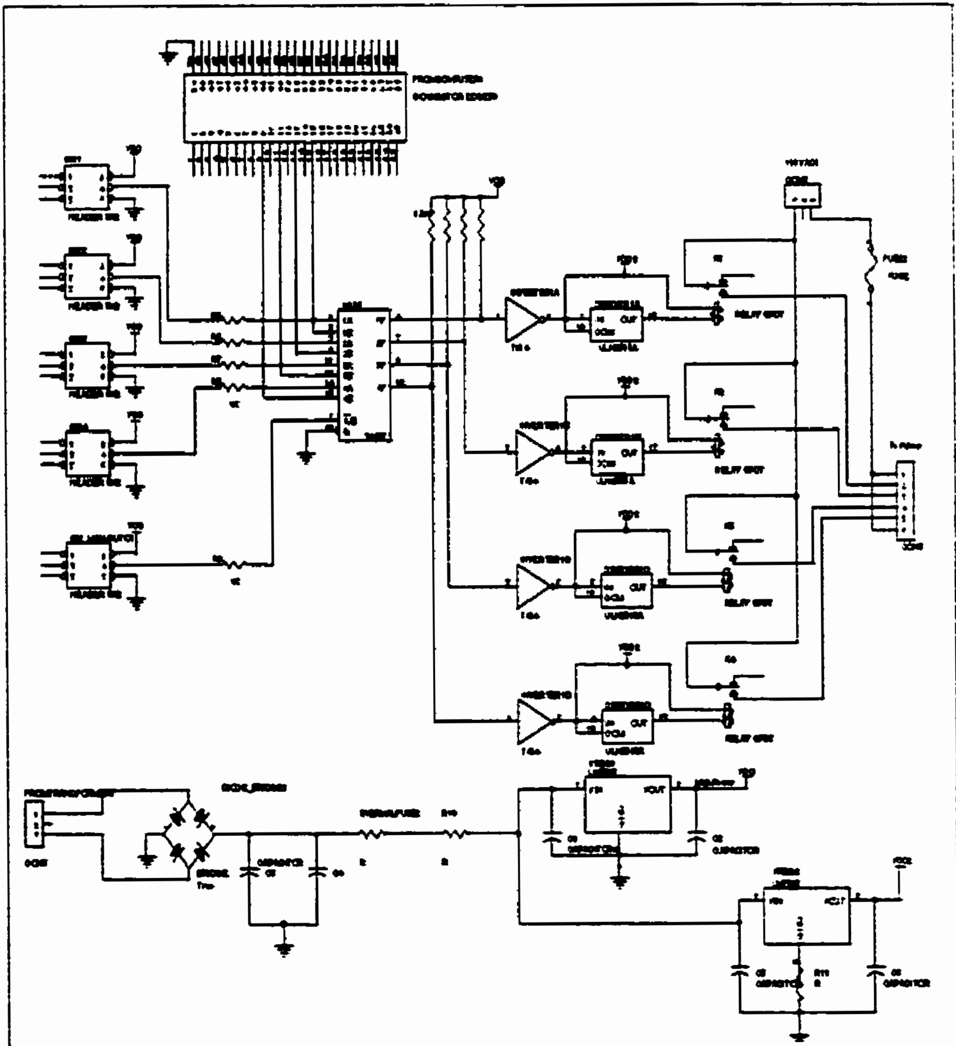

Figure A–2. Final electronic circuitry for control board.

voltage circuit. The control circuitry also included a power supply board to provide the required supply voltages for different parts of the circuit.

A series of experiments were successfully performed with the electronic board described above. However, that design was slightly modified. The required time for actuation of the valves is about one second. This property obviates the need for debouncing circuitry. In this case, the filtering function is done by the valves themselves. A deriver chip was used instead of the transistors and their related components (Figure A-2). This change considerably reduced the total number of components.

Relays were also replaced with more reliable ones, since the relays originally used were sensitive to vibrations of the board.

The power supply for the relay deriver section is also separated from the rest of circuit to allow using relays with different activation voltages, if necessary.

Appendix B: Flowchart of Etching Control Software

In this appendix the flowcharts of different sections of the control software are given. To avoid confusion a simplified form of the flowcharts is presented. As mentioned in thesis, the control software was written by LabView. One of the important features of LabView is its ability to run different subroutines in parallel. It was this property that let us run the timer or schematic subroutines at the same time as the main application was controlling the system. Obviously, this could not be illustrated using flowcharts, since flowcharts are commonly used to represent serial processing. But if the reader is aware of this point, the given flowcharts can be very helpful to obtain an overall understanding of how the control software works in reality.

Appendix B: Flowchart of Etching Control Software

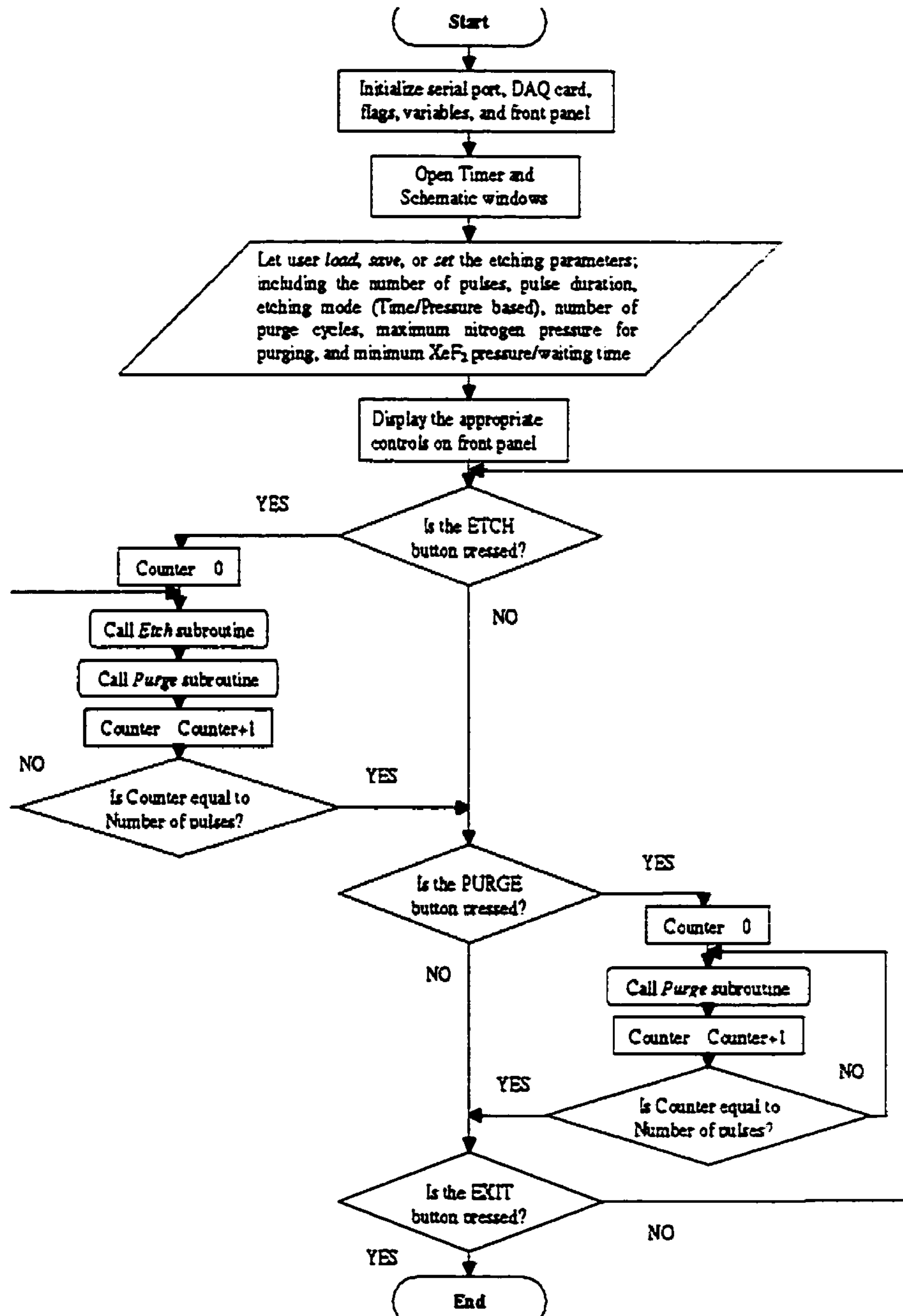

Figure B−1. Main subroutine in automatic mode.

Appendix B: Flowchart of Etching Control Software

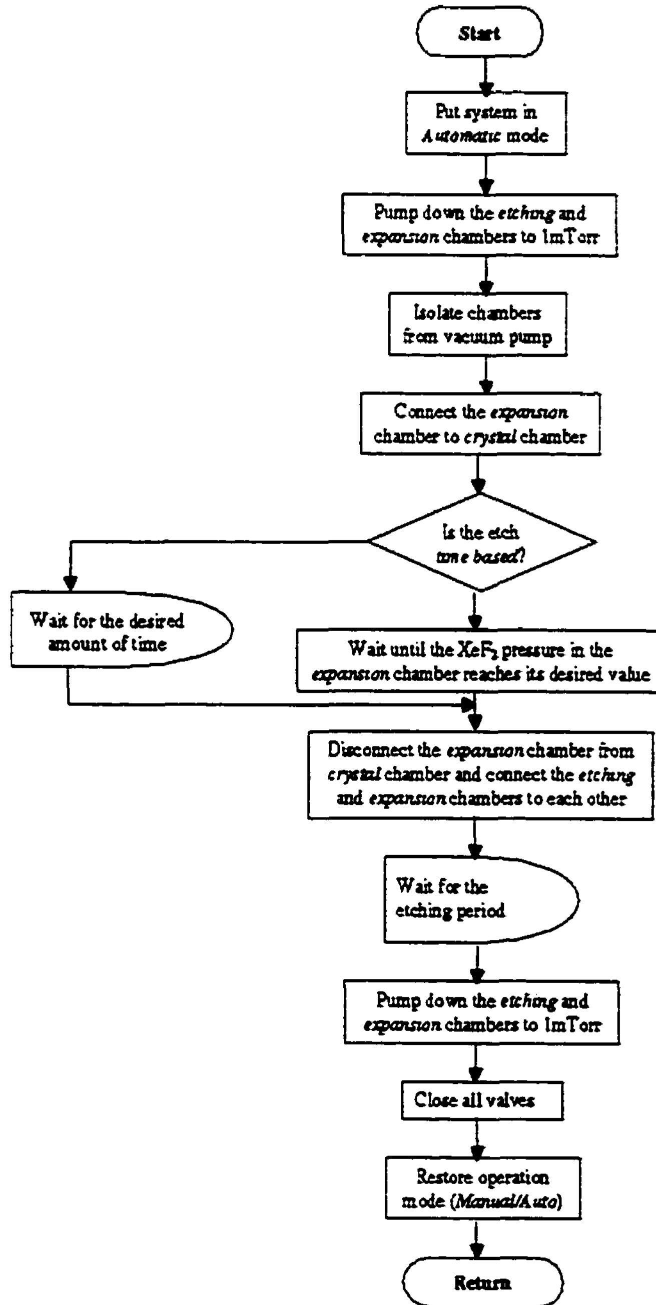

Figure B−2. Etch subroutine.

Appendix B: Flowchart of Etching Control Software

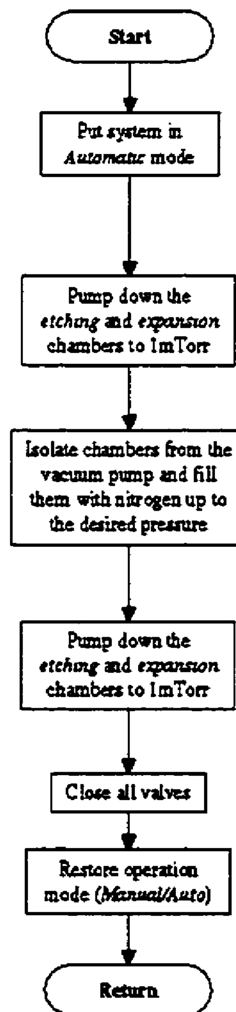

Figure B-3. Purge subroutine.

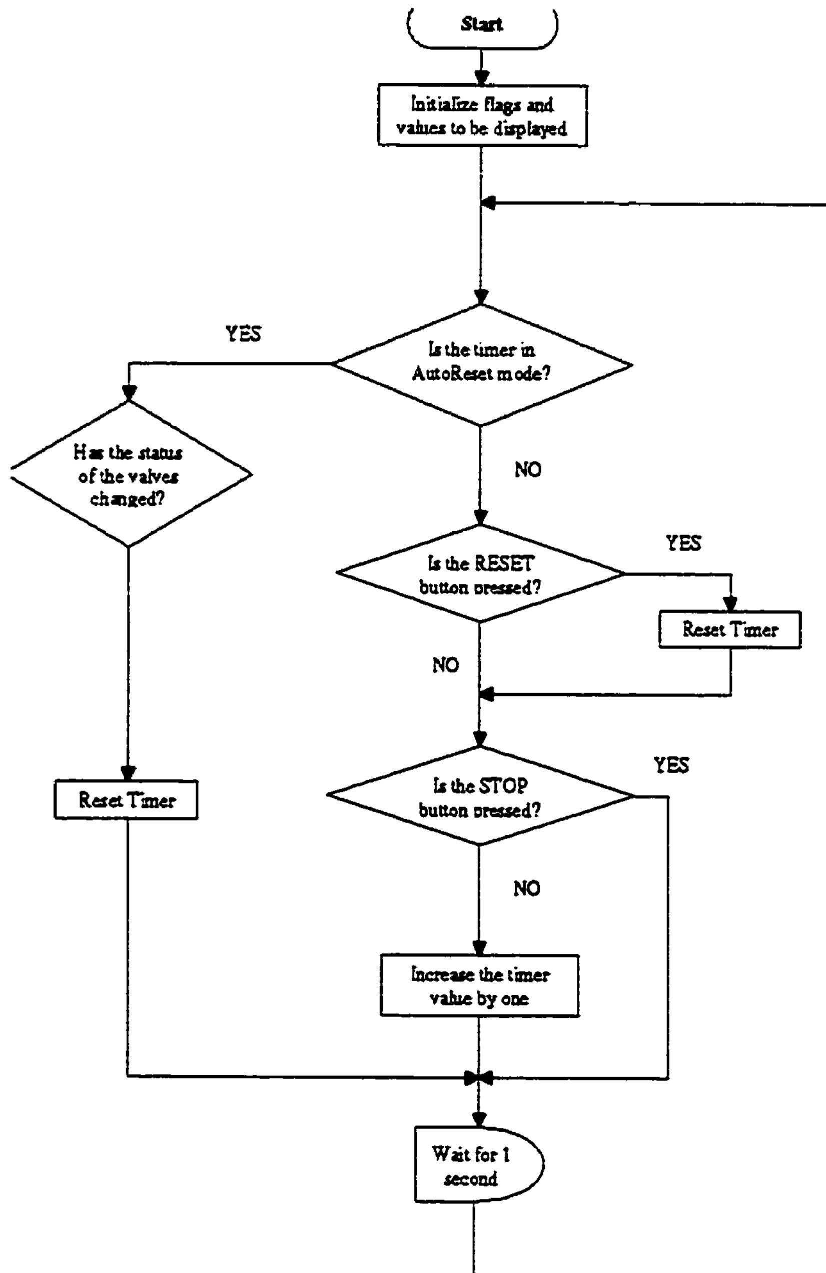

Figure B–4. Timer subroutine.

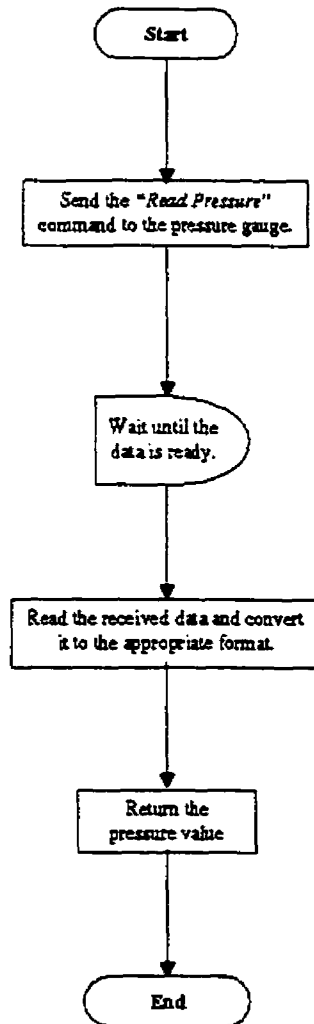

Figure B−5. Subroutine for reading the pressure.

Appendix C: Simulation Program Code

In this appendix, the simulation software code is given. The code is almost self-explanatory. Comments are added to help understanding different sections and functions. Whenever possible a comment is given to help improving the code in future.

Appendix C: Simulation Program Code

```
#include <stdio.h>
#include <stdlib.h>
#include <math.h>
#include <string.h>
#include <sys/stat.h>
#include <sys/types.h>

#define DIRECTORY "/var/tmp/EtchSimulation/"    /*Can be any other desired direcotry*/
#define ZERO 48
#define FALSE 0
#define TRUE 1
#define NULL_STRING "\0"
#define SILICON 128
#define MASK 255
#define AIR 0
#define PI 3.14152692
#define MAXINT 32768

#define MASK_HEIGHT 40
#define WINDOW_WIDTH 1001
#define WINDOW_HEIGHT 500
#define MAX_NUM_OF_WINDOWS 1  /*Can be lager than 1. The upper limit is imposed by the system
memory*/
#define MAX_MOVE 100
#define NUM_OF_MOVEMENTS 32768
#define EMPTY_SPACE 40

typedef unsigned char BYTE;

void CreateFileName(char *Name, int FileNo, int SegmentNo);

BYTE data[MAX_NUM_OF_WINDOWS][WINDOW_WIDTH][WINDOW_HEIGHT],
PixelHit[MAX_NUM_OF_WINDOWS][WINDOW_WIDTH][WINDOW_HEIGHT];
```

Appendix C: Simulation Program Code

```
int NumHoles, ImpingeNo, Scale, EtchWindowSize, NumOfFiles, NumOfSiAtoms, MaskThickness;
float ReactionP, Lambda_0;
float Lambda[MAXINT], URV[MAXINT], NRV[MAXINT];
int HoleOffset[10], HoleWidth[10];

int main () {

        void GetData(void);

        void Initialize(void);

        void CreateUniform(void);

        void CreateNormal(void);

        void Simulate(void);

        void SaveData(int FileNo);

        void SaveInformation(void);

        void FillMoveArray(void);

        long int i;

        CreateUniform();

        CreateNormal();

/*Create the directory for saving the simulation results*/

        if(mkdir(DIRECTORY, 448)!=0)
```

```
		if(chmod(DIRECTORY, 448)!=0){
			printf("\nUnable to create the directory for saving data\nExit due to
error...\n\n");
			exit(0);
		}


/*Gets the simulation data from user*/

	GetData();

/*Initializes the simulation parameters*/

	Initialize();

/*Saves the simulation parameters in a file for furture access*/

	SaveInformation();

/*Simulation starts here; data is saved regularly*/

	for(i=0; i<NumOfFiles; i++){

		Simulate();

		SaveData(i);

	}


	return 0;
}
```

```
void SaveInformation(void){
/*Saves the simulation parameters in a file for furture access*/

        static int FileCounter=0;

        FILE *InformationFile;
        char *InformationFileName;
        int n;

        InformationFileName=(char *) malloc(60);

        CreateFileName(InformationFileName, FileCounter++, 0);
        strcat(InformationFileName, ".inf");

        InformationFile=fopen(InformationFileName, "w");

        fprintf(InformationFile, "\nScale = %d\n", Scale);

        fprintf(InformationFile, "\nNumber of holes = %d\n", NumHoles);

        for(n=0; n<NumHoles; n++){
                fprintf(InformationFile, "\nHole #%d width in microns= %d", n+1, HoleWidth[n]);
                fprintf(InformationFile, "\nDistance from previous hole in microns= %d\n",
HoleOffset[n]);
        }

        fprintf(InformationFile, "\n\nMean free path in microns = %f\n", Lambda_0);

        fprintf(InformationFile, "\nMask thickness in microns = %d\n", MaskThickness);
```

```
        fprintf(InformationFile, "\nReaction probability = %f\n", ReactionP);

        fprintf(InformationFile, "\nNumber of impingements before reaction takes place = %d\n",
ImpingeNo);

        fprintf(InformationFile, "\nNumber of removed silicon atoms between two successive saves of
data = %d\n", NumOfSiAtoms);

        fprintf(InformationFile, "\nTotal number of output files for each segment = %d\n",
NumOfFiles);

        fclose(InformationFile);

        free(InformationFileName);


        return;
}


void CreateUniform(void){
/*Creates an array whose elements are Uniform Random Variables between 0 and 1*/

        long int i;

        for(i=0; i<MAXINT; i++)
                URV[i]=(float) rand()/(MAXINT-1);

        return;
}


void CreateNormal(void){
```

Appendix C: Simulation Program Code

```
/*Creates an array whose elements are Normal Random Variables with a mean of 0 and variance of
~0.1*/

        long int i,j;

        for(i=0; i<MAXINT; i++){
                NRV[i]=0;
                for(j=0; j<50; j++)
                        NRV[i]+=URV[rand()];
                NRV[i]=(NRV[i]-25)/50;
        }

        return;
}


void GetData(){
/*Gets the data required to generate the desired mask properties (i.e. number of holes, their distance from
each other, and their width), and also the Mean Free Path of gas molecules and Reaction Probability upon
a collision between a gas molecule and Si atom*/

        long int i;

        printf("\n\nEtching window width = 1001*Scale \nEnter the value for scale (must be an integer
<= 26): ");
        scanf("%d", &Scale);

        printf("\n\nEnter number of holes (must be an integer <= 10): ");
        scanf("%d", &NumHoles);

        for(i=0; i<NumHoles; i++){
                printf("\n\nEnter the data for position of the hole #%d on mask.", i+1);
                printf("\nHole width in microns: ");
```

```
            scanf("%d", &HoleWidth[i]);
            printf("Distance from previous hole in microns: ");
            scanf("%d", &HoleOffset[i]);
        }

    printf("\n\nEnter mean free path in microns (~10microns @ 3Torr): ");
    scanf("%f", &Lambda_0);

    printf("\n\nEnter the mask thickness in microns: ");
    scanf("%d", &MaskThickness);

    printf("\n\nEnter reaction probability (between 0 and 1): ");
    scanf("%f", &ReactionP);

    printf("\n\nEnter number of impingements before reaction takes place (must be an integer >= 1):
");
    scanf("%d", &ImpingeNo);

    printf("\n\nEnter the number of silicon atoms that have to be removed between two successive
saves of data (~1000's): ");
    scanf("%d", &NumOfSiAtoms);

    printf("\n\nEnter the total number of output files for each segment: ");
    scanf("%d", &NumOfFiles);

    printf("\n\nSimulation started\nResulting files will be saved at %s\n", DIRECTORY);
    printf("\nSimulation may take several minutes or even hours to finish, please wait...\n");

    return;
}
```

Appendix C: Simulation Program Code

```
void Initialize(void){
/*Initializes all the data to do the simulation in the next step*/

        long int i, j, k, index=0, Var1, Var2;

        for(i=0; i<MAXINT; i++)
                Lambda[i]=Lambda_0*(1+NRV[rand()]);

        for(i=0;i<Scale;i++)
                for(j=0;j<WINDOW_WIDTH;j++)
                        for(k=0;k<WINDOW_HEIGHT;k++)
                                PixelHit[i][j][k]=0;

        for(i=0; i<WINDOW_WIDTH; i++)
                for(j=0;j<MASK_HEIGHT;j++)
                        for(k=0; k<Scale; k++)
                                data[k][i][j]=AIR;

        for(k=0; k<NumHoles; k++){
                for(i=0; i<HoleOffset[k]; i++){
                        Var1=(int) ((index+i)/WINDOW_WIDTH);
                        Var2=(int) ((index+i)%WINDOW_WIDTH);
                        for(j=MASK_HEIGHT; j<(MASK_HEIGHT+MaskThickness); j++)
                                data[Var1][Var2][j]=MASK;
                }

                index+=HoleOffset[k];

                for(i=0; i<HoleWidth[k]; i++){
                        Var1=(int) ((index+i)/WINDOW_WIDTH);
                        Var2=(int) ((index+i)%WINDOW_WIDTH);
                        for(j=MASK_HEIGHT; j<(MASK_HEIGHT+MaskThickness); j++)
```

```
                        data[Var1][Var2][j]=AIR;
            }

            index+=HoleWidth[k];
    }


    for(i=index; i<EtchWindowSize; i++){
            Var1=(int) (i/WINDOW_WIDTH);
            Var2=(int) (i%WINDOW_WIDTH);
            for(j=MASK_HEIGHT; j<(MASK_HEIGHT+MaskThickness); j++)
                    data[Var1][Var2][j]=MASK;
    }


    for(i=0; i<WINDOW_WIDTH; i++)
            for(j=(MaskThickness+MASK_HEIGHT); j<WINDOW_HEIGHT; j++)
                    for(k=0;k<Scale;k++)
                            data[k][i][j]=SILICON;


    return;
}


void Simulate(){
/*Simulates the etch process by resembling movement of gas molecules and their collisions with each
other, mask and silicon*/

    BYTE CheckMask(long int LastX, long int LastY, long int NextX, long int NextY);
    BYTE MoveIndex=0;
    long int LastX, LastY, NextX=0, NextY=0, MidX, MidY, deltaX, deltaY, Counter=0,
MoveCounter=0, MaxMove, SegmentNo, RelativeX;
```

```
float angle, radius;

MaxMove=(int) (MAX_MOVE*EtchWindowSize/Lambda_0);

while (Counter<NumOfSiAtoms){

        if(MoveCounter==MaxMove){
                MoveCounter=0;
                LastX=(int) (EtchWindowSize*URV[rand()]);
                LastY=(int) (MASK_HEIGHT-3*Lambda[rand()]);
        }
        else{

                angle=2*PI*URV[rand()];
                radius=Lambda[rand()];
                deltaX=(int) (radius*cos(angle));
                deltaY=(int) (radius*sin(angle));

                NextX=LastX+deltaX;
                NextY=LastY+deltaY;
                MoveCounter++;

                if (CheckMask(LastX, LastY, NextX, NextY)==TRUE){
                        if((LastY<=(MASK_HEIGHT-MaskThickness)) &&
(LastY>=(MASK_HEIGHT)))
                                NextY=LastY+2*(URV[rand()]-.5)*Lambda_0;
                        else
                                NextX=LastX+2*(URV[rand()]-.5)*Lambda_0;

                }
                else{
```

```
				if ((NextX>(EtchWindowSize+10*Lambda_0)) || (NextX<(-
10*Lambda_0)) || (NextY<0)){
					LastX=(int) (EtchWindowSize*URV[rand()]);
					LastY=(int) (MASK_HEIGHT-3*Lambda[rand()]);
					MoveCounter=0;
				}

				else if ((NextX>=0) && (NextX<EtchWindowSize) && (NextY>0)){

					SegmentNo=NextX/WINDOW_WIDTH;
					RelativeX=NextX%WINDOW_WIDTH;

					if
(data[NextX/WINDOW_WIDTH][NextX%WINDOW_WIDTH][NextY]==AIR){
						LastX=NextX;
						LastY=NextY;
					}


					if (data[SegmentNo][RelativeX][NextY]==MASK){
						angle=-angle*(1+NRV[rand()]);
						radius=Lambda[rand()];
						deltaX=(int) (radius*cos(angle));
						deltaY=(int) (radius*sin(angle));
						NextX=LastX+deltaX;
						NextY=LastY+deltaY;

					}
					else if (data[SegmentNo][RelativeX][NextY]==SILICON){

						do{
							deltaX>>=1;
							deltaY>>=1;
```

```
                        MidX=LastX+deltaX;
                        MidY=LastY+deltaY;

                        SegmentNo=MidX/WINDOW_WIDTH;
                        RelativeX=MidX%WINDOW_WIDTH;

                        if
(data[SegmentNo][RelativeX][MidY]==AIR){
                                LastX=MidX;
                                LastY=MidY;
                        }
                        else if
(data[SegmentNo][RelativeX][MidY]==SILICON){
                                NextX=MidX;
                                NextY=MidY;
                        }

                }while ((abs(deltaX)>=2) || (abs(deltaY)>=2));

                if (URV[rand()]<=ReactionP){

                        if(PixelHit[NextX/WINDOW_WIDTH][Ne
xtX%WINDOW_WIDTH][NextY]==ImpingeNo){

                                data[NextX/WINDOW_WIDTH][
NextX%WINDOW_WIDTH][NextY]=AIR;

                                Counter++;
                        }
                        else
                                PixelHit[NextX/WINDOW_WIDT
H][NextX%WINDOW_WIDTH][NextY]++;

                        LastX=(int)
```

```
EtchWindowSize*URV[rand()];
                                                        LastY=(int) MASK_HEIGHT-
3*Lambda[rand()];
                                                        MoveCounter=0;
                                                  }
                                             }
                                        }
                                   }
                              }
                         }

                         return;
}


BYTE CheckMask(long int LastX, long int LastY, long int NextX, long int NextY){
/*Checks to see if the gas molecule tries to pass mask*/

          long int x1, x2, index=0;
          int i, HitMask=FALSE;

          if (NextY!=LastY)
          {
                    x1=(int) ((NextX-LastX)*(MASK_HEIGHT-LastY)/(NextY-LastY)+LastX);
                    x2=(int) ((NextX-LastX)*(MASK_HEIGHT+MaskThickness-LastY)/(NextY-
LastY)+LastX);

                    for(i=0; i<NumHoles; i++){
                              if (((x1>=index) && (x1<=(index+HoleOffset[i]))) || ((x2>=index) &&
(x2<=(index+HoleOffset[i])))){
                                        HitMask=TRUE;
                                        break;
                              }
```

```
			index+=HoleOffset[i]+HoleWidth[i];
		}

		if (((x1>=index) && (x1<=EtchWindowSize)) || ((x2>index) &&
(x2<=EtchWindowSize)))
			HitMask=TRUE;

	}

	return(HitMask);

}


void SaveData(int FileNo){
/*Saves the processed data to file for later access*/

	FILE *OutputFile;
	char *OutputFileName;
	long int i, j, k, MyVar;
	BYTE tmp[WINDOW_WIDTH][WINDOW_HEIGHT];


	OutputFileName=(char *) malloc(60);

	if(Scale!=1){
		for(k=MASK_HEIGHT;k<WINDOW_HEIGHT;k++)
			for (i=0;i<WINDOW_WIDTH;i++){
				MyVar=0;
				for(j=(i*Scale);j<((i+1)*Scale);j++)
					MyVar+=data[j/WINDOW_WIDTH][j%WINDOW_WIDTH
][k];
				tmp[i][k]=(int) ((MyVar/Scale)+0.5);
```

```
                }

        CreateFileName(OutputFileName, FileNo, 0);
        strcat(OutputFileName, ".cmp");

        OutputFile=fopen(OutputFileName,"w");

/*Remove EMPTY_SPACE in this function to get rid of the empty space above the mask in output file*/

        for (j=0; j<EMPTY_SPACE; j++){
                for(i=0; i<WINDOW_WIDTH; i++)
                        fprintf(OutputFile,"%d ", AIR);

                fprintf(OutputFile,"\n");
        }

        for (j=MASK_HEIGHT; j<(MASK_HEIGHT+MaskThickness); j++){
                for(i=0; i<WINDOW_WIDTH; i++)
                        fprintf(OutputFile,"%d ", tmp[i][j]);

                fprintf(OutputFile,"\n");
        }

        for (j=(MASK_HEIGHT+MaskThickness); j<(WINDOW_HEIGHT-EMPTY_SPACE);
j++){
                for(i=0; i<WINDOW_WIDTH; i++)
                        fprintf(OutputFile,"%d ", tmp[i][j]);

                fprintf(OutputFile,"\n");
        }

        fclose(OutputFile);
```

```
	}

	for(k=0;k<Scale;k++){

		CreateFileName(OutputFileName, FileNo, k);
		strcat(OutputFileName, ".dat");

		OutputFile=fopen(OutputFileName,"w");

/*Remove EMPTY_SPACE in this function to get rid of the empty space above the mask in output file*/

		for (j=0; j<EMPTY_SPACE; j--){
			for(i=0; i<WINDOW_WIDTH; i++)
				fprintf(OutputFile,"%d ", AIR);

			fprintf(OutputFile,"\n");
		}

		for (j=(MASK_HEIGHT); j<(MASK_HEIGHT+MaskThickness); j++){
			for(i=0; i<WINDOW_WIDTH; i++)
				fprintf(OutputFile,"%d ", data[k][i][j]);

			fprintf(OutputFile,"\n");
		}

		for (i=(MASK_HEIGHT+MaskThickness); i<WINDOW_HEIGHT; i--){
			for(j=0; j<WINDOW_WIDTH; j++)
				fprintf(OutputFile,"%d ", data[k][j][i]);

			fprintf(OutputFile,"\n");
		}
```

```
                fclose(OutputFile);
        }

        free(OutputFileName);

        return;
}

void CreateFileName(char *Name, int FileNo, int SegmentNo){
/*Creates an appropriate file name for each of the output files*/

        long int i;
        char c;

        strcpy(Name, NULL_STRING);
        strcat(Name, DIRECTORY);

        strcat(Name, "S");

        i=Scale;
        c=(int) ((i/10)+ZERO);
        strcat(Name, &c);
        i%=10;
        c=i+ZERO;
        strcat(Name, &c);

        strcat(Name, "H");
```

```
i=NumHoles;
c=(int) ((i/10)+ZERO);
strcat(Name, &c);
i%=10;
c=i+ZERO;
strcat(Name, &c);

strcat(Name, "L");

i= (int) Lambda_0;
c=(int) ((i/100)+ZERO);
strcat(Name, &c);
i%=100;
c=(int) ((i/10)+ZERO);
strcat(Name, &c);
i%=10;
c=i+ZERO;
strcat(Name, &c);

strcat(Name, "M");

i= (int) MaskThickness;
c=(int) ((i/100)+ZERO);
strcat(Name, &c);
i%=100;
c=(int) ((i/10)+ZERO);
strcat(Name, &c);
i%=10;
c=i+ZERO;
strcat(Name, &c);

strcat(Name, "P");
```

```
	i= (int) (ReactionP*1000);
	if (i>=1000)
		i=999;
	c=(int) ((i/100)+ZERO);
	strcat(Name, &c);
	i%=100;
	c=(int) ((i/10)+ZERO);
	strcat(Name, &c);
	i%=10;
	c=i+ZERO;
	strcat(Name, &c);

	strcat(Name, "I");

	c=ImpingeNo+ZERO;
	strcat(Name, &c);

	strcat(Name, "_");

	c='a'+SegmentNo;
	strcat(Name, &c);

	i=FileNo;
	c=(int) ((i/10)+ZERO);
	strcat(Name, &c);
	i%=10;
	c=i+ZERO;
	strcat(Name, &c);

	return;
}
```

Appendix D: Etching Data for Different Etching Methods

In this appendix the etching data, consisting of the etching pressures and pulse duration, are given for different etching methods whose results have been used in different sections of this thesis. It should be mentioned that the pressure gauge itself was attacked by XeF_2. However, the pressure readings were consistent and reproducible.

The data presented in this appendix correspond to four samples with different surface areas. These samples were etched by basic, triple, and quick pulse methods. In following tables all pressures are given in Torr.

I. Sample with an Initial Surface Area of ~60mm^2

A. Basic Pulse Method

Appendix D: Etching Data for Different Etching Methods

Pulse #	Expansion Chamber Pressure before Etch	Initial Pressure in Etching Chamber	Pulse Duration (second)	Etch Depth (μm)
1	0.3	0.26	150	
2	0.3	0.26	150	
3	0.3	0.26	150	
4	0.3	0.26	150	22

B. Triple Pulse Method

#	Expansion Chamber Pressure before Etch			Initial Pressure in Etching Chamber			Pulse Duration (second)			Final Pressure in Etching Chamber			Etch Depth (μm)
	1st	2nd	3rd	1st	2nd	3rd	1st	2nd	3rd	1st	2nd	3rd	
1	0.44	0.42	0.28	0.42	0.3	0.11	75	45	30	0.5	0.32	0.12	
2	0.35	0.42	0.31	0.29	0.26	0.14	75	45	30	0.42	0.31	0.17	
3	0.35	0.4	0.29	0.3	0.25	0.14	75	45	30	0.4	0.29	0.16	
4	0.31	0.33	0.25	0.27	0.21	0.12	75	45	30	0.33	0.25	0.15	10

C. Quick Pulse Method

Pulse #	Expansion Chamber Pressure before Etch	Initial Pressure in Etching Chamber	Pulse Duration (second)	Etch Depth (μm)
1	0.8	0.65	150	
2	0.65	0.56	150	

Pulse #	***Expansion Chamber Pressure before Etch***	***Initial Pressure in Etching Chamber***	***Pulse Duration (second)***	***Etch Depth (µm)***
3	0.51	0.45	150	
4	0.42	0.39	150	
5	0.39	0.35	150	
6	0.39	0.29	150	24

II. Sample with an Initial Surface Area of ~110mm²

A. Basic Pulse Method

Pulse #	***Expansion Chamber Pressure before Etch***	***Initial Pressure in Etching Chamber***	***Pulse Duration (second)***	***Etch Depth (µm)***
1	0.3	0.26	150	
2	0.3	0.26	150	
3	0.3	0.26	150	8

B. Triple Pulse Method

#	***Expansion Chamber Pressure before Etch***			***Initial Pressure in Etching Chamber***			***Pulse Duration (second)***			***Final Pressure in Etching Chamber***			***Etch Depth (μm)***
	1st	*2nd*	*3rd*	*1st*	*2nd*	*3rd*	*1st*	*2nd*	*3rd*	*1st*	*2nd*	*3rd*	
1	0.37	0.42	0.3	0.32	0.27	0.13	75	45	30	0.42	0.29	0.17	
2	0.33	0.39	0.28	0.28	0.25	0.14	75	45	30	0.38	0.28	0.16	
3	0.3	0.32	0.24	0.26	0.22	0.12	75	45	30	0.32	0.24	0.15	8

C. Quick Pulse Method

Pulse #	***Expansion Chamber Pressure before Etch***	***Initial Pressure in Etching Chamber***	***Pulse Duration (second)***	***Etch Depth (μm)***
1	0.5	0.43	150	
2	0.41	0.37	150	
3	0.37	0.34	150	
4	0.35	0.3	150	9

III. Sample with a Surface Area of ~85mm²

A. Basic Pulse Method

Pulse #	***Expansion Chamber Pressure before Etch***	***Initial Pressure in Etching Chamber***	***Pulse Duration (second)***	***Etch Depth (μm)***
1	0.3	0.26	150	
2	0.3	0.26	150	
3	0.3	0.26	150	13
4	0.3	0.26	150	
5	0.3	0.26	150	
6	0.3	0.26	150	20

B. Triple Pulse Method

#	***Expansion Chamber Pressure before Etch***			***Initial Pressure in Etching Chamber***			***Pulse Duration (second)***			***Final Pressure in Etching Chamber***			***Etch Depth (μm)***
	1st	***2nd***	***3rd***	***1st***	***2nd***	***3rd***	***1st***	***2nd***	***3rd***	***1st***	***2nd***	***3rd***	
1	0.32	0.4	0.28	0.27	0.23	0.13	75	45	30	0.4	0.28	0.16	
2	0.3	0.36	0.28	0.26	0.23	0.15	75	45	30	0.36	0.28		
3	0.3	0.32	0.24	0.26	0.2	0.11	75	45	30	0.32	0.24	0.17	12
4	0.31	0.38	0.27	0.25	0.23	0.12	75	45	30	0.37	0.27	0.16	
5	0.29	0.32	0.27	0.25	0.23	0.11	75	45	30	0.32	0.27	0.15	
6	0.31	0.43	0.27	0.32	0.25	0.15	75	45	30	0.42	0.26	0.18	
7	0.3	0.34	0.25	0.25	0.21	0.11	75	45	30	0.33	0.25		30

C. Quick Pulse Method

Pulse #	*Expansion Chamber Pressure before Etch*	*Initial Pressure in Etching Chamber*	*Pulse Duration (second)*	*Etch Depth (μm)*
1	0.44	0.39	150	
2	0.36	0.32	150	7
3	0.69	0.51	150	
4	0.4	0.34	150	15

Appendix E: Experimental Data for Trenching Effect

I. Dependance of Trenching Effect on Hole Diameter

As discussed in Chapters 3 and 4, the trenching effect can only be observed at the edges of those holes whose diameters are much larger than the mean free path of the gas molecule at the etching pressure. The following figures are bottom profiles of many holes with different diameters. They clearly illustrate the dependance of trenching effect on the hole diameter.

All of the holes were on one sample and the profiles were taken after 10 etching pulses. The etching method was triple pulse. The initial pressure was 0.3Torr and pulse duration was 150sec.

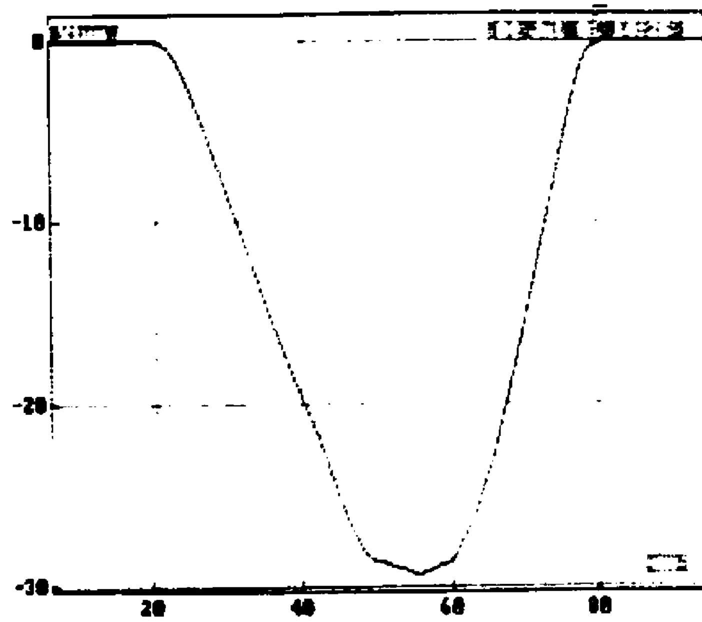

Figure E-1. Profile of a 60μm hole.

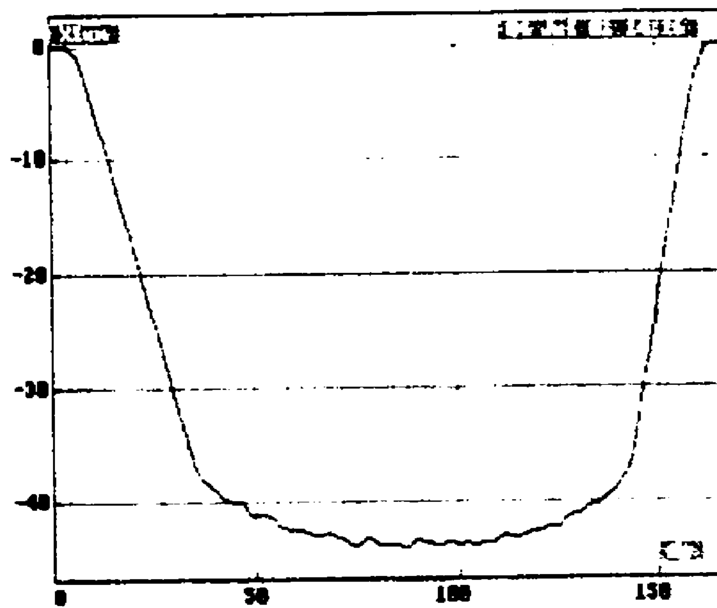

Figure E-2. Profile of a 158μm hole.

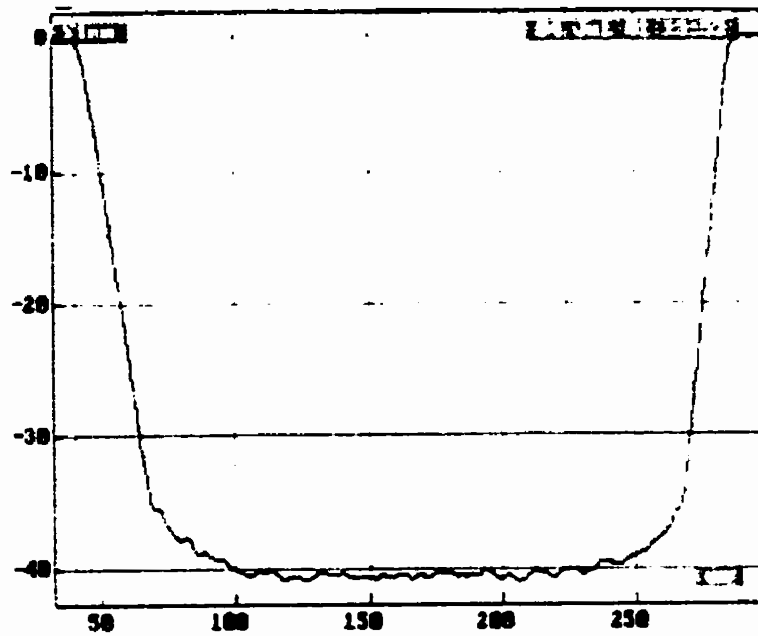

Figure E−3. Profile of a 249µm hole.

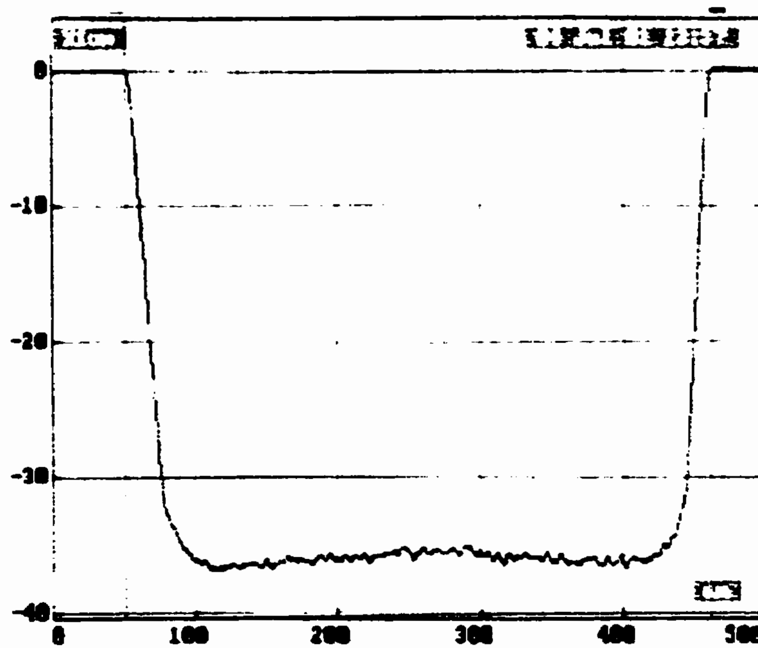

Figure E−4. Profile of a 411µm hole.

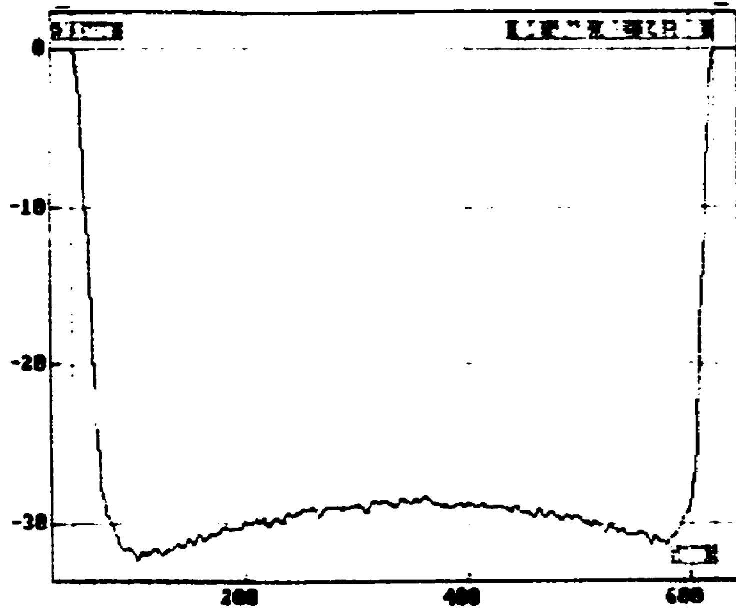

Figure E–5. Profile of a 576µm hole.

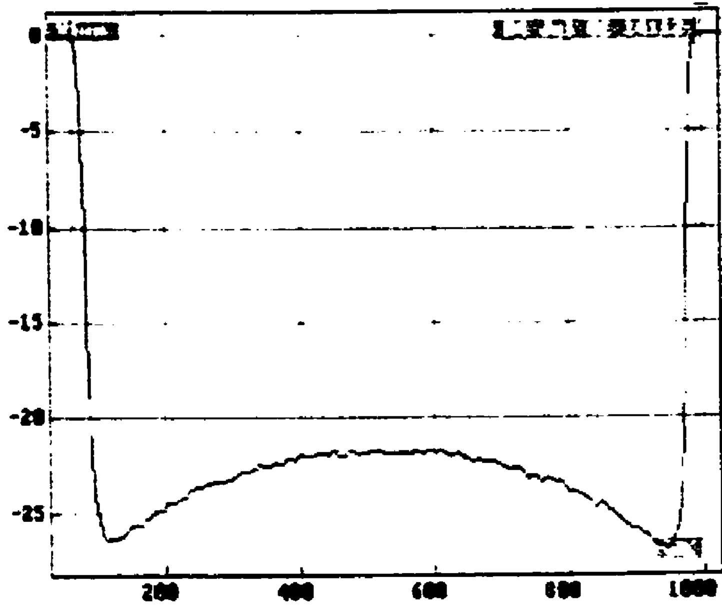

Figure E–6. Profile of a 924µm hole.

II. Dependance of Trenching Effect on Number of Etching Pulses

In addition to the etching pressure and hole size, trenching effect also depends on the etch depth. The following figures illustrate these variations for holes with roughly the same size. These pictures show this dependance for two groups of holes. In one of these groups the hole diameter is around 600μm and for the other group, the hole diameter is around 900μm. As can be seen, the trenching effect is more obvious on larger hole profiles.

The etching method was triple pulse, with 150sec pulses and an initial pressure of 0.3Torr.

A. Results after 4 Etching Pulses

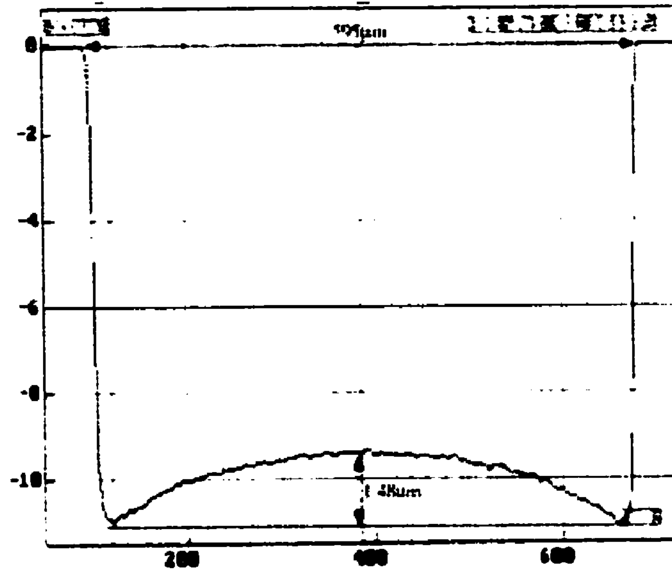

Figure E-7. Profile of a 595μm hole.

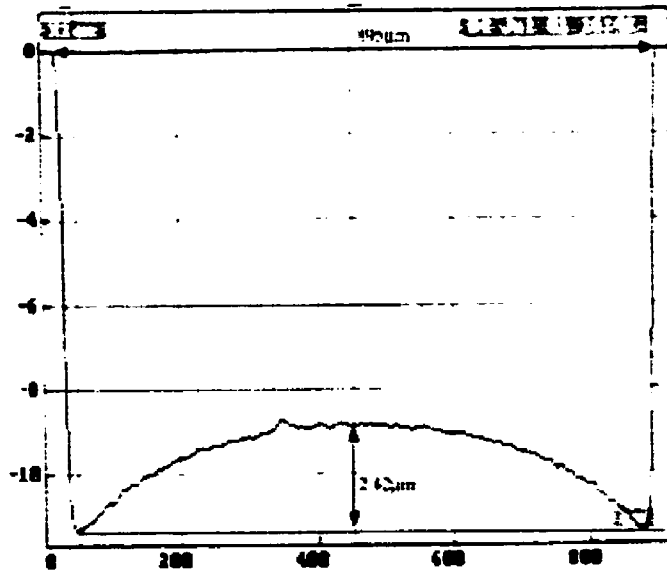

Figure E-8. Profile of a 895μm hole.

B. Results after 7 Etching Pulses

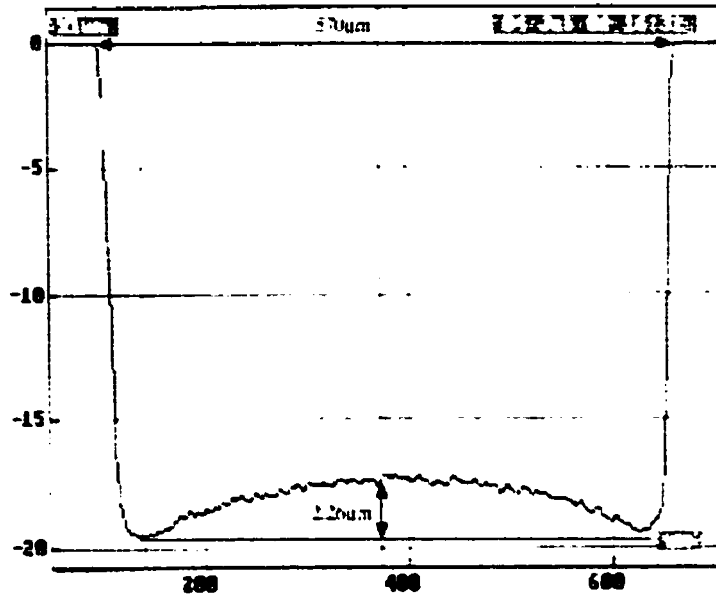

Figure E-9. Profile of a 570μm hole.

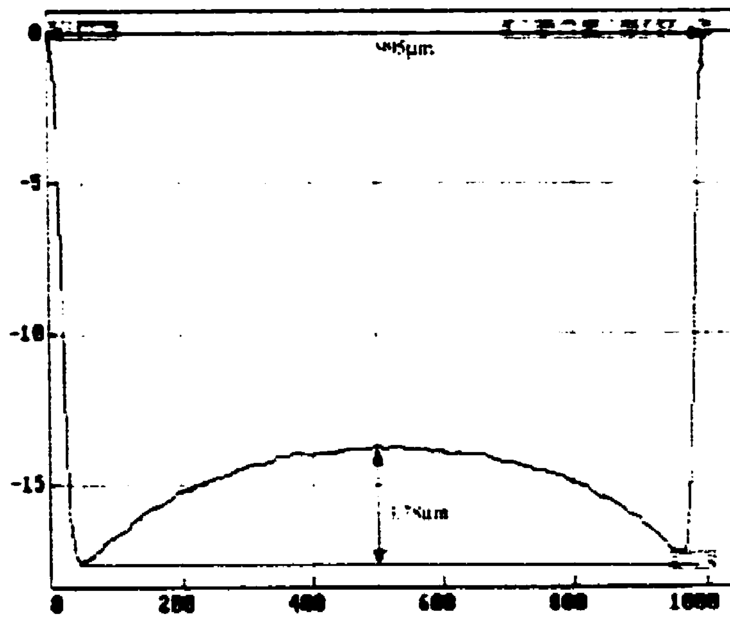

Figure E-10. Profile of a 995μm hole.

C. Results after 10 Etching Pulses

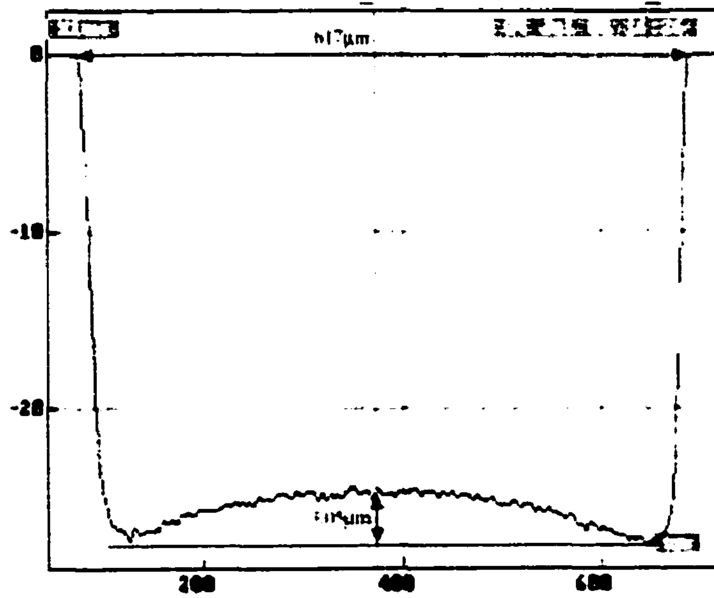

Figure E-11. Profile of a 617µm hole.

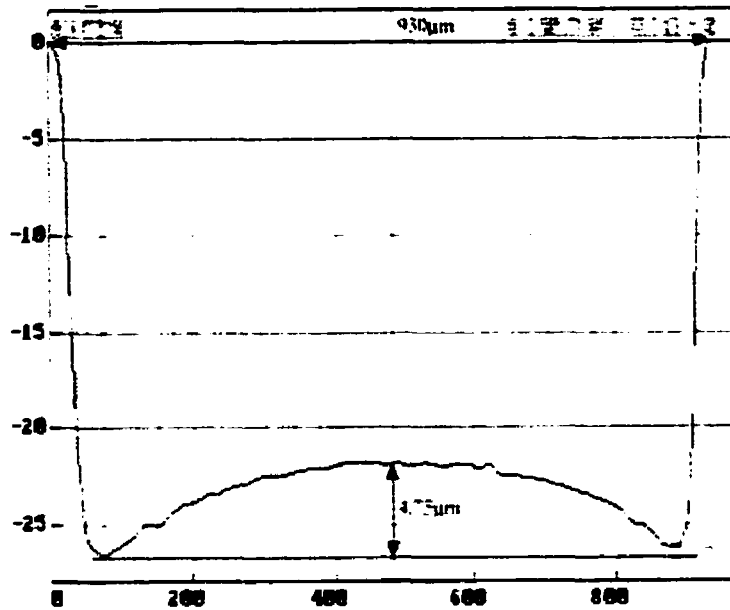

Figure E-12. Profile of a 930µm hole.

III. Comparison of Simulation and Experimental Results

In this section, the experimental results taken from a specific sample are compared to simulation results for similar etching conditions and hole sizes. After measuring the etch depth on the real sample, the simulation was run so that it resulted in almost the same etch depth. This was done to verify the accuracy of simulation program in predicting the etch profiles.

As can be seen in following figures, the simulation results for the overall shape of the bottom profile of different holes match the experimental data in all cases. However, the simulation slightly overestimated the depth of trenches for large holes.

Sidewall shapes of holes may be different from what is shown in measured profiles. This is due to the size of probe of the profilometer which was about the size of small holes.

For simulations, the reaction probability was set to 0.1 and the mean free path was assumed to be 10μm. The simulation was run for each hole separately to avoid loading effect. The hole diameters in simulations were set to be equal to the real holes.

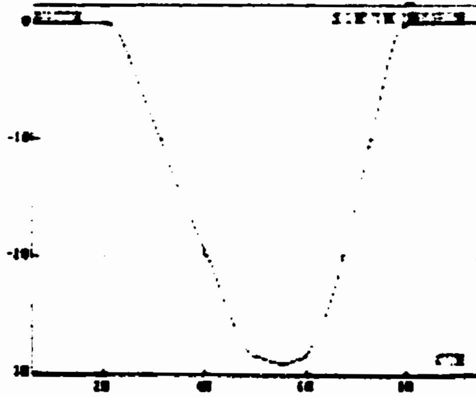

Figure E−13. Experimental and simulation results for a 60μm hole.

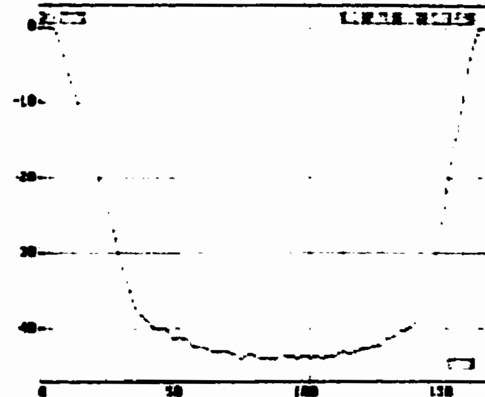

Figure E−14. Experimental and simulation results for a 160μm hole.

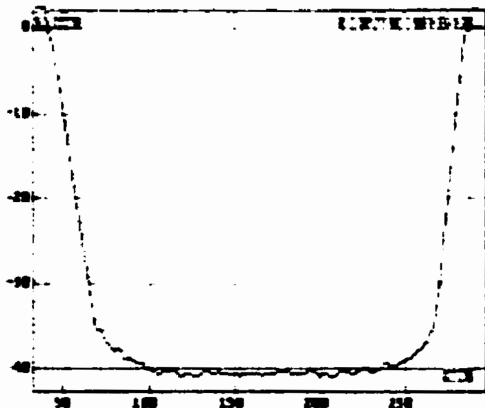

Figure E−15. Experimental and simulation results for a 250μm hole.

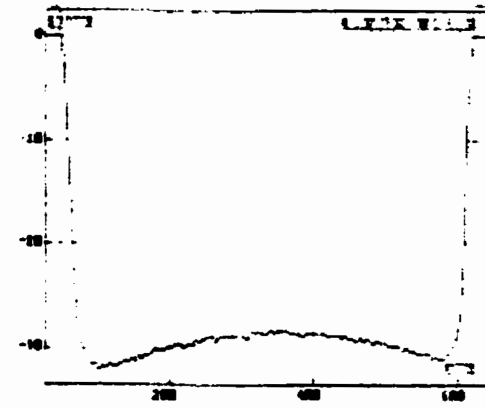

Figure E−16. Experimental and simulation results for a 580μm hole. The actual trench depth is 2.9μm versus 5μm for simulated result.

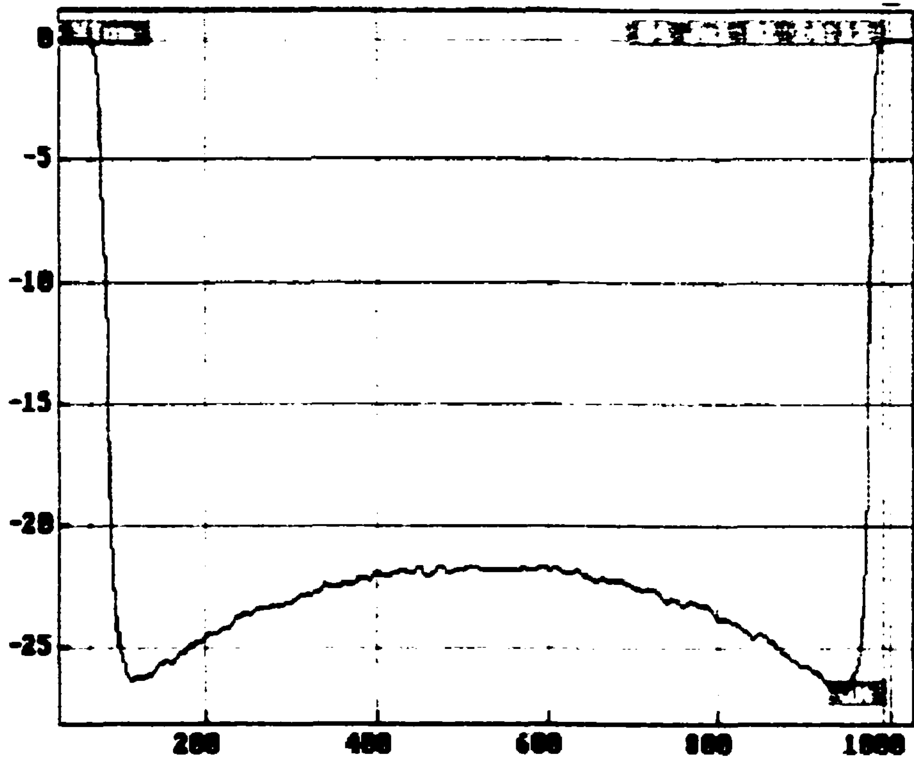

Figure E−17. Experimental and simulation results for a 1000μm hole. The actual trench depth is 4.9μm versus 7μm for simulated result.

Appendix F: Fabricated System

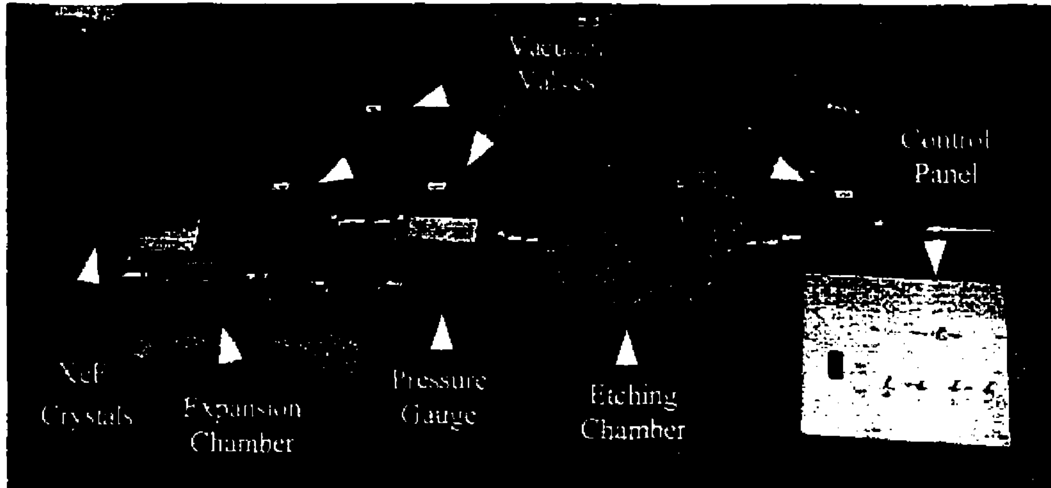

Figure F–1. Final setup of the system.

Etching chamber volume = $1100 cm^3$

Expansion chamber volume = $550 cm^3$

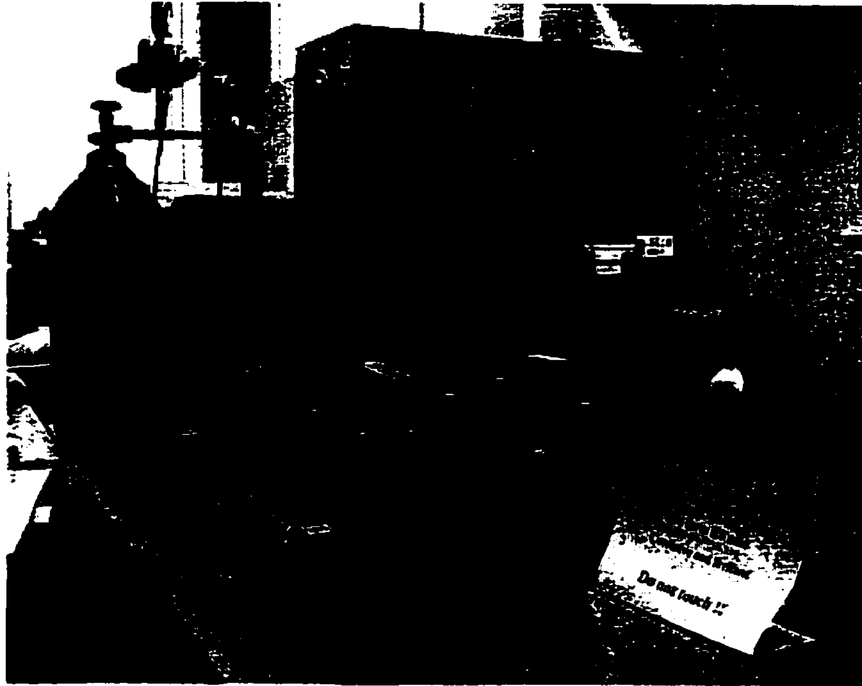

Figure F-2. Another view of the etching system.

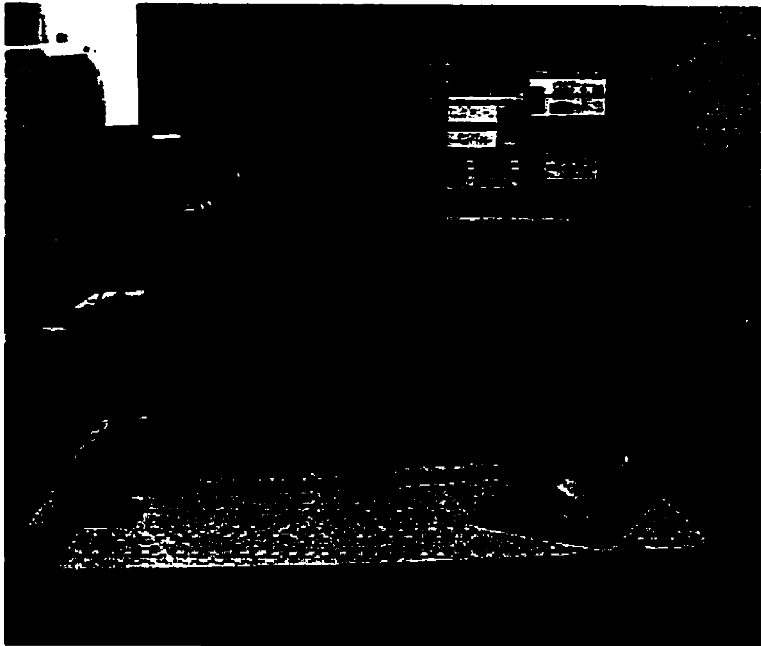

Figure F-3. Computer interface.

NOTE TO USERS

Page(s) not included in the original manuscript and are unavailable from the author or university. The manuscript was microfilmed as received.

134

This reproduction is the best copy available.

UMI®

References

[1]. *http://www.ee.ucla.edu/labs/laser/index.html*

[2]. *http://mems.engr.wisc.edu/publications/online.html*

[3]. A. Selvakumar and K. Najafi, "A high sensitivity Z-axis capacitive silicon microaccelerometer with a torsional suspension," *Journal of Microelectromechanical Systems*, vol. 7, no. 2, pp 192-200, 1998.

[4]. M. J. Madou, *Fundamentals of microfabrication*, CRC Press, 1997.

[5]. N. Maluf, *An introduction to microelectromechanical systems engineering*, Artech House, 1999.

[6]. S. T. Picraux and P. J. McWhorter, "The broad sweep of integrated microsystems," *IEEE Spectrum*, vol. 35, no. 12, 1998.

[7]. *http://www.mdl.sandia.gov/micromachine/overview.html*

[8]. *http://www.dbanks.demon.co.uk/ueng/*

[9]. S.M. Sze, *Semiconductor devices: physics and technology*, John Wiley, 1985.

[10]. R.C. Jaeger, *Introduction to microelectronic fabrication (Vol. V of Modular Series on Solid State Devices)*, Addison-Wesley 1989.

[11]. K.E. Petersen, "Silicon as a mechanical material," *Proceedings of the IEEE*, vol. 70, no. 5, pp 420-457, 1982.

[12]. S. A. Campbell, *The science and engineering of microelectronic fabrication*, Oxford University Press, 1996.

[13]. G. T. A. Kovacs, *Micromachined transducer sourcebook*, WCB/McGraw-Hill,

1998.

[14]. K. R. Williams, "Micromachining etch rate database," *http://www-bsac.EECS.Berkeley.EDU/db/*

[15]. W. H. Ko, J. T. Suminto, and G. J. Yeh, "Bonding techniques for microsensors," *Micromachining and Micropackaging of Transducers*, C.D. Fung, P.W. Cheung, W.H. Ko and D.G. Fleming, eds. Elsevier Science Publishers B. V., Amsterdam, pp 41–61, 1985.

[16]. A. Hanneborg, "Silicon wafer bonding techniques for assembly of micromechanical elements," *Proceedings of the IEEE 4th International Conference on Micro Electro Mechanical Systems: MEMS '91*, pp 92–98, 1991.

[17]. V. D. Samper, A. J. Sangster, R. L. Reuben, and U. Wallrabe, "Torque evaluation of a LIGA fabricated electrostatic micromotor," *Journal of Microelectromechanical Systems*, vol. 8, no. 1, pp 115–123, 1999.

[18]. M. McCormick, E. Chowanietz, and A. Lees, "Microengineering design and manufacture using the LIGA process," *Engineering Science and Education Journal*, vol. 3, no. 6, pp 255 –262,1994.

[19]. H. Debeda,T. V. Freyhold, J. Mohr,and U. Wallrabe, and J. Wengelink, "Development of miniaturized piezoelectric actuators for optical applications realized using LIGA technology," *Journal of Microelectromechanical Systems*, vol. 8, no. 3, pp 258 –263, 1999.

[20]. H. Miyajima and M. Mehregany, "High–aspect–ratio photolithography for MEMS applications," *Journal of Microelectromechanical Systems*, vol. 4, no. 4, pp 220–229, 1995.

[21]. F. Ayazi and K. Najafi, "High aspect–ratio combined poly and single–crystal silicon (HARPSS) MEMS technology," *Journal of Microelectromechanical Systems*, vol. 9, no. 3, pp 288–294, 2000.

[22]. V. Aksyuk, B. Barber, C. R. Giles, R. Ruel,L. Stulz, and D. Bishop, "Low insertion loss packaged and fiber connectorised MEMS reflective optical switch," *Electronics Letters* , vol. 34, no. 14 , pp. 1413–1414, 1998.

[23]. K. Najafi and K. D. Wise, "An implantable multielectrode array with on–chip signal processing," *1986 Digest of Technical Papers, International Solid–State Circuits Conference*, pp. 98–99, Los Angeles, 1986.

[24]. K. Wang and C. T–C. Nguyen, "High–order medium frequency micromechanical electronic filters," *IEEE Journal of Microelectromechanical Systems*, vol. 8, no. 4, pp 534–557, 1999.

[25]. H. F. Winters and J. W. Coburn, "The etching of silicon with XeF_2 vapor," *Applied Physics Letters*, vol. 34, no. 1, pp 70–73, 1979.

[26]. X. Wang, X Yang, K. Walsh, and Y. Tai, "Gas–phase silicon etching with bromine trifluoride," *International Conference on Solid State Sensors and Actuators; TRANSDUCERS '97*, Chicago, vol. 2, pp 1505 –1508, 1997.

[27]. P. B. Chu, J. T. Chen, R. Yeh, G. Lin, J. C. P. Haung, B. A. Warneke, and K. S. J. Pister, "Controlled pulsed–etching with Xenon Difluoride," *Proceedings of The Ninth International Conference on Solid State Sensors and Actuators*, June 1997.

[28]. F. A. Houle, "A reinvestigation of the etch products of silicon and XeF_2: doping and pressure effects," *Journal of Applied Physics*, vol. 60, no. 9, pp 3018–3026, 1986.

[29]. D. E. Ibbotson, J. A. Mucha, and D. L. Flamm,"Plasmaless dry etching of silicon with fluorine–containing compounds," *Journal of Applied Physics*, vol. 56, no. 10, pp 2939–2942, 1984.

[30]. D. L. Flamm, V. M. Donnelly, and J. A. Mucha, "XeF_2 and F–atom reactions with Si: their significance for plasma etching," *Solid State Technology*, pp 117–121, April 1983.

[31]. D. L. Flamm, D. E. Ibbotson, J. A. Mucha, and V. M. Donnelly "The reaction of fluorine atoms with silicon," *Journal of Applied Physics*, vol. 52, no. 5, pp 3633–3639, 1981.

[32]. V. M. Donnelly and D. L. Flamm, "Studies of chemilumiescence accompanying fluorine atom etching of silicon," *Journal of Applied Physics*, vol. 51, no. 10, pp 5273–5276, 1980.

[33]. J. A. Gibson and A. F. Janzen, "Reaction of xenon difluoride with organosilicon compounds," *Canadian Journal of Chemistry*, vol. 49, pp 2168–2171, 1971.

[34]. D. E. Ibbotson, D. L. Flamm, J. A. Mucha, and V. M. Donnelly, "Comparison of

XeF_2 and F–atom reactions with Si and SiO_2," *Applied Physics Letters*, vol. 44, no. 12, pp 1129–1131, 1984.

[35]. M. J. Vasile, "The reaction probability of XeF_2 with silicon," *Journal of Applied Physics*, vol. 54, no. 11, pp 6697–6704, 1983.

[36]. N. H. Tea, V. Milanović, C. A. Zincke, J. S. Suehle, M. Gaitan, M. E. Zaghloul, and J. Geist, "Hybrid postprocessing etching for CMOS–compatible MEMS," *Journal of Microelectromechanical Systems*, vol. 6, no. 4, pp 363–372, 1997.

[37]. *http://hyperphysics.phy–astr.gsu.edu/hbase/hframe.html*

[38]. C. Shafai, M. J. Brett, and T. M. Hrurey, "Etch–induced stress failures of SiO_2 cantilever beams," *Sensors and Actuators A*, vol. 70, pp 283–290, 1998.

[39]. A. Misaka and K. Harafuji, "Simulation study of micro–loading phenomena in silicon dioxide hole etching," *IEEE Transactions on Electron Devices*, vol. 44, no. 5, pp 751–760, 1997.

[40]. A. Papulis, *Probability and Statistics*, Prentice Hall, 1996.